REPUBLIC OF TURKEY

ACIBADEM MEHMET ALI AYDINLAR UNIVERSITY

INSTITUTE OF NATURAL AND APPLIED SCIENCES

PREPARATION AND *IN VITRO* EVALUATION OF TARGETED AND ANTI-INFLAMMATORY DRUG LOADED PLGA NANOPARTICLES

DENİZ GÖL

MASTER THESIS

DEPARTMENT OF BIOMATERIALS

SUPERVISOR

Assist. Prof. Özgül Gök Özatay

ISTANBUL-2024

REPUBLIC OF TURKEY

ACIBADEM MEHMET ALI AYDINLAR UNIVERSITY

INSTITUTE OF NATURAL AND APPLIED SCIENCES

PREPARATION AND *IN VITRO* EVALUATION OF TARGETED AND ANTI-INFLAMMATORY DRUG LOADED PLGA NANOPARTICLES

DENİZ GÖL

MASTER THESIS

DEPARTMENT OF BIOMATERIALS

SUPERVISOR

Assist. Prof. Özgül Gök Özatay

ISTANBUL-2024

Department:	Biomaterials
Program:	Biomaterials Master Program
Thesis Title:	Preparation and *in vitro* Evaluation of Targeted and Anti-Inflammatory Drug Loaded PLGA Nanoparticles
Student's name and Surname:	Deniz Göl
Date of Defence:	08/03/2024

This is to certify that I have examined this copy of master thesis. I have found that she/he prepared after fulfilling the specified requirements in the associated legislations before the final examining committee whose signatures are below.

Jury Member (Jury President)	Assist. Prof. Özgül Gök Özatay Acıbadem Mehmet Ali Aydınlar University	……
Jury Member (Supervisor of the Thesis)	Assist. Prof. Özgül Gök Özatay Acıbadem Mehmet Ali Aydınlar University	……
Jury Member	Assoc. Prof. Merve Açıkel Elmas Acıbadem Mehmet Ali Aydınlar University	……
Jury Member	Assoc. Prof. Ahmet Erdi Sözen Marmara University	……

DECLARATION

I declare that this thesis work is my own work, I had no unethical behavior at any stages from the planning to the writing of the thesis, I obtained all the information in this thesis in accordance with academic and ethical rules, I cited all the information and comments that were not obtained with this thesis work, and I provided resources in the list of references. I also declare that there was no violation of any patents and copyrights during the study and writing of this thesis.

08/03/2024
Deniz Göl

PREFACE AND ACKNOWLEDGEMENT

First of all, I would like to express my sincere gratitude to my thesis supervisor Assist. Prof. Özgül Gök Özatay for her patience, motivation, support, and encouragement throughout conducting my research. Her guidance and trust -both in my personal and academic life- paved the way for the completion of this thesis. I am grateful to her for enhancing my laboratory skills and pushing me further.

Moreover, I would like to thank former and present Gök Research Group members for supporting and encouraging me. I feel so lucky to work with all of you. I also extend my appreciation to my colleagues, Begüm Yalçın and Gülnaz Yükselen. They always encouraged me and believed in my success. The collaborative spirit of our departments in the university has also enhanced my academic experience.

Last but not least, I would like to express my greatest appreciation to my parents (Mesut Göl and Hülya Göl), to my sister (Damla Göl Adıgüzel), and to my cousin (Nehir Ünal) for their lifetime support, love, and continuous encouragement throughout the completion of my master's degree. Also, I would like to extend my sincere appreciation to my beloved cat, Balım, whose presence has been a constant source of my motivation.

I would like to express my sincere gratitude to The Scientific and Technological Research Council of Türkiye (TÜBİTAK). This master's thesis was supported by TÜBİTAK Directorate of Science Fellowships and Grant Programmes (BİDEB) 2211-National Graduate Scholarship Program. Being a recipient of this scholarship is an honor, and I am truly thankful for the opportunity.

Furthermore, the first project of this thesis was supported by TÜBİTAK 1001 (titled “Makrofaj Hedefli Uzun Zincirli Vitamin E Metaboliti α-13′-COOH Yüklenmiş Nanopartiküllerin Hazırlanması ve *In Vitro* ve *In Vivo* Deney Modellerinde İncelenmesi”, project no. 121S687). Also, the other study conducted within the scope of first project was supported by Acıbadem Mehmet Ali Aydınlar University Scientific Research Projects Commission (ABAPKO, titled "Garcinoik Asit Yüklenmiş Makrofaj Hedefli Nanopartiküllerin Hazırlanması ve Primer Makrofaj Hücrelerinde Etkinliğinin İncelenmesi”, project no. ABAPKO 2022/01-15). In addition, the third project of this thesis was also supported by ABAPKO (titled “Antiinflamatuar İlaç İçeren ve Hedefli PLGA Nanoparçacıkların Hazırlanması ve *in vitro* Değerlendirilmesi”, project no. FYL-2024-2149).

TABLE OF CONTENTS

LIST OF ABBREVIATIONS AND SYMBOLS

^{1}H NMR	Proton nuclear magnetic resonance
1.25%PPT-PLGA NPs	1.25% PPT by weight containing targeted empty NPs
1.25%PPT-QCT-PLGA NPs	1.25% PPT by weight containing targeted QCT-loaded NPs
2.50%PPT-PLGA NPs	2.50% PPT by weight containing targeted empty NPs
2.50%PPT-QCT-PLGA NPs	2.50% PPT by weight containing targeted QCT-loaded NPs
10%TT80-PLGA NPs	10% TT80 by weight containing targeted empty NPs
10%TT80-QCT-PLGA NPs	10% TT80 by weight containing targeted QCT-loaded NPs
20%TT80-PLGA NPs	20% TT80 by weight containing targeted empty NPs
20%TT80-QCT-PLGA NPs	20% TT80 by weight containing targeted QCT-loaded NPs
α-13′-COOH PLGA NPs	Non-targeted α-13′-COOH loaded NPs
ACN	Acetonitrile
ANOVA	Analysis of variance
AS	Atherosclerosis
αTCP	α-tocopherol
αTCP-PLGA NPs	αTCP loaded non-coated NPs
CCCP	Carbonyl cyanide 3-chlorophenylhydrazone

CCK-8	Cell Counting Kit-8
$CDCl_3$	Deuterated chloroform
CS	Chitosan
CS-CUR-PLGA NPs	CS-coated CUR loaded NPs
CS-PLGA NPs	CS-coated empty NPs
CS-αTCP-PLGA NPs	CS-coated αTCP loaded NPs
CUR	Curcumin
CUR-PLGA NPs	CUR loaded non-coated NPs
DCC	N,N′-Dicyclohexylcarbodiimide
DCM	Dichloromethane
ddH_2O	Double-distilled water
DDS	Drug delivery systems
DIC	N,N'-Diisopropylcarbodiimide
DLS	Dynamic light scattering
DMAP	4-(Dimethylamino)pyridine
DMEM/F-12	Dulbecco's Modified Eagle Medium F-12 Nutrient Mixture (Ham)
DMF	N,N-Dimethylformamide
DMSO	Dimethyl sulfoxide
DPBS	Dulbecco's Phosphate Buffered Saline
DSPE	1,2-distearoyl-sn-glycero-3-phosphatidylethanolamine

DSPE-PEG	Poly(ethylene glycol) grafted 1,2-distearoyl-sn-glycero-3-phosphatidylethanolamine
DSPE-PEG-Mal	1,2-distearoyl-sn-glycero-3-phosphoethanolamine-N-[maleimide(polyethylene glycol)]
DSPE-PEG-S2P	S2P peptide-conjugated DSPE-PEG
EE	Encapsulation efficiency
EPR	Enhanced permeability and retention
Et_3N	Triethylamine
FBS	Fetal Bovine Serum
FDA	US Food and Drug Administration
FITC	Fluorescein isothiocyanate
FITC-PLGA NPs	FITC-labeled non-targeted empty NPs
FITC-S2P-PLGA NPs	FITC-labeled targeted empty NPs
FT-IR	Fourier transform infrared spectroscopy
G	Glycolide
GA	Garcinoic acid
GA-PLGA NPs	Non-targeted GA loaded NPs
L	Lactide
LC/MS-MS	Liquid chromatography/mass spectrometry-mass spectrometry
LPS	Lipopolysaccharide
MW	Molecular weight
Non-coated PLGA NPs	Non-coated empty PLGA NPs
Non-targeted PLGA NPs	Non-targeted empty PLGA NPs

NPs	Nanoparticles
PBS	Phosphate buffered saline
PDI	Polydispersity index
PEG	Poly(ethylene glycol)
PES	Polyethersulfone
PFA	Paraformaldehyde
PLGA	Poly(D, L-lactide-co-glycolide)
PLGA NPs	Non-targeted empty NPs
PNPs	Polymeric nanoparticles
PPT	PLGA-PEG-TPP
Prep-HPLC	Preparative high-performance liquid chromatography
PVA	Poly(vinyl alcohol)
QCT	Quercetin
QCT-PLGA NPs	Non-targeted QCT-loaded PLGA NPs
RhB	Rhodamine B
RhB-FITC-PLGA NPs	RhB-conjugated FITC-labeled non-targeted empty NPs
RhB-FITC-S2P-PLGA NPs	RhB-conjugated FITC-labeled targeted empty NPs
RhB-FITC-S2P-α-13′-COOH PLGA NPs	RhB-conjugated FITC-labeled targeted α-13′-COOH-loaded NPs
RhB-FITC-α-13′-COOH PLGA NPs	RhB-conjugated FITC-labeled non-targeted α-13′-COOH-loaded NPs
ROS	Reactive oxygen species

RT	Room temperature
S2P-GA-PLGA NPs	Targeted GA loaded NP
S2P-PLGA NPs	Targeted empty NPs
S2P-α-13′-COOH PLGA NPs	Targeted α-13′-COOH-loaded NPs
SEM	Scanning electron microscopy
TCP	Tocopherol
TEM	Transmission electron microscopy
TFA	Trifluoroacetic acid
TIS	Triisopropylsilane
TPP	Triphenylphosphate
TPP-Br	(4-Bromobutyl) triphenylphosphonium bromide
TT80	TPP-Tween80
VitE	Vitamin E

LIST OF FIGURES

LIST OF TABLES

SUMMARY

Inflammation is derived from certain pathogenic disorders and its persistence leads to chronic inflammatory diseases such as atherosclerosis (AS) and cancer, posing life-threatening risks. For its treatment, conventional drug delivery systems (DDS) have several limitations including the toxicity, insufficient delivery, weak bioavailability, and high dosage requirements. For this reason, nanoparticles (NPs) have been recently used as a contemporary DDS since they can overcome the shortcomings of traditional treatment methodologies. In this thesis, which is comprised of three projects, it is aimed to develop poly(D, L-lactide-co-glycolide) (PLGA) NPs loaded with anti-inflammatory drugs for the treatment of AS-induced inflammation or oxidative stress-induced inflammation. In the first project, macrophage-targeted and anti-inflammatory vitamin E metabolites containing NPs were synthesized while in the second project, chitosan-coated, antioxidant and anti-inflammatory drug containing core-shell PLGA NPs were produced. In these projects, sustained drug release was successfully achieved through monodisperse and stable NPs against AS-induced inflammation. In the third project, mitochondria-targeted, quercetin-loaded monodisperse and highly stable PLGA NPs were synthesized. Cell culture studies proved that NPs showed higher cell viability compared to free drug. Moreover, all targeted NPs effectively decreased the production of reactive oxygen species in the presence of an inflammation compared to non-targeted NPs and free drug. Also, the dose-dependent targeting efficacy of targeted NPs was proved against free drug and non-targeted NPs via JC-1 assay. In conclusion, three different PLGA NPs that have a great potential to serve as an effective DDS for treating chronic inflammatory diseases were developed in this thesis study.

Keywords: Controlled drug release, Inflammation, Nanoparticle, Poly(D, L-lactide-co-glycolide), Targeted drug delivery system

ÖZET

Anti-İnflamatuar İlaç İçeren ve Hedefli PLGA Nanoparçacıkların Hazırlanması ve *in vitro* Değerlendirilmesi

İnflamasyon, belirli patojenik bozukluklardan kaynaklanır ve sürekliliği, ateroskleroz (AS) ve kanser gibi insan yaşamını tehdit eden kronik inflamatuar hastalıklara yol açar. Geleneksel ilaç taşıma sistemlerinin (İTS) inflamasyon tedavisinde kullanılmasının toksisite, yetersiz dağılım, düşük biyoyararlanım ve yüksek doz gereksinimleri gibi çeşitli sınırlamaları vardır. Bu nedenle, nanoparçacıklar (NP) geleneksel tedavi yöntemlerinin eksikliklerini aşabildikleri için modern İTS olarak son zamanlarda kullanılmaktadır. Üç projeden oluşan bu tezde, AS tarafından ya da oksidatif stres tarafından indüklenen inflamasyonun tedavisi için anti-inflamatuar ilaçlarla yüklenmiş poli(laktik-ko-glikolik asit) (PLGA) NP'lerin geliştirilmesi hedeflenmiştir. İlk projede, makrofaj hedefli ve anti-inflamatuar vitamin E metaboliti içeren NP'ler sentezlenirken, ikinci projede, kitosan kaplı, antioksidan ve anti-inflamatuar ilaç içeren çekirdek-kabuk PLGA NP'ler üretildi. Bu projelerde, AS kaynaklı inflamasyona karşı oluşturulan monodispers ve stabil NP'lerden sürekli ilaç salınımı başarılı bir şekilde elde edildi. Üçüncü projede ise, mitokondri hedefli, kuersetin yüklü, monodispers ve yüksek stabiliteye sahip PLGA NP'ler sentezlendi. Hücre kültürü çalışmaları bütün NP'lerin serbest ilaca kıyasla daha yüksek hücre canlılığı gösterdiğini kanıtladı. Ayrıca, tüm hedefli NP'ler inflamasyon durumunda reaktif oksijen türlerinin üretimini serbest ilaç ve hedeflendirilmemiş NP'lere kıyasla etkili bir şekilde azalttı. Bununla beraber, hedeflendirilmiş NP'lerin doza bağlı hedefleme etkinliği hedeflendirilmemiş NP'lere ve serbest ilaca karşı kanıtlandı. Sonuç olarak, bu tez çalışmasında, kronik inflamatuar hastalıkların tedavisinde etkili bir İTS olarak hizmet etme potansiyeline sahip olan üç farklı PLGA NP geliştirilmiştir.

Anahtar Sözcükler: Hedeflendirilmiş ilaç taşıma sistemi, İnflamasyon, Kontrollü ilaç salınımı, Nanoparçacık, Poli(laktik-ko-glikolik asit)

1. BACKGROUND AND AIM OF THE STUDY

This thesis comprises three projects. Project 1 is the "Preparation of macrophage-targeted poly(D, L-lactide-co-glycolide) (PLGA) nanoparticles (NPs) containing different vitamin E (VitE) metabolites for the treatment of atherosclerosis (AS)-induced inflammation", project 2 is the "Preparation of chitosan (CS)-coated curcumin (CUR) and α-tocopherol (αTCP) loaded core-shell PLGA NPs for the treatment of AS-induced inflammation", and project 3 is the "Preparation and *in vitro* evaluation of mitochondria-targeted quercetin (QCT) loaded PLGA NPs for the treatment of oxidative stress-induced inflammation".

In general, the projects of this thesis focusing on the synthesis and evaluation of different types of PLGA NPs loaded with specific drugs for the treatment of inflammation. The main purpose behind this thesis is to develop NPs with optimized properties, to assess the effectiveness of them, and to evaluate their potential as anti-inflammatory agents.

The studies conducted in all projects demonstrate originality in terms of contributions to the science. Although the chosen polymer, drug molecules, or targeting agents used in this thesis are previously studied in the literature, their combination is not used. For instance, for the first project, there is no available study demonstrating the anti-inflammatory impact of α-13'-COOH-loaded S2P-conjugated NPs and garcinoic acid (GA)-loaded S2P-conjugated NPs specifically on macrophages. Also, for the studies conducted in second project, there is a lack of existing literature on CUR-loaded and αTCP-loaded, CS-coated PLGA NPs against the inflammation induced by AS. Last but not least, for the third project, there is currently no literature examining the use of triphenylphosphate (TPP)-conjugated QCT-loaded PLGA NPs for addressing inflammation which is induced by oxidative stress. Additionally, within the framework of this project, two distinct conjugates

containing TPP were synthesized to assess and compare their effectiveness as targeting agents. These targeting agents were then conjugated onto the NPs at varying ratios. Similar study is also not available in the literature. All of these contributes to the uniqueness and originality of this thesis.

Thanks to the data obtained at the end of all these experiments, it becomes possible to develop polymeric PLGA NPs, with a specific targeting agent conjugated on their surface, containing anti-inflammatory drug molecules. This could provide effective reduction in the inflammation and improvement in the quality of life for patients suffering from chronic inflammatory disorders such as diabetes, cancer, and AS. The studies conducted within the scope of this thesis will pave the way for many future investigations.

2. INTRODUCTION

2.1. Drug Delivery Systems

Most of the traditional administration routes for drug molecules have a number of drawbacks that must be overcome before achieving desired pharmacological effects. These limitations include toxicity, high dosage requirements, low therapeutic potency, inadequate delivery mechanism at the target site, serious side effects, and poor biodistribution and bioavailability (1,2). For instance, oral pills for delivering small drug molecules and injections for administrating peptides and proteins are prevalently used therapy modalities nowadays. Although oral pills provide predictable dosing intervals and are non-invasive in nature, their usage is limited in delivering larger therapeutic compounds to the body. On the contrary, injections can be used to deliver macromolecules, but because of their intrusive nature and high risk of infection, their use is limited (3). All in all, the administration route of pharmaceutical substances and organ physiology and metabolism significantly affect the clinical success of therapeutic compounds. When the drug is given systematically in the conventional delivery, the bioavailability of the drug is often relatively low, and the plasma level of the drug may drop abruptly below a minimally effective level. As a result, additional doses can be necessary, which reduces patient convenience and raises the danger of an overdose (4). In order to overcome the risks and shortcomings related to conventional drug delivery routes, drug delivery systems (DDS) have been utilized in recent years (2).

A DDS is a formulation or method that enables the administration of therapeutic molecules into the body by improving their therapeutic effect and safety. DDS could be utilized to successfully overcome biological barriers to reach the intended region effectively and also regulate the amount and release of drug molecules in this desired site (2). In this way, the plasma drug level could be attained between the maximum

desired level and the minimum effective level, in a sustained manner (4). This leads to reduced toxicity and undesirable side effects, enhanced efficiency, and patient convenience. DDS can prevent the therapeutic substance from being quickly metabolized and eliminated from the body, allowing for the administration of lower dosages of drug molecules (5). Consequently, compared to traditional drug delivery, DDS enhance the administration and effectiveness of pharmaceutical compounds in the body.

2.1.1. Nanoparticles

Solid, colloidal particles which have a diameter between 10-1000 nm, known as NPs, can be obtained using a variety of materials such as polymers, metals, or ceramics (6,7). Ideally, NPs need to be biocompatible, non-toxic, biodegradable, non-immunogenic, non-thrombogenic, non-inflammatory, and cost-effective for use in clinical applications. The size and surface properties of these NPs and the release mechanism of therapeutic molecules carried by them could be adjusted depending on their intended use (5).

For both diagnostic and therapeutic purposes, NPs serve as commonly used DDS, offering several advantages over conventional methods thanks to their small size and large surface area. These include regulating drug release, maintaining the concentration of drug molecules at a therapeutic level, and allowing targeting tissues (5,8). NPs can be obtained using biodegradable materials and this allows sustained release of encapsulated molecules in the targeted region over a certain period of time (6). Based on the preparation method, they can be obtained as either nanocapsules or nanospheres. The drug molecule is physically and uniformly spread in nanospheres. On the other hand, in nanocapsules, the drug is placed into a cavity and protected by a polymeric membrane (9).

Furthermore, there are numerous methods to load NPs with various therapeutic agents in order to overcome most of the drug delivery challenges (6,10). The drug molecule can be dispersed, trapped, adsorbed, attached, and/or encapsulated to NPs based on the design and purpose (6). In terms of encapsulated therapeutic agents, NPs could enhance the solubility and stability of them, and this increases the safety and efficiency of treatment (10). For instance, NPs offer a stealth mode, especially for water-insoluble pharmacological compounds, to prevent immune system recognition. In this way, they could provide prolonged circulation time compared to conventional DDS. Moreover, thanks to their nano-size, they can easily penetrate biological barriers and provide an accumulation of small drug molecules at the target site. This leads to a decrease in the toxicity and side effects of drug molecules (7). Also, NPs can provide high drug-loading capacity (5). In conclusion, NPs are commonly used DDS because the release rate of pharmacological agents at the targeted regions in the body could be controlled thanks to their usage (9).

2.1.1.1. Polymeric nanoparticles

Polymeric nanoparticles (PNPs) that have a hydrodynamic diameter smaller than 1000 nm are known as solid colloidal particles. They can be produced easily and cheaply in large quantities using natural (e.g., CS, gelatin), synthetic (e.g., poly(vinyl alcohol (PVA), PLGA) and even semisynthetic sources that can be either biodegradable or non-biodegradable (11,12). The usage of non-biodegradable polymers in the synthesis of NPs leads to some shortcomings including chronic toxicity and severe immune response. Because of this, PNPs obtained using biodegradable polymers have been preferred widely in studies at the present time. The US Food and Drug Administration (FDA) has certified that some polymers, such as PLGA, are safe for use in clinical applications (12). These PNPs can also be loaded with therapeutically active compounds that have received FDA approval. As a result, PNPs allow administering drugs to the desired specific site at a controlled rate (12).

Furthermore, PNPs are widely preferred promising DDS since they can enhance the safety of therapeutic agents by delivering higher amounts of them to targeted regions properly. Thanks to their nano-size, most of the PNPs can effectively pass through biological barriers and have a long circulation through the bloodstream without being detected by the immune system of the body (11,13). It is possible to widen the application areas of PNPs by altering their properties such as size, surface charge, solubility, or surface functionality (14). By taking these into account, PNPs are commonly used DDS for the treatment of various diseases including cancer, inflammation, and cardiovascular disorders (12).

PLGA nanoparticles

Biodegradable PNPs are DDS that allow sustained and controlled release of therapeutic agents due to their nano-size and compatibility with the human body. These particles also possess several advantageous properties such as stability during blood circulation, non-inflammation, non-toxicity, non-immunogenicity, non-thrombogenicity, and biodegradability (15).

Specifically, PLGA, which is recognized by FDA as an ideal material to be used as a DDS, is a biocompatible and biodegradable hydrophobic copolymer made of lactic acid and glycolic acid (15,16). Non-toxic lactic and glycolic acids are linked together through the ester bonds and form PLGA. After PLGA hydrolyses into these two monomers in the body as in Figure 2.1, they are then metabolized into simpler byproducts such as CO_2 and H_2O via the Krebs Cycle (17). Therefore, the systemic toxicity caused by the usage of PLGA as a part of DDS is significantly low (15).

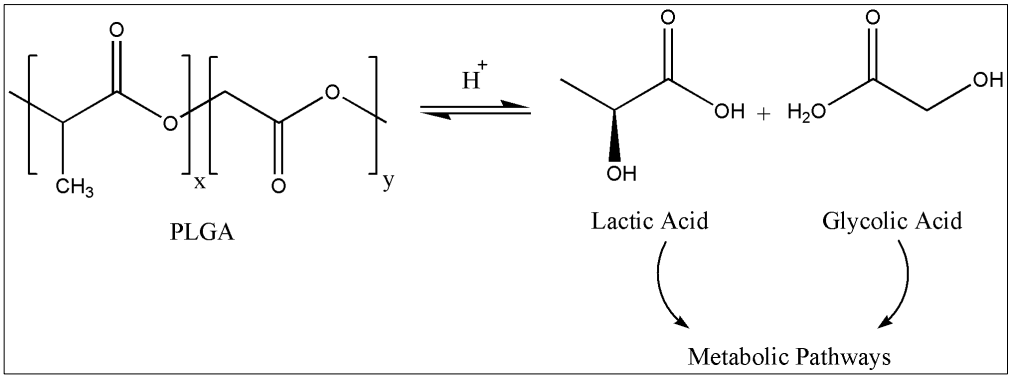

Figure 2. 1. Schematic representation of the hydrolysis of PLGA.

Different kinds of molecules can be encapsulated by PLGA NPs (17). Depending on the properties such as the ratio of lactic acid to glycolic acid, molecular weight (MW), surface modifications, and the degree of crystallinity, the degradation rate of PLGA polymer varies (18). As lactic acid/glycolic acid ratio increases, the hydrophobicity of PLGA polymer increases. Moreover, as the MW of the polymer decreases, the degradation and drug release rate of PLGA NPs increases (19). For instance, if the polymer has low MW and high glycolic acid content, it will be more hydrophilic. This results in a shorter degradation time. On the other hand, when the polymer has higher lactic acid content, it will be more hydrophobic and so degrade slowly. By adjusting these ratios and MW, it is also possible to adjust the drug release rate from PLGA NPs (17).

There are several methods for preparing PLGA NPs such as emulsification-solvent evaporation, nanoprecipitation, and spray drying. Among these, nanoprecipitation is one of the most commonly used ones since it is a relatively easy process. This method is generally used to encapsulate hydrophobic drug molecules in the polymer matrix. First of all, polymer and drug are dissolved in an organic solvent such as acetone and acetonitrile as in Figure 2.2. Then, while continuously stirring, this organic solution is added dropwise to the aqueous solution. Instantaneous solvent diffusion takes place during this procedure, and PLGA NPs are produced as a result (17).

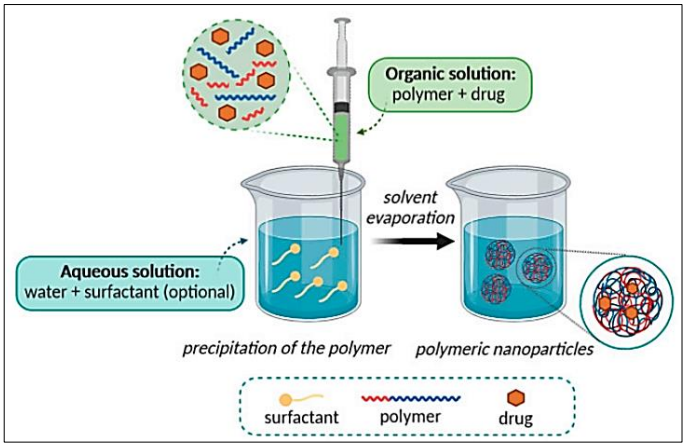

Figure 2. 2. Schematic representation of the nanoprecipitation method (12).

2.1.2. Targeted nanoparticles

Therapeutically active substances must penetrate biological barriers to carry out their desired functions in required regions regardless of their dosage. The components of those barriers, such as cellular membranes and enzymatic barriers, are complicated in nature. Especially, when the therapeutic target is inside of the cell, most of the conventional drug molecules are ineffective since they cannot diffuse into the cells by themselves. In this regard, it can be said that the biggest challenge in treating infectious, malignant, and hereditary diseases is the proper delivery of therapeutic agents to a particular tissue, organ, or cell. To address this, targeted DDS have been developed. Since NPs typically circulate in the bloodstream for a longer period of time compared to conventional drug molecules, they are frequently used to transport therapeutic agents to target sites in effective concentration (20).

There are two methods available for obtaining targeted NPs and these are known as passive targeting and active targeting as in Figure 2.3. Active targeting is based on the interaction between the targeting ligands located on the surface of NPs and the receptors on the target cell, whereas passive targeting depends on the physicochemical features (21).

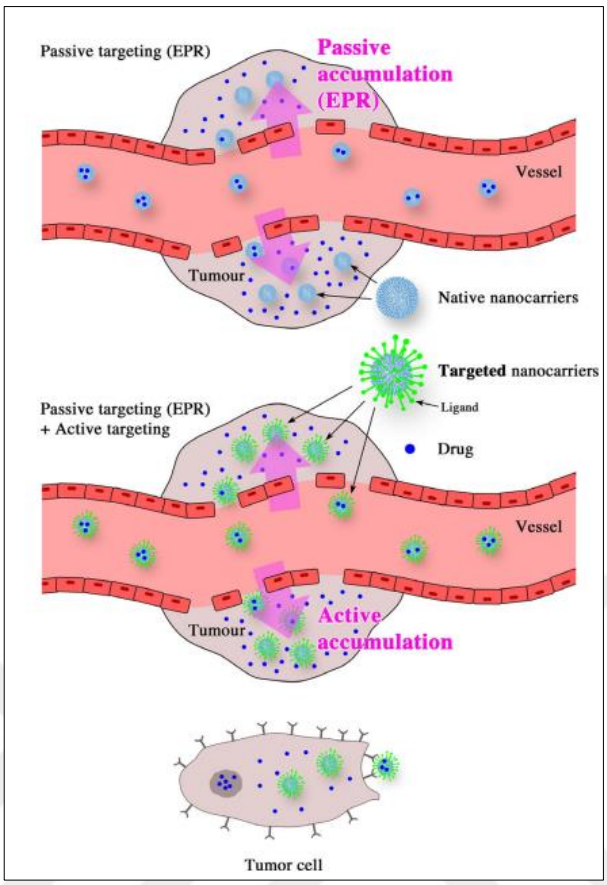

Figure 2. 3. Schematic representation of the passive and active targeting (12).

In healthy tissues, the endothelium of blood vessels is tightly packed. On the other hand, tumour tissues have a highly permeable vasculature that allows the entry of macromolecules and nanocarriers. They also possess impaired lymphatic drainage so therapeutic molecules can be retained inside the tissues longer. This phenomenon is defined as the enhanced permeability and retention (EPR) effect which provides an accumulation of nanocarriers in the tumour site through passive targeting (22). The properties of particles and the structure of tumours are both important in passive targeting. It does not contain any targeting ligands on the surface of the carrier. The threshold diameter value for extravasation is approximately 400 nm in tumours while particles smaller than 10 nm are filtered from the kidney. Therefore, the sizes of NPs should be adjusted accordingly to improve passive targeting ability. In a similar manner, the charge and surface functionalization of NPs are additional parameters affecting the rate of passive targeting. Passive targeting, however, does not ensure or

improve the uptake of NPs by cancer cells. This situation leads to the usage of active targeting that utilizes receptor-ligand interactions (22).

Moreover, NPs can reach the tumour site thanks to the EPR effect both in passive and active targeting. Besides, active targeting can further improve their internalization and also the intracellular release of therapeutic molecules (22). In active targeting, some biological targeting ligands such as antibodies, peptides, proteins, nucleic acids, or small molecules are located on the surface of NPs. These ligands are capable of binding to specific receptors overexpressed on the surface of targeted cells. This enhances the cellular uptake of NPs containing drug molecules, decreases the side effects, and so increases the therapeutic effect. Consequently, the amount of drug delivered to the disease site is obtained considerably higher in active targeting compared to free drug and passive targeting (21).

2.1.2.1. Macrophage-targeted nanoparticles

Innate immune cells called macrophages are present in all tissues and are capable of engulfing cells, presenting antigens, and secreting cytokines. They are crucial in controlling the initialization and progression of inflammation and immunological processes and also play a critical role in providing tissue homeostasis. However, under pathological conditions, the plasticity of macrophages remarkably alters, and this can cause the onset and progression of chronic diseases such as inflammatory disorders, cancer, diabetes, AS, and obesity. In various stages of these diseases, macrophages play crucial roles, and they have emerged as a key therapeutic target for the treatment of several illnesses. Therefore, the limitations of conventional drug molecules could be overcome by using macrophage-targeted drug-loaded NPs with targeting ligands on their surfaces (23-25). Among these targeting ligands, the S2P peptide with a sequence of CRTLTVRKC can be used as a macrophage-targeting ligand since it

recognizes the stabilin-2 receptor which is highly expressed on the surface of macrophages (26).

2.1.2.2. Mitochondria-targeted nanoparticles

Mitochondrion which is composed of a lipid bilayer structure is a significant organelle found in eukaryotic cells. It primarily consists of four parts, each of which performs a particular role. These are the outer mitochondrial membrane, the inner-membranous space, the inner mitochondrial membrane, and also the matrix. The permeability of these parts differs from each other. For instance, the outer membrane generally allows the passage of small molecules while the inner mitochondrial membrane is much more selective, and passage through it is controlled by some specialized channel proteins (27).

Mitochondria differ from other cellular components in terms of their distinct electrochemical potential and composition. Moreover, the mitochondrion is the only organelle that has its own genomes that play a crucial role in the production of proteins responsible in the electron transport chain for oxidative phosphorylation. It performs a variety of cellular functions as an organelle, including energy production, signalling, cell growth and differentiation, cell cycle control, and cell death. Since it has such precious functions, mitochondrial dysfunctions or mutations that trigger the cascade of cell death signals could cause severe diseases such as AS, cardiovascular disease, neurodegenerative disease, cancer, and even organ failure. Therefore, mitochondria are one of the emerging pharmaceutical targets for the treatment of various diseases and mitochondrial targeting strategies have gained importance (27).

It is difficult to carry drug molecules efficiently to the mitochondria due to their highly negative potential, complex nature, and double-membrane structure which have

different permeability from each other (28). For this reason, NPs that are aimed to be delivered could be functionalized with specific mitochondrial targeting ligands to improve drug delivery and treatment efficacy (29). In order to enhance the penetration of therapeutic agents into the mitochondria, specific targeting ligands could be conjugated onto the NPs. Among these ligands, TPP which is a lipophilic cation is one of the most commonly used to target mitochondria. As in Figure 2.4, it has a positively charged phosphorus atom. This atom is surrounded by three hydrophobic phenyl groups which make the TPP molecule lipophilic (30). There are several advantageous properties of using TPP as a targeting ligand including in vivo stability, lipophilic nature, ease of preparation and functionalization, and insignificant amount of chemical reactivity against cellular components. Thanks to its positive charge, it can cross the negatively charged phospholipid bilayer of mitochondria and can deliver the therapeutic molecule encapsulated into the NPs to desired location (28,31). Moreover, the transport of TPP-conjugated NPs from the cytoplasm into mitochondria is facilitated up to a hundred times compared to non-functionalized NPs thanks to the higher negative potential of the mitochondria in cancer cells (32).

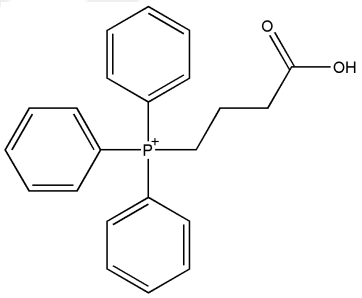

Figure 2. 4. The chemical structure of TPP.

2.2. Therapeutic Agents for Drug-Loaded Nanoparticles

An ideal DDS should possess a high drug-loading capacity to reduce the administration amount of drug molecules. This is beneficial to diminish side effects. Different methods could be used for loading drug molecules such as the incorporation method and the adsorption/absorption method. In the incorporation method, drugs are

incorporated into the NPs during their synthesis. In the other method, drug molecules are absorbed after formation of NPs. To actualize this, synthesized NPs are incubated with a concentrated drug solution (8). Depending on the application, nanospheres or nanocapsules can be obtained. In nanospheres, drug molecules are found on the surface of particles while in nanocapsules, they are located inside particles (15). In the literature, numerous synthetic or natural drug molecules are available, and they are commonly used as therapeutic agents to develop drug-loaded NPs depending on their advantages.

2.2.1. Quercetin

A naturally occurring polyphenolic flavonoid, QCT is found in fruits and vegetables. It is commonly used as a therapeutic agent in the prevention and treatment of various chronic diseases (33,34). Its structure can be seen in Figure 2.5. It has several beneficial biological properties such as being antioxidant, antiviral, antimicrobial, anti-inflammatory, and anti-carcinogenic (34). Its antioxidant property allows the protection of cells from the oxidative stress caused by reactive oxygen species which could eventually lead to severe chronic inflammatory diseases. Considering these, QCT is commonly used as a therapeutic agent for the treatment. It can also be combined with other drug molecules to reduce the overall required dose and possible side effects. However, due to its solubility and bioavailability problems, some alternative delivery methods have been studied for their effective use (35). The highly poor solubility of QCT in water could be solved by encapsulating it in NPs, especially in polymeric ones. Carrying hydrophobic drug molecules such as QCT with nanocarriers enhances the stability, bioavailability, and pharmacokinetic profile of the drug while reducing its toxicity to the body (36).

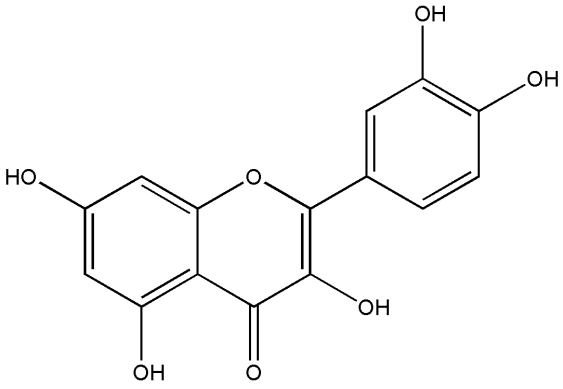

Figure 2. 5. The chemical structure of QCT.

2.2.2. Curcumin

Turmeric is one of the natural plants that has been commonly used for medical purposes for years thanks to its antioxidant, anti-inflammatory, anticancer, and antimicrobial properties (37). CUR derived from turmeric is a polyphenol commonly used as a natural drug molecule and its chemical structure can be seen in Figure 2.6. It has neuroprotective, antioxidant, anti-inflammatory, anticarcinogenic, antibacterial, antidiabetic, antiviral, and antifungal properties (38,39). CUR is able to target several signalling molecules which demonstrate its activity at the cellular level (37). It has been shown that CUR can be highly tolerated by the body even at high levels without having any negative effects. For this reason, it is one of the most commonly used therapeutic agents to treat several diseases (38). It has several beneficial properties, but because of some difficulties, its usage and delivery to the body are restricted. It has low water solubility, rapid metabolism, low absorption, and poor bioavailability in the body. Different approaches have been developed to address these stability, durability, and bioavailability limitations. One of these commonly used strategies is the encapsulation of CUR in various nanocarriers to deliver it to the body properly (38).

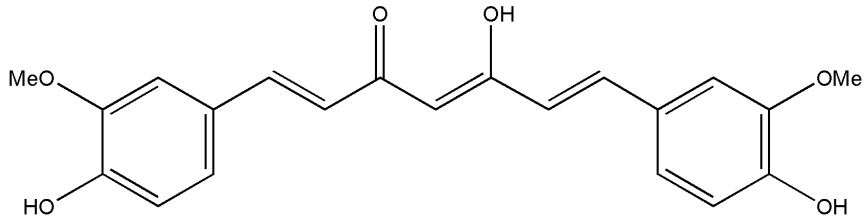

Figure 2. 6. The chemical structure of CUR.

2.2.3. Vitamin E metabolites

One of the essential nutrients for the body is fat-soluble VitE (40). It is commonly found in dietary fats, oils, and seeds (41). It has antioxidant and anti-inflammatory properties that enable its usage in both preventing and treating chronic inflammatory diseases such as AS, neurological disorders, and cardiovascular diseases (42,43). Moreover, it also plays an important role in modulating gene expression and regulating signal transduction (42). It consists of eight isomers which are α-, β-, γ-, and δ-tocopherol (TCP), and α-, β-, γ-, and δ- tocotrienol that differs from each other depending on the position and quantity of methyl groups present (41,42).

Furthermore, TCPs are one of the most commonly used forms of VitE derivatives. These lipid-soluble molecules are known for their antioxidant and anti-inflammatory properties (44). Among them, αTCP is the most active form, and its chemical structure can be seen in Figure 2.7 (42). Its nature is phenolic (41). Since it is an abundant form in the human body and exhibits superior antioxidant and anti-inflammatory effects compared to other isomers, it is widely used (40).

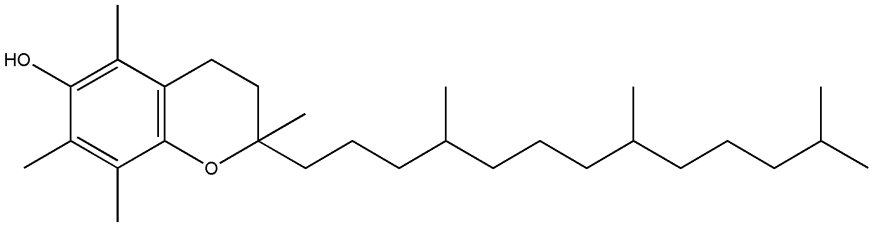

Figure 2. 7. The chemical structure of αTCP.

Moreover, αTCP is metabolized in the liver by enzymatic degradation, and alcohol derivative α-13′-OH is formed. It is then converted to acid derivative α-13′-COOH by α-oxidation. These alcohol and acid derivatives are the bioactive forms of VitE and are known as long-chain metabolites of αTCP (41,42). α-13′-COOH acts as a regulatory molecule in the body and its chemical structure can be seen in Figure 2.8. In the literature, α-13′-COOH molecule shows promising results, especially in inflammatory diseases and cancer (45). Additionally, is also important in regulating some metabolism genes, atherogenic and inflammatory pathways, and also cell death (41).

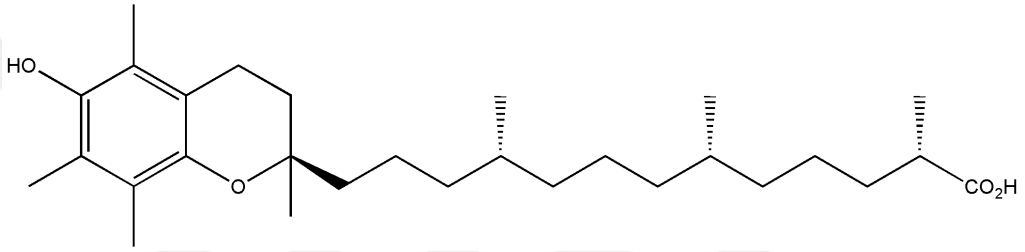

Figure 2. 8. The chemical structure of α-13′-COOH.

In addition to these, GA is one of the derivatives of δ- tocotrienols and it is obtained from Garcinia kola which is conventionally used as medicine for years by people. GA is commonly known for its antimicrobial, antioxidant, and anti-inflammatory features. Its chemical structure can be seen in Figure 2.9. δ-tocotrienols from which GA is derived are found effective both in inflammation and oxidative stress. They could be also useful in the treatment of AS since they can affect macrophage recruitment (46,47).

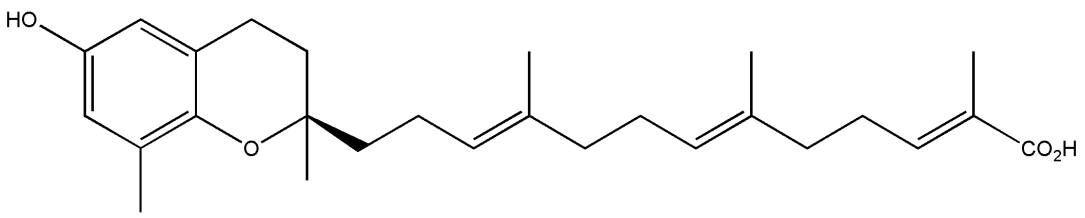

Figure 2. 9. The chemical structure of GA.

2.3. Surface Modification of Nanoparticles

The number of NPs entering the targeted cells has an important role in the efficacy and possible side effects of designed nanomedicine. For this reason, the surface properties such as surface charge, size, and shape of NPs need to be properly adjusted to improve the possible applications and therapeutic effects. Therefore, surface modifications could be done to enhance the interaction between NPs and cells. Biomolecule conjugation and/or polymer coating are under these surface modifications that could be carried out to promote the therapeutic efficiency of NPs (48).

2.3.1. Biomolecule conjugation as a surface modification

Biomolecules which are the fundamental components of both cells and tissues include proteins, carbohydrates, some small molecules, and even nucleic acids. These small biomolecules could be used as targeting agents for desired cells that have overexpressed specific receptors or antigens on their surface. This could lead to improved therapeutic efficiency and diminished side effects since it provides more specific treatment for diseases (49).

For example, stabilin-2 is one of the receptors that have a role in the engulfment of apoptotic cells, and it is highly expressed on the surface of macrophages which are responsible for reducing inflammation and eliminating apoptotic cells. S2P peptide with a sequence of CRTLTVRKC is able to specifically bind to the stabilin-2 receptors. Therefore, the conjugation of S2P peptide as a biomolecule enables the effective delivery of S2P-modified NPs to macrophages in vivo (50,51). As another example, TPP is a positively charged small biomolecule that is able to cross the

mitochondrial matrix space. Therefore, TPP-conjugated NPs promote mitochondria targeting (52).

2.3.2. Polymer coating as a surface modification

Modification of NPs surface could be required to enhance the interaction between cells and NPs as well as improve the therapeutic efficiency. For example, PLGA NPs have several advantageous properties including stability, safety, biocompatibility, and proper drug release. Besides these, they also have some limitations. For example, it degrades into its acidic components through the cleavage of ester bonds. This would lead to local tissue damage. Also, they have a short circulation time through blood since they are hydrophobic in their nature and recognized as a foreign material from the body. Therefore, some modifications are needed to obtain suitable NP formations. Its properties such as circulation time, drug release profile, surface charge, and hydrophilicity/hydrophobicity could be adjusted depending on the need by coating its surface with some polymers (53,54).

For example, poly(ethylene glycol) grafted 1,2-distearoyl-sn-glycero-3-phosphatidylethanolamine (DSPE-PEG) is one of the FDA-approved amphiphilic copolymers composed of hydrophobic 1,2-distearoyl-sn-glycero-3-phosphoethanolamine (DSPE) and hydrophilic poly(ethylene glycol) (PEG) (55). It could be used as a coating polymer in order to provide better drug loading, enhance the stability of NPs, and decrease the rapid clearance of them from the body (26). Moreover, the usage of hydrophilic and biocompatible PEG-based coatings can improve the blood circulation time of nanocarriers since they can diminish the risks of opsonization, unwanted protein adsorption, and rapid clearance from the body (56). Furthermore, desired targeting agents can be linked to the activated terminal groups of PEG. For example, DSPE-PEG can be functionalized with a maleimide group and 1,2-distearoyl-sn-glycero-3-phosphoethanolamine-N-[maleimide(polyethylene glycol)]

(DSPE-PEG-Mal) is formed as in Figure 2.10 and it is widely preferred due to its successful interaction with targeting ligands such as peptides. In this way, the surface of NPs could be functionalized with targeting agents such as S2P peptide during the coating procedure. This enhances the tissue specificity and drug delivery (55).

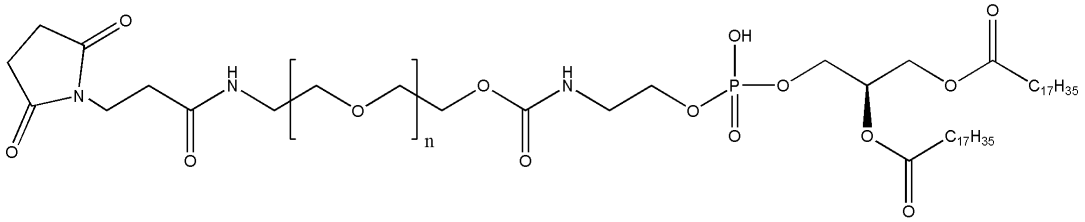

Figure 2. 10. The chemical structure of DSPE-PEG-Mal.

As another example, CS is a positively charged linear cationic polysaccharide and it is made up of glucosamine and N-acetylglucosamine units. It is obtained from the outer skeleton of crustaceans such as shrimp and crabs. It is a biocompatible, non-toxic, and biodegradable natural polymer. These characteristics also make it inexpensive, retainable, and renewable. It is therefore one of the polymers that is frequently utilized, particularly for surface coating and modifications (57). Moreover, CS-coated core-shell NPs can be synthesized in two different ways. In the first one, the already-formed NPs are mixed with a CS solution (57). Since CS is a positively charged polymer, it is also possible to incorporate them into the previously formed NPs made up of negatively charged polymers. In this way, core-shell NPs could be obtained which is suitable for sustained drug release (58). In the second one, CS solution is added while the NPs are being prepared. Depending on the application purpose and also the results of characterization studies, the optimum MW and concentration of CS are chosen for further coating studies (57). Furthermore, coating the surface of NPs with CS could provide some favourable properties. First of all, the stability of NPs during blood circulation is improved since it can prevent the rapid clearance and removal of NPs. Drug release from these NPs can also be controlled more precisely since the burst effect is decreased in the presence of CS coating. Moreover, CS coating could also enhance tissue penetration and mucoadhesiveness while modulating the interactions between cells and NPs thanks to its cationic charge. Additionally, it can provide improved antimicrobial effects, reduced toxicity,

enhanced bioavailability, and drug efficacy. Overall, CS polymer might be employed as a surface modification agent to modify and enhance several properties of nanocarriers, including surface charge and drug release time (53,57).

2.4. Nanomedicine for the Treatment of Inflammation

Inflammation which is related to some pathogenic disorders is known as a defence mechanism of the body against pathogens, infections, and tissue damage (59,60). There are several reasons that induce inflammation, and it has to be resolved properly since the persistence of the inflammation process leads to tissue damage and other correlated diseases (60). To solve problems associated with inflammation, several mechanisms are available, and their proper functioning provides resolution. In case of any deficiency in the resolution process such as excessive inflammatory response, nonresolution occurs. This hardens the development of anti-inflammatory treatments (61).

2.4.1. Atherosclerosis-induced inflammation

One of the leading causes of death among older people is a severe chronic inflammatory disease known as AS (62). Atherosclerotic plaques are formed as a result of the deposition of lipids in the arteries, gradually. Inflammatory cells and factors greatly affect the initiation and progression of AS by causing some pathological and physiological differences (62). In this progression process, immune cells such as monocytes, macrophages, neutrophils, and some lymphocytes play critical roles. Macrophages, for example, have some receptors that can take up the oxidized low-density lipoproteins which leads to the formation of plaques. For this reason, they are important in the resolution of inflammation and immune response in AS. Therefore, these cells are promising targets for therapeutic intervention intended to treat or

prevent AS (63). Because inflammation plays a crucial role in the development of AS, some treatment modalities for this disease are needed to be designed by regulating some anti-inflammatory and immunological pathways (62).

2.4.2. Oxidative stress-induced inflammation

Mitochondria is one of the important organelles found in the body that carry out several functions including biosynthesis, metabolism, apoptosis, and even cell survival. Also, mitochondria which are the main resource of reactive oxygen species (ROS) are also responsible for regulating both oxidative stress and immune responses (64). The excessive production of oxidants such as free radicals and ROS in the body causes the formation of oxidative stress which is one of the leading causes of inflammatory diseases (59,65). ROS production must be kept at an optimum level in order to maintain homeostasis and regulate some physiological and cellular functions such as differentiation, cellular signalling, and apoptosis. Its excessive production causes the formation of oxidative stress and mitochondrial dysfunctions. These situations could damage the cells and some biomolecules and eventually lead to the development of chronic inflammatory disorders (59,66). All in all, ROS-induced modifications and oxidative stress are the major cause of many inflammatory diseases (65). Considering the great impact of oxidative stress on inflammation, effective treatment methodologies are required to be developed against this to prevent severe diseases.

3. MATERIALS AND METHODS

In this section of the thesis, the materials, and methodologies essential for the synthesis of NPs across all three projects are presented in detail, respectively.

3.1. Materials

3.1.1. Materials for project 1: macrophage-targeted NPs

For the synthesis of macrophage-targeted NPs, PLGA (lactide (L):glycolide (G) 50:50, MW 45000 g/mol), N,N-Dimethylformamide (DMF, anhydrous, 99.8%), triethylamine (Et_3N, MW 101.19 g/mol, ≥ 99%), acetic acid (99.8-100.5%), triisopropylsilane (TIS, MW 158.36 g/mol, 98%), and PLGA-Rhodamine B (RhB) (L:G 50:50, Mn 10000-30000) were purchased from Sigma-Aldrich. DSPE-PEG (physical state: chloroform solution, 25 mg/mL, MW 3774.654 g/mol) was obtained from Avanti. DSPE-PEG-Fluorescein isothiocyanate (FITC) (MW 3400 g/mol) and DSPE-PEG-Mal (MW 3400 g/mol) were purchased from Nanocs. All other solvents used were obtained from Merck unless indicated otherwise together with piperidine (99%), N,N'-Diisopropylcarbodiimide (DIC, 99.8%), DMF for peptide synthesis, and trifluoroacetic acid (TFA) for protein sequence analysis. Acetonitrile (ACN, MW 41.05 g/mol, ≥ 99.9%), was purchased from ISOLAB Chemicals. Fmoc-Arg(Pbf)-OH (arginine, MW 648.77 g/mol), Fmoc-Cys(Trt)-OH (cysteine, MW 585.71 g/mol), Fmoc-Lys(Boc)-OH (lysine, MW 468.54 g/mol), Fmoc-Thr(tBu)-OH (threonine, 397.46 g/mol), Fmoc-Val-OH (valine, 339.39 g/mol), and oxyma pure (MW 142.11 g/mol) were used from Novabiochem. Fmoc-L-Leu-OH (leucine, MW 353.4 g/mol) and rink amide proTide (resin, loading: 0.59 mmol/g) was obtained from CEM Corporation. Dialysis membrane (Spectra/Por 6 Trial Kit, MWCO: 2 kD), phosphate buffered saline (PBS) tablets and diethyl ether (MW 74.12 g/mol, ≥ 99.7%) were

obtained from Spectrum Labs, MP Biomedicals, and Merck, respectively. One of the VitE derivatives which is α-13′-COOH (MW 460.7 g/mol) was obtained from Assoc. Francesco Galli, University of Perugia, Italy. GA (MW 426.6 g/mol) which is used as another drug molecule within the scope of this project was supplied from Asst. Prof. Ahmet Erdi Sözen from Marmara University. S2P-SH (MW 1078.57 g/mol) was synthesized using The Liberty Blue™ (CEM) Automated Microwave Peptide Synthesizer by following previously reported method in general (67). S2P peptide-conjugated DSPE-PEG (DSPE-PEG-S2P) was also synthesized considering the previously reported procedure (26).

3.1.2. Materials for project 2: CS-coated NPs

In order to synthesize CS-coated NPs, PLGA (L:G 50:50, MW 100000-125000 g/mol, PURASORB PDLG 5008) was requested from Corbion. Acetone (MW 58.08 g/mol) and Tween80 for synthesis (pH 5-7 (1.07 g/mL, H_2O, 20°C)) were purchased from Merck. CUR (MW 368.38 g/mol), (±)-αTCP (MW 430.71 g/mol, ≥ 96%), acetic acid (99.8-100.5%), PVA (MW 31.000-50.000 g/mol, 98-99% hydrolysed) and CS (low MW, MW 50000-190000 g/mol) were obtained from Sigma-Aldrich. Dialysis membrane (Spectra/Por 6 Trial Kit, MWCO: 2 kD) and PBS tablets were purchased from Spectrum Labs and MP Biomedicals, respectively.

3.1.3. Materials for project 3: mitochondria-targeted NPs

For the synthesis of mitochondria-targeted NPs, PLGA (L:G 50:50, MW 100000-125000 g/mol, PURASORB PDLG 5008) and PLGA (L:G 85:15, MW 59000 kg/mol, PURASORB PDLG 8505A) were again obtained from Corbion. PEG (BioUltra, MW 2000 g/mol), N,N′-Dicyclohexylcarbodiimide (DCC, MW 206.33 g/mol, 99%), 4-(Dimethylamino)pyridine (DMAP, MW 122.17 g/mol, ≥ 98.0% (NT)), QCT (MW

302.24 g/mol, ≥ 95%), acetic acid (99.8-100.5%), Et_3N (MW 101.19 g/mol, ≥ 99%), and (4-Bromobutyl) triphenylphosphonium bromide (TPP-Br, MW 478.20 g/mol, 98%) were purchased from Sigma-Aldrich. Acetone (MW 58.08 g/mol), ethanol (MW 46.07 g/mol, 96%), dichloromethane (DCM, MW 84.93 g/mol), diethyl ether (MW 74.12 g/mol,), and Tween80 for synthesis (pH 5-7 (1.07 g/mL, H_2O, 20°C)) were purchased from Merck. ACN (MW 41.05 g/mol, ≥ 99.9%) was supplied from ISOLAB Chemicals. Dialysis membrane (Spectra/Por 6 Trial Kit, MWCO: 2 kD), syringe filter (0.45µm, polyethersulfone (PES) membrane), and PBS tablets were obtained from Spectrum Labs, TPP, and MP Biomedicals respectively. The procedure previously reported in the literature was adapted and TPP-Tween80 (TT80, 1703.2 g/mol) and PLGA-PEG-TPP (PPT, 62000-63000 g/mol) conjugates were synthesized in the laboratory (68). Moreover, PLGA-PEG (62 kD) was also produced in the laboratory through an esterification reaction between hydroxy group of PEG and the carboxyl group of PLGA by following the general steps of the previously reported method (69).

For cell culture studies of the mitochondria-targeted NPs, sterile dimethyl sulfoxide (DMSO) (MW 78.13 g/mol, 99.9%) was used from Cell Signaling Technology. Moreover, Dulbecco's Modified Eagle Medium F-12 Nutrient Mixture (Ham) (DMEM/F-12, (1:1) (1X)), 0.25% Trypsin-EDTA (1X), Dulbecco's Phosphate Buffered Saline (DPBS (1X)), and also Fetal Bovine Serum (FBS, Qualified, Heat Inactivated) were obtained from Gibco while penicillin-streptomycin (10000 units penicillin and 10 mg streptomycin/mL, 0.1 µm filtered) was used from Sigma-Aldrich. The Cell Counting Kit-8 (CCK-8) was purchased from Glpbio Technology. Moreover, the DCFDA/H2DCFDA-Cellular ROS Assay Kit (ab113851) and MitoProbe JC-1 Assay Kit (M34152) were supplied from Abcam and Invitrogen, respectively.

3.2. Methods

3.2.1. Methods for project 1: macrophage-targeted NPs

3.2.1.1. Non-targeted NP synthesis

In general, NPs were formed and characterized as previously reported in the literature by changing some parameters according to the conducted optimization experiments (26). For the synthesis of non-targeted empty (without drug) NPs **(PLGA NPs)**, PLGA (2.5 mg, 0.05 μmol) was dissolved in 500 μL of acetone. DSPE-PEG (2 mg, 0.53 μmol, 80 μL from its stock solution which is 25 mg/mL in chloroform) was dissolved in 10 mL of double-distilled water (ddH_2O) and PLGA solution was added dropwise onto this solution. This mixture was stirred for 1h at 1100 rpm. Then, the prepared NPs were centrifuged three times against ddH_2O for 20 min at 4000 rpm to remove the impurities. The purified PLGA NPs were finally resuspended in 1 mL of ddH_2O and stored at -20°C.

The same procedure was followed for the synthesis of non-targeted drug-loaded NPs. As a difference, α-13′-COOH molecules (0.25 mg, 0.54 μmol) and PLGA (2.5 mg, 0.05 μmol) and GA molecules (0.25 mg, 0.59 μmol) and PLGA (2.5 mg, 0.05 μmol) were dissolved together in 500 μL of acetone for the preparation of α-13′-COOH loaded NPs **(α-13′-COOH PLGA NPs)** and GA loaded NPs **(GA-PLGA NPs),** respectively. After following the other steps, the prepared drug-loaded NPs were centrifuged three times against ddH_2O for 20 min at 4000 rpm to remove the unbound drug molecules and impurities. The purified α-13′-COOH PLGA NPs and GA-PLGA NPs were resuspended in 1 mL of ddH_2O. Different from the α-13′-COOH PLGA NPs, GA-PLGA NPs were centrifuged for additional 2 min at 4000 rpm to remove the aggregates and finally, they were stored at -20°C.

Moreover**, non-coated NPs** were also synthesized in order to understand whether the DSPE-PEG coating was achieved successfully or not. For this, PLGA (2.5 mg, 0.05 μmol) was dissolved in 500 μL of acetone and this solution was added dropwise onto 10 mL of ddH_2O while continuous stirring at 1100 rpm. This reaction lasted for 1h. At the end, the prepared NPs were centrifuged three times against ddH_2O for 20 min at 4000 rpm and obtained non-coated NPs were resuspended in 1 mL of ddH_2O and stored at -20°C.

3.2.1.2. S2P peptide synthesis

The stabilin-2 receptor-specific S2P peptide (CRTLTVRKC) was synthesized using The Liberty Blue™ (CEM) Automated Microwave Peptide Synthesizer. For this, the previously reported method was followed in general (67). The synthesis scale was adjusted to 0.1 mmol. 0.143 g resin was weighted and left to swell for at least 30 min before starting the peptide synthesis. For the peptide synthesis, 1.56 g arginine, 0.71 g cysteine, 0.22 g leucine, 0.29 g lysine, 0.48 g threonine, and 0.21 g valine were weighed and dissolved in 12 mL, 6 mL, 3 mL, 3 mL, 6 mL, and 3mL DMF, respectively. DIC and oxyma were used as an activator and activator base, respectively while piperidine was used for deprotection. DIC solution was prepared by mixing 1.1 mL DIC with 12.9 mL DMF while piperidine solution was obtained by adding 40 mL DMF onto 10 mL piperidine. Similarly, 0.995 g oxyma was dissolved in 7 mL of DMF. After placing them, the peptide synthesis was initiated. At the end of the synthesis, the peptide was cleaved from the resin with RazorTM Peptide Cleavage System (CEM) at 37°C for 30 min. The cleavage cocktail consists of 4.75 mL of TFA, 125 μL of TIS, and 125 μL of ddH_2O. Then, the obtained S2P peptide was precipitated using cold diethyl ether and centrifuged at 6000 rpm for 3 min against cold diethyl ether three times. After centrifugation, the diethyl ether was carefully removed. The pellet was dried in the desiccator and then purified using a preparative High-Performance Liquid Chromatography (prep-HPLC, The CombiFlash® NextGen 300+, EZ Prep) device to remove impurities that may be present in the reaction mixture. To achieve this, S2P

peptide was dissolved in the mixture of ddH_2O and ACN and injected into hydrophobic C18 column (RediSep® Silver C18 Reversed Phase columns, 4.3 g). The flow rate was set to 18 mL/min while run length was adjusted to 15 min. The mobile phase consisted of A and B which were ddH_2O with 0.025% TFA and ACN with 0.025% TFA, respectively. S2P peptide was first run at 100% ddH_2O for 2 min, increased linearly over 10 min from 0% ACN to 100% ACN and then run at 100% ACN for last 3 min. Relevant pure peaks coming from S2P were collected and the excess ACN was evaporated using rotary evaporator (BUCHI Rotavapor® R-100). The chemical characterization of the synthesized S2P peptide was completed using an LC/MS-MS device (6420 Triple Quad LC/MS, Agilent Technologies). At the end, the peptide was lyophilized (HyperCOOL 8080) and stored at +4°C.

3.2.1.3. DSPE-PEG-S2P conjugation synthesis

The structure of DSPE-PEG-S2P can be seen in Figure 3.1, and it was synthesized as previously reported (26). For this, 2.6 mL of anhydrous DMF and 0.4 mL of DMSO were added to the S2P peptide (19 mg, 0.018 mmol, 1.2 eq.). At the same time, DSPE-PEG-Mal (50 mg, 0.015 mmol, 1 eq.) was dissolved in 2 mL of DMF. Then, the DSPE-PEG-Mal solution was added to the peptide solution. Finally, 10 µL of Et_3N was injected into the mixture while stirring. This reaction continued for 2 days at 1500 rpm at room temperature (RT). The final product was purified by removing impurities using a dialysis membrane (MW cut-off: 2kD). The obtained DSPE-PEG-S2P conjugate was lyophilized and stored at +4°C. This conjugate was analysed using proton nuclear magnetic resonance (^1H NMR) to determine the presence of all components within the conjugate.

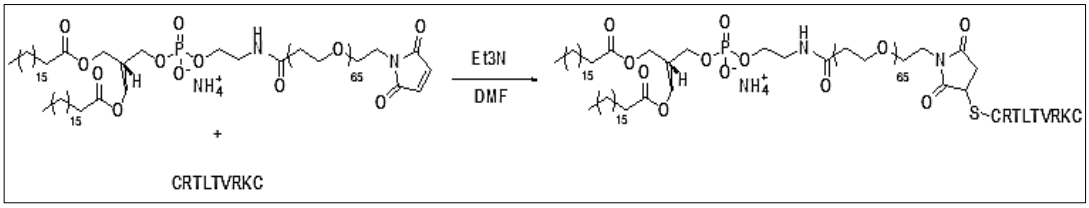

Figure 3. 1. Schematic representation of the synthesis of DSPE-PEG-S2P conjugation.

3.2.1.4. Targeted NP synthesis

As a targeting agent, S2P peptide was added to the surface of NPs. For this purpose, free thiol groups from cysteine amino acids in the structure of the S2P peptide were used. PLGA (2.5 mg, 0.05 μmol) was dissolved in 500 μL of acetone. DSPE-PEG (1.8 mg, 0.48 μmol, 72 μL from its stock solution which is 25 mg/mL in chloroform) and DSPE-PEG-S2P (0.2 mg, 0.044 μmol) were dissolved in 10 mL of ddH_2O and PLGA solution was added dropwise onto this solution. This mixture was stirred for 1h at 1100 rpm. Then, the prepared NPs were centrifuged three times against ddH_2O for 20 min at 4000 rpm to remove the impurities. The purified targeted empty NPs **(S2P-PLGA NPs)** were resuspended in 1 mL of ddH_2O and centrifuged for another 2 min at 4000 rpm to remove the aggregates. Finally, the NPs were stored at -20°C.

The same procedure was followed for the synthesis of targeted α-13′-COOH loaded NPs (**S2P-α-13′-COOH PLGA NPs**) and targeted GA loaded NPs **(S2P-GA-PLGA NPs)** with a slight variation. In this part, α-13′-COOH molecules (0.25 mg, 0.54 μmol) and PLGA (2.5 mg, 0.05 μmol) and GA molecules (0.25 mg, 0.59 μmol) and PLGA (2.5 mg, 0.05 μmol) were together dissolved in 500 μL of acetone for the synthesis of S2P-α-13′-COOH PLGA NPs and S2P-GA-PLGA NPs, respectively. The remaining procedure was followed, and the prepared NPs were centrifuged three times against ddH_2O for 20 min at 4000 rpm. This process aimed to eliminate any unbound drug molecules and impurities. The NPs were finally resuspended in 1 mL of ddH_2O,

and aggregates were removed via centrifugation for 2 min at 4000 rpm. At the end, the obtained NPs were stored at -20°C.

3.2.1.5. FITC-labelled NP synthesis

To enable the visualization of both the non-targeted and targeted NPs *in vitro*, FITC was conjugated onto the surface of NPs as an imaging agent. The general procedure for NP synthesis was followed with some modifications. For the synthesis of FITC-labelled non-targeted empty NPs **(FITC-PLGA NPs)**, PLGA (2.5 mg, 0.05 μmol) was dissolved in 500 μL of acetone. DSPE-PEG (1.4 mg, 0.37 μmol, 56 μL from its stock solution which is 25 mg/mL in chloroform) and DSPE-PEG-FITC (0.6 mg, 0.18 μmol) were dissolved in 10 mL of ddH_2O and PLGA solution was added dropwise onto this solution. Moreover, for the synthesis of FITC-labelled targeted empty NPs **(FITC-S2P-PLGA NPs)**, PLGA (2.5 mg, 0.05 μmol) was again dissolved in 500 μL of acetone. DSPE-PEG (1.2 mg, 0.32 μmol, 48 μL from its stock solution which is 25 mg/mL in chloroform), DSPE-PEG-S2P (0.2 mg, 0.044 μmol) and DSPE-PEG-FITC (0.6 mg, 0.18 μmol) were dissolved in 10 mL of ddH_2O and PLGA solution was added drop by drop onto this solution. Then, the prepared NPs were centrifuged three times against ddH_2O for 20 min at 4000 rpm to remove the unbound FITC molecules and impurities. The purified NPs were resuspended in 1 mL of ddH_2O, and aggregates were removed by centrifugation for 2 min at 4000 rpm. Finally, NPs were stored at -20°C.

3.2.1.6. RhB-conjugated FITC-labelled NP synthesis

Since the detachment of fluorescently labelled lipid-PEG chains and dispersion of NPs could lead false-positive signals, RhB and FITC was used to obtain dual-labelled NPs. In this way, red fluorescence was obtained in the core due to the RhB-conjugated

PLGA polymer while green fluorescence was achieved in the exterior coating layer due to the presence of DSPE-PEG-FITC molecule.

For the synthesis of RhB-conjugated FITC-labelled non-targeted empty NPs **(RhB-FITC-PLGA NPs),** PLGA (2.5 mg, 0.05 μmol) and PLGA-RhB (0.25 mg) were dissolved in 500 μL of acetone. Simultaneously, DSPE-PEG (1.4 mg, 0.37 μmol, 56 μL from its stock solution which is 25 mg/mL in chloroform) and DSPE-PEG-FITC (0.6 mg, 0.18 μmol) were dissolved in 10 mL of ddH_2O. Then, the solution in acetone was added drop by drop to the aqueous solution at 1100 rpm while stirring. The reaction continued for 1h and then prepared NPs were centrifuged for three times against cold ddH_2O for 20 min at 4000 rpm to remove the unbound dye molecules and polymers. The purified NPs were resuspended in 1 mL of ddH_2O and finally centrifuged for 2 min at 4000 rpm to optimize the size of NPs by removing aggregates. Eventually, NPs were stored at -20°C.

For the synthesis of RhB-conjugated FITC-labelled non-targeted and targeted drug-loaded NPs, α-13′-COOH was used as a drug molecule and the experiment was conducted accordingly. Considering this, for the synthesis of RhB-conjugated FITC-labelled non-targeted α-13′-COOH-loaded NPs **(RhB-FITC-α-13′-COOH PLGA NPs),** PLGA (2.5 mg, 0.05 μmol), α-13′-COOH molecules (0.25 mg, 0.54 μmol), and PLGA-RhB (0.25 mg) were dissolved in 500 μL of acetone and remaining procedure was followed. On the other hand, to synthesize RhB-conjugated FITC-labelled targeted empty NPs **(RhB-FITC-S2P-PLGA NPs),** PLGA (2.5 mg, 0.05 μmol) and PLGA-RhB (0.25 mg) were dissolved in 500 μL of acetone. Simultaneously, DSPE-PEG (1.2 mg, 0.32 μmol, 48 μL from its stock solution which is 25 mg/mL in chloroform), DSPE-PEG-S2P (0.2 mg, 0.044 μmol), and DSPE-PEG-FITC (0.6 mg, 0.18 μmol) were dissolved in 10 mL of ddH_2O. Then, the solution in acetone was added drop by drop to the aqueous solution at 1100 rpm. Similarly, for the synthesis of RhB-conjugated FITC-labelled targeted α-13′-COOH-loaded NPs **(RhB-FITC-S2P-α-13′-COOH PLGA NPs),** PLGA (2.5 mg, 0.05 μmol), α-13′-COOH molecules

(0.25 mg, 0.54 μmol), and PLGA-RhB (0.25 mg) were dissolved in 500 μL of acetone and remaining procedure was followed as described.

3.2.1.7. Characterization of NPs

Dynamic Light Scattering (DLS) Analysis: All of the synthesized NPs were resuspended in ddH_2O, and their hydrodynamic diameters and polydispersity indexes (PDI) were measured using DLS (Wyatt Technologies Dynapro Nanostar instrument) in ddH_2O at RT. To perform the analysis, 100μL of NP solution was transferred into a DLS cuvette. The cuvette was then subjected to a series of 10 process runs, with each run having a 5 second equilibrium time. This was repeated three times to confirm the obtained data.

Zeta Potential Analysis: For the evaluation of surface charge, NPs were diluted 10% by volume using 0.001M sodium chloride (NaCl) solution. These solutions were placed in zeta potential cuvettes and measurements were completed to determine the surface charges of synthesized NPs via Malvern Zetasizer Nano ZS at RT with 10 runs. Three repetitions were done to take the average of the obtained measurements.

Morphological Analysis: The dimensions of the obtained NPs, the presence of coating, and whether they formed aggregation or not were determined using Transmission Electron Microscopy (TEM) (Thermo Fischer Scientific, Talos L120C). To actualize this, lacey carbon film supported copper TEM grids were used. NPs that were prepared in ddH_2O were dropped on these grids, and they were waited to dry before conducting the analysis under high vacuum. Moreover, morphologies of these NPs were analysed using Scanning Electron Microscopy (SEM) (Thermo Fischer Scientific, Quattro ESEM). In this analysis, NP solutions were dropped on metal stubs

having carbon tape, and they were waited to dry. Subsequently, they were coated with gold under vacuum and the analysis was conducted.

Fourier Transform Infrared Spectroscopy (FT-IR) Analysis: Characteristic functional groups of the α-13′-COOH drug molecule, PLGA polymer, DSPE-PEG, non-coated NPs, PLGA NPs, and α-13′-COOH PLGA NPs were recorded using the IR spectra coming from FT-IR spectroscopy (Thermo Scientific NICOLET iS10 instrument). This was conducted to confirm the presence of the polymer, DSPE-PEG coating, and also drug molecule in the structure of obtained NPs. Moreover, the formation of DSPE-PEG-S2P conjugate was proven by comparing its functional groups that were coming from both DSPE-PEG-Mal and S2P peptide. Each sample spectrum was recorded from 400 cm^{-1} to 4000 cm^{-1} with 32 scans at RT.

Stability Analysis: PLGA NPs, α-13′-COOH PLGA NPs, and GA-PLGA NPs were incubated in 1M pH 7.4 PBS at different temperatures (25˚C and 37˚C). After certain times of incubation (0h, 0.25h, 0.5h, 0.75h, 1h, 2h, 3h, 4h, 5h, 6h, 7h, 8h, 24h, 48h, 72h, 96h, 120h, 168h, and longer), the hydrodynamic diameter of these NPs was measured using DLS with three repetitions for each time point. To what extent the NPs could maintain their initial stable structure under different environmental conditions was investigated.

NanoDrop Analysis: For determining the net protein concentration in S2P-PLGA NPs and S2P-α-13′-COOH PLGA NPs, nanodrop device (Thermo Scientific™ NanoDrop™ One Microvolume UV-Vis Spectrophotometer) was used. The absorbance of the peptide at 214 nm was measured for both targeted and non-targeted empty and drug-loaded NPs. Non-targeted ones were used as a reference. The net protein concentration in the targeted NPs was calculated by subtracting the measured concentration values of the non-targeted NPs from the measured concentration values of targeted NPs. This was used to prove the presence of targeting peptide on NPs.

Total Drug Amount Determination: The amount of drug molecules that were used during the synthesis of α-13′-COOH-loaded NPs and GA-loaded NPs were indicated in the procedure. By using the Liquid Chromatography/Mass Spectrometry-Mass Spectrometry (LC/MS-MS) (AB Sciex 4000 QTRAP) device, how much of the α-13′-COOH and GA molecules added to the polymer solution during the preparation phase were encapsulated into the final NPs was calculated in terms of μg/mL. This was also expressed as a percentage of drug encapsulation efficiency (EE) by using the given equation (eq.1). The total drug concentration found inside of NPs was determined by bursting them with acetone (1:1 by volume).

$$Drug\ EE\% = \left(\frac{encapsulated\ drug\ amount}{initially\ added\ drug\ amount}\right) \times 100 \quad \text{(eq.1)}$$

Firstly, a specific multiple reaction monitoring (MRM) method was developed for the α-13'-COOH drug in an LC/MS-MS device, using a C18 column as the stationary phase. A mixture of ACN and deionized water (50%:50% (v/v)) was used as the mobile phase at a flow rate of 0.5 mL/min. A sample of 5 μL was taken from the pure drug solution, and a scanning dependent on ionization in the range of 50-1500 Da was performed in the MS2Scan mode. For the α-13'-COOH drug with a theoretical MW of 460.69 g/mol, a value of 459.2 m/z was observed as the +1 charged state in the scanning method as can be seen in Figure 3.2.

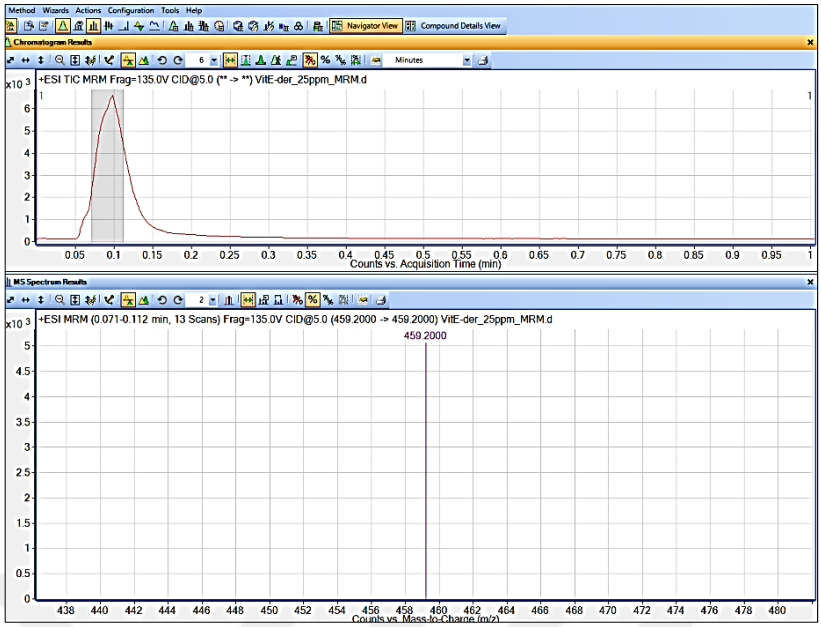

Figure 3. 2. The results of the MRM method prepared for the α-13'-COOH.

Afterward, using this method, the analysis of drug molecules prepared at different concentrations (0.1953, 0.7813, 3.1250, 6.2500, and 12.0 ppb) was conducted. The software of the device was used to draw a specific calibration curve for the drug molecule as in Figure 3.3. This curve was then used to analyse the total drug concentration in the NPs as well as drug release rate from NPs.

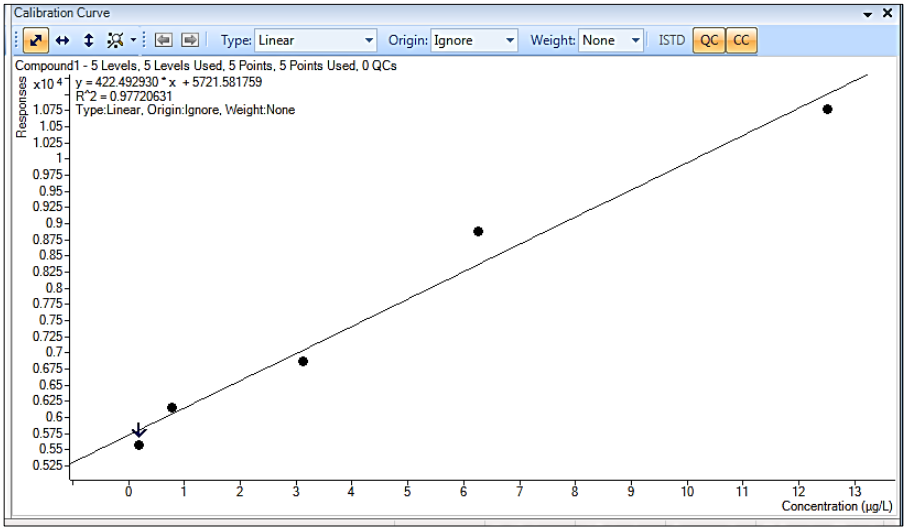

Figure 3. 3. Calibration curve prepared for α-13′-COOH.

In order to determine the amount of drug in GA-PLGA NPs and S2P-GA-PLGA NPs, the GA molecules were prepared at various concentrations for analysis. Using the software of the LC/MS-MS device, a specific calibration curve for the drug molecule was constructed, as illustrated in Figure 3.4. This calibration curve serves as a reference for determining the total GA concentration found in the NPs and the released drug amount from these NPs at certain time intervals.

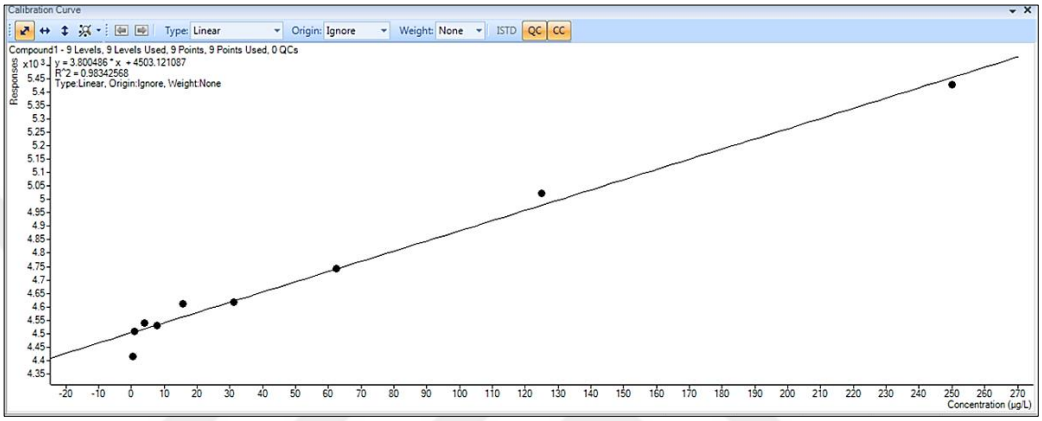

Figure 3. 4. Calibration curve prepared for GA.

Measurement of Drug Release Profiles from NPs: To assess the release rate of α-13′-COOH from α-13′-COOH PLGA NPs and GA from the GA-PLGA NPs, two different release media which were 1M pH 7.4 PBS and pH 5.5 acetate buffer solution were used to mimic the healthy and inflammatory conditions of the human body fluid, respectively. Samples were put in the dialysis bag (MW cut-off: 2kD) and placed in an orbital shaker (Ohaus Incubating Light Duty Orbital Shaker) at 37°C and 200 rpm. In drug release studies, 'sink' conditions were achieved by using 40 mL of receptor solution in the external phase. Thus, the effect of increasing volume on the drug release profile when NP solution was given to the blood was mimicked. Samples from the release medium were collected at specified time intervals (0h, 0.25h, 0.5h, 0.75h, 1h, 2h, 3h, 4h, 5h, 6h, 7h, 24h, 48h, 72h, 96h, 144h, 192h, 288h, 366h, 384h, 456h, 504h, and 627h). The amount of free drug in these samples were quantitatively analysed by LC/MS-MS device using the calibration curve seen in Figure 3.3 and Figure 3.4. This analysis allowed the measurement and determination of the amount of α-13′-COOH

and GA released from the NPs over the specified time intervals in two different release media.

Fluorescence Spectrophotometer Analysis: FITC is a fluorescent dye with maximum excitation wavelength at 494 nm and maximum emission wavelength at 520 nm. For the quantification of this dye, a calibration curve was prepared using commercially bought DSPE-PEG-FITC polymer containing free FITC dye as in Figure 3.5. With the help of this curve, the concentration of FITC molecules on the surface of FITC-PLGA NPs, FITC-S2P-PLGA NPs, RhB-FITC-PLGA NPs, RhB-FITC-α-13′-COOH PLGA NPs, RhB-FITC-S2P-PLGA NPs, and RhB-FITC-S2P-α-13′-COOH PLGA NPs was determined based on absorbance using a fluorescent spectrophotometry (VarioSCAN II instrument).

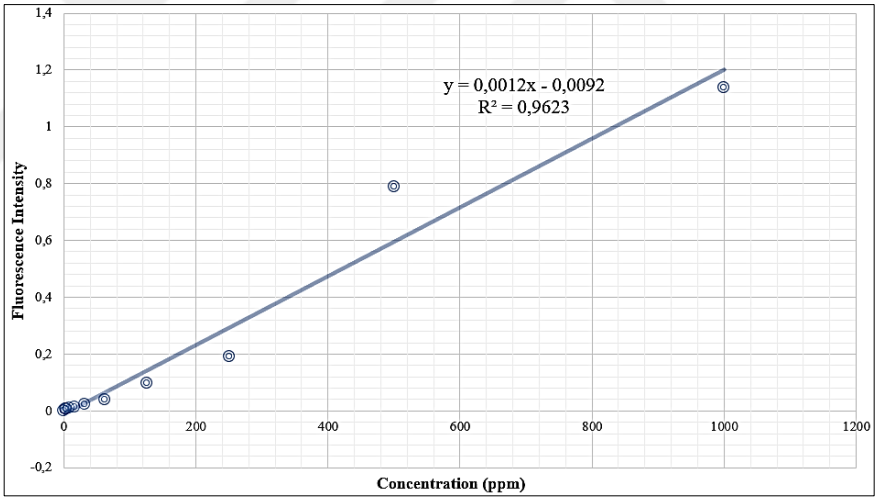

Figure 3. 5. Calibration curve prepared for FITC.

Moreover, RhB is another dye that has maximum excitation wavelength at 553 nm and maximum emission wavelength at 627 nm. In order to determine the amount of this dye found in NPs, a calibration curve was prepared at 553 nm using commercially bought RhB-conjugated PLGA polymer as it can be seen in Figure 3.6. With the help of this curve, the concentration of RhB molecules found in RhB-FITC-PLGA NPs, RhB-FITC-α-13′-COOH PLGA NPs, RhB-FITC-S2P-PLGA NPs, and

RhB-FITC-S2P-α-13′-COOH PLGA NPs was determined based on their absorbance at 553 nm using a fluorescent spectrophotometry.

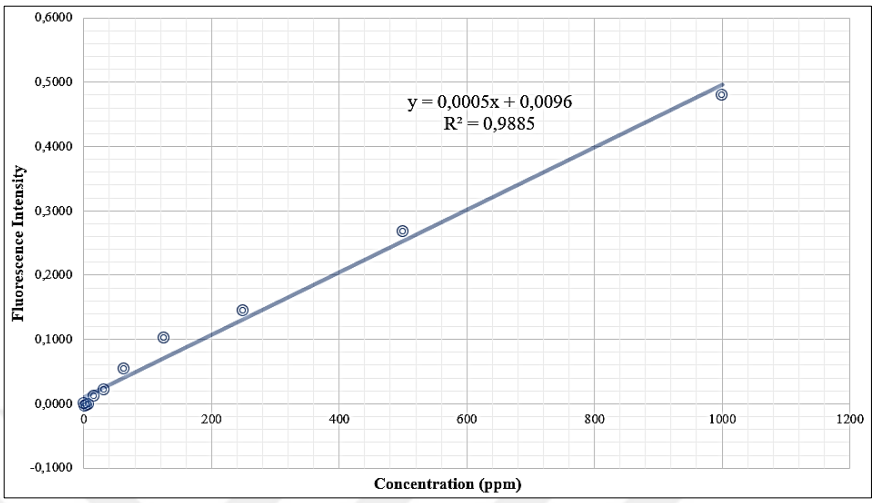

Figure 3. 6. Calibration curve prepared for RhB.

3.2.1.8. Statistics

Statistical analyses for this project were conducted using GraphPad Prism 10 and presented through two-way analysis of variance (ANOVA). The results were shown as mean ± standard deviation. A p-value less than 0.05 was considered statistically significant.

3.2.2. Methods for project 2: CS-coated NPs

3.2.2.1. Preparation of non-coated NPs

First of all, non-coated empty PLGA NPs **(non-coated PLGA NPs)** were synthesized by following the general principles given in the literature with some modifications (70,71). For this, PLGA (25 mg, 0.20-0.25 μmol) was dissolved in 1 mL

of acetone. 10 µL of Tween80 was added to the 4 mL of 1.5% (w/v) PVA solution prepared in ddH_2O at 100 rpm while stirring. It was dispersed at 300 rpm. Then, the prepared PLGA solution was added dropwise onto the PVA solution at 1500 rpm using an insulin syringe. This reaction was continued for 1h at 1500 rpm. Then, the prepared NPs were centrifuged three times against cold ddH_2O for 10 min at 10000 rpm to remove the impurities. The purified non-coated PLGA NPs were finally resuspended in 10 mL of ddH_2O, and the remaining aggregates were removed by centrifuging at 6000 rpm until achieving the desired NP size. These NPs were stored at -20°C.

Almost the same procedure was followed for the synthesis of non-coated drug-loaded NPs. Both CUR loaded non-coated NPs (**CUR-PLGA NPs**) and αTCP loaded non-coated NPs (**αTCP-PLGA NPs**) were prepared. The only difference from non-coated PLGA NPs was the dissolution of drug molecules and PLGA together in the acetone. CUR (2.5 mg, 6.79 µmol) and PLGA (25 mg, 0.20-0.25 µmol) were dissolved in 1 mL of acetone for the synthesis of CUR-PLGA NPs. Similarly, αTCP (2.5 mg, 5.8 µmol) and PLGA (25 mg, 0.20-0.25 µmol) were dissolved in 1 mL of acetone for the synthesis of αTCP-PLGA NPs. Then, the prepared NPs were centrifuged three times against cold ddH_2O for 10 min at 10000 rpm to remove the unbound drug molecules and impurities. After resuspending CUR-PLGA NPs and αTCP-PLGA NPs in 10 mL of ddH_2O, the size of these NPs was optimized by removing aggregates using a centrifuge at 6000 rpm. Finally, they were also stored at -20°C.

3.2.2.2. Preparation of CS-coated NPs

To synthesize CS-coated NPs, the process was carried out in accordance with the general principles outlined in the literature, with certain adjustments made (70,71). At the beginning, non-coated empty and drug-loaded NPs were added dropwise onto a 0.2% (w/v) low MW CS solution with a 1:1 (v/v) ratio while stirring continuously at 1100 rpm. This reaction continued overnight. After that, CS-coated empty NPs (**CS-**

PLGA NPs), CS-coated CUR loaded NPs (**CS-CUR-PLGA NPs**), and CS-coated αTCP loaded NPs (**CS-αTCP-PLGA NPs**) were centrifuged three times against cold ddH_2O for 50 min at 16000 rpm at 2°C to remove the impurities. The obtained CS-coated NPs were then resuspended in 10 mL of ddH_2O, and the remaining aggregates were removed by centrifuging at 10000 rpm until achieving the desired NP size. These NPs were also stored at -20°C.

3.2.2.3. Characterization of NPs

For the characterization of NPs, DLS, zeta potential, and morphological SEM analysis were conducted as they were explained in Section 3.2.1.7. Moreover, some other additional characterization tests were carried out.

Stability Analysis: All of the synthesized non-coated and CS-coated empty and drug-loaded NPs were incubated in 1M pH 7.4 PBS at different temperatures (25˚C and 37˚C). After certain times of incubation (0h, 0.25h, 0.5h, 0.75h, 1h, 2h, 3h, 4h,5h, 6h, 7h, 24h, 48h, 72h, 96h, 193h, 267h, and longer), the hydrodynamic diameter of these NPs was measured via DLS with three repetitions for each time point. This was used to understand how long they maintained their initial stable structure under different environmental conditions.

Total Drug Amount Determination: The amount of CUR and αTCP molecules that were used during the synthesis of drug-loaded NPs was indicated in Section 3.2.2.1. LC/MS-MS was used to measure the amount of CUR and αTCP that were encapsulated inside the NPs in terms of μg/mL and also EE was calculated as a percentage using eq.1. The total drug concentration in the NPs was determined by bursting the NPs using acetone in a 1:1 volume ratio. The CUR and αTCP were prepared at different concentrations and by using LC/MS-MS device, dedicated calibration curves were

created for these drug molecules, as shown in Figure 3.7 and Figure 3.8. These graphs were used as a benchmark for determining the overall drug concentration found in NPs.

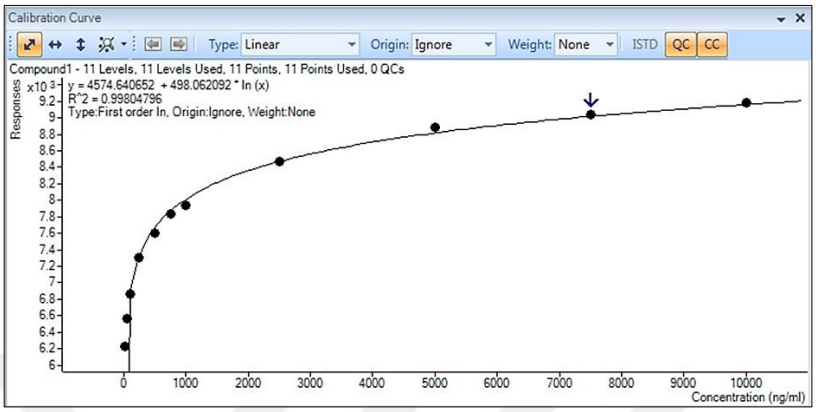

Figure 3. 7. Calibration curve prepared for CUR.

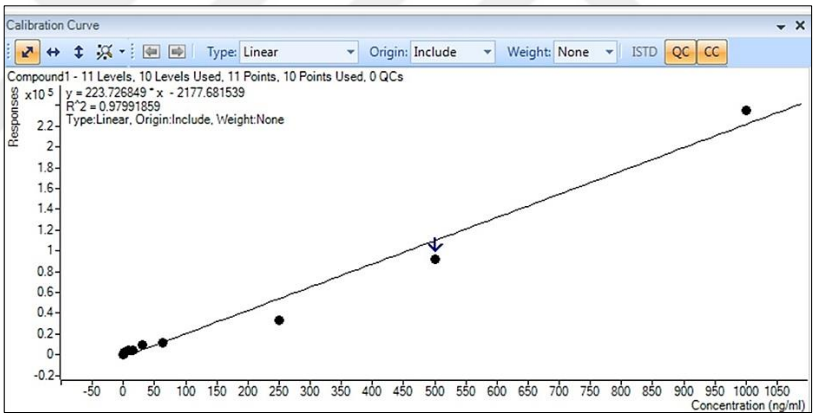

Figure 3. 8. Calibration curve prepared for αTCP.

Measurement of Drug Release Profiles from NPs: The release rate of CUR from the CUR-PLGA NPs and CS-CUR-PLGA NPs as well as the release rate of αTCP from αTCP-PLGA NPs and CS-αTCP-PLGA NPs were investigated using two different release media. One was a 1M pH 7.4 PBS, which simulates the conditions of a healthy human body fluid while the other was a pH 5.5 acetate buffer solution, which mimics the inflammatory conditions of the human body fluid. The remaining drug release experiments were carried out following the procedures described in Section 3.2.1.7. At specified time intervals (0h, 0.25h, 0.5h, 0.75h, 1h, 2h, 3h, 4h, 5h, 6h, 7h,

24h, 48h, 72h, 96h, 168h, and 197h), samples were collected from the release medium. These samples were then analysed using an LC/MS-MS device and previously prepared calibration curve seen in Figure 3.7 and Figure 3.8. This analysis allowed the measurement of the amount of drug molecules released from the NPs over the specified time intervals in two different release media.

3.2.2.4. Statistics

Statistical analyses were performed using GraphPad Prism 10, employing two-way ANOVA. The results were shown as mean ± standard deviation, with statistical significance defined as a p-value below 0.05.

3.2.3. Methods for project 3: mitochondria-targeted NPs

3.2.3.1. Non-targeted NP synthesis

Nanoprecipitation method was followed in general as previously reported in the literature to synthesize NPs (17). First of all, for the synthesis of non-targeted empty PLGA NPs **(non-targeted PLGA NPs)**, PLGA (L:G 50:50, 25 mg, 0.20-0.25 μmol) was dissolved in 1 mL of acetone. Simultaneously, 10 μL of Tween80 was added to the 10 mL of slightly heated ddH_2O while stirring at 100 rpm. The solution was left to disperse at 300 rpm for 5 min, after which it was homogenized for a total of 1 min, with intervals of 2 second every 10 second. Subsequently, PLGA solution was added dropwise onto this solution at 1100 rpm using an insulin syringe. The reaction proceeded for 1h, followed by an additional 1 min homogenization of the NP solution. Then, the synthesized NPs were centrifuged three times against cold ddH_2O for 10 min at 15000 rpm for purification. The non-targeted PLGA NPs were eventually

resuspended in 10 mL of ddH_2O, and homogenization was applied for 2 min. Finally, obtained NP solution was filtered through a 0.45 µm PES syringe filter and stored at -20°C.

In order to synthesize non-targeted QCT-loaded PLGA NPs (**QCT-PLGA NPs**), a similar procedure was employed with a slight modification. The key distinction was that QCT (2.5 mg, 8.27 µmol) and PLGA (L:G 50:50, 25 mg, 0.20-0.25 µmol) were dissolved together in 1 mL of acetone. The subsequent steps remained unchanged and were carried out accordingly.

3.2.3.2. TT80 conjugate synthesis

To synthesize TT80 conjugate, previously reported method was followed in general (68). Initially, Tween80 (50 mg, 0.038 mmol) was weighted in round bottom flask and nitrogen gas was applied. Meanwhile, TPP-Br (73 mg, 0.153 mmol) was prepared in glass vial and nitrogen gas was passed through. 1 mL and 9 mL of anhydrous DCM was added on TPP-Br and Tween80, respectively. TPP-Br was dissolved using sonicator. After that, Et_3N (21.3 µL, 0.153 mmol) was added directly into the Tween80 solution while stirring on magnetic stirrer at 800 rpm. Subsequently, TPP-Br solution was also added in this solution. This reaction continued overnight. Then, the excess amount of DCM was evaporated using rotary evaporator and TT80 conjugate was precipitated using cold diethyl ether. This was waited at -20°C overnight. The next day, suction filtration was applied using gooch funnel (por.4) with sintered glass disc. After removing the diethyl ether, DCM was passed through the samples that remained on the filter. In this way, TT80 conjugate was collected, and DCM was again evaporated using rotary evaporator. At the end, TT80 conjugate was purified using a prep-HPLC device. To accomplish this, the first step involved dissolving TT80 in DMSO and injecting it into a C18 column. The flow rate was set at 18 mL/min, and the run length was adjusted to 15 min. The mobile phase was

composed of two components, A and B. Mobile phase A consisted of ddH_2O with 0.025% TFA, while mobile phase B consisted of ACN with 0.025% TFA. The TT80 conjugate was initially run with 100% ddH_2O for 2 min, followed by a linear increase over 10 min from 0% ACN to 100% ACN, and finally run at 100% ACN for the last 3 min. The relevant pure peaks obtained from TT80 were collected, and any excess ACN was removed using a rotary evaporator. The chemical characterization of the synthesized TT80 conjugate was carried out via LC/MS-MS device. Ultimately, the TT80 conjugate which was used as one of the targeting agents in this project was lyophilized and stored at +4°C. Also, the chemical structure of this conjugate was investigated with the help of ^1H NMR to confirm the presence of both TPP and Tween80 within the conjugate.

3.2.3.3. PPT synthesis

To compare the therapeutic effectiveness of TT80-functionalized NPs with PPT-functionalized NPs, PPT conjugate was utilized as an additional targeting agent. For this purpose, first of all, PLGA-PEG conjugate was synthesized by adapting the previously reported method (69). In a round-bottom flask, PLGA with a carboxylic acid group at the end (L:G 85:15, 1 g, 0.0166 mmol) and DCC coupling agent (17.4 mg, 0.042 mmol) were weighed and placed under nitrogen gas. Subsequently, 2 mL of anhydrous DCM was added to the flask. Additionally, PEG with a hydroxyl group at the end (66.6 mg, 0.033 mmol) and DMAP (3 mg, 0.012 mmol) were weighed in a glass vial and exposed to nitrogen gas. Following that, 3 mL of anhydrous DCM was added to the vial. The solution containing PEG and DMAP was then directly introduced into the solution containing PLGA and DCC. This reaction proceeded for 2 days at 1000 rpm. Subsequently, the obtained PLGA-PEG conjugate was precipitated by adding it into cold diethyl ether and left at -20°C overnight. The following day, suction filtration was performed using a gooch funnel (por.4) equipped with a sintered glass disc to eliminate diethyl ether. DCM was passed through the retained samples on the filter, allowing for the collection of the PLGA-PEG conjugate.

The excess DCM was then completely evaporated using a rotary evaporator. The obtained dry PLGA-PEG conjugate was stored at +4°C.

To synthesize the PPT conjugate, PLGA-PEG (100 mg, 1.613 μmol) and TPP-Br (6.17 mg, 12.9 μmol) were weighed in a round-bottom flask and a glass vial, respectively. Nitrogen gas was then applied to both substances. 1 mL and 9 mL of anhydrous DCM were added to TPP-Br and PLGA-PEG, respectively and the TPP-Br solution was dissolved using a sonicator. After that, Et_3N (1.8 μL, 12.9 μmol) was directly added into the PLGA-PEG solution while stirring on a magnetic stirrer at 800 rpm. Subsequently, the TPP-Br solution was also added to this mixture. This reaction continued for 2 days. Following the reaction, the obtained PPT conjugate was precipitated using cold diethyl ether and left at -20°C overnight. The next day, suction filtration was carried out using a gooch funnel (por.4) equipped with a sintered glass disc. After removing the diethyl ether, DCM was passed through the remaining samples on the filter, collecting the PPT conjugate in DCM. To achieve phase separation and purification, extraction was performed as a final step. For this purpose, 5% sodium bicarbonate ($NaHCO_3$), 10% sodium carbonate (Na_2CO_3), and brine were sequentially used. Anhydrous sodium sulphate (Na_2SO_4) was employed at the end to remove any remaining water molecules. The precipitates formed due to the usage of Na_2SO_4 were removed using filter paper, and the excess DCM was eliminated using a rotary evaporator. The purified PPT conjugate was then placed in a vacuum until dried and the dried conjugate was stored at +4°C. The chemical structure of both PLGA-PEG copolymer and PPT conjugate was investigated using ^1H NMR.

3.2.3.4. Targeted NP synthesis

Targeted NP synthesis using TT80

Different amounts of the targeting agent by weight were employed in order to compare the obtained characterization results and identify the formulation that yielded the most favourable outcomes. It is stated in the literature that the critical limit for cationic TPP molecule concentration is 10 μM. Above this concentration value, it could cause the formation of adverse effects including the proton leakage and mitochondrial membrane depolarization (27). For this reason, while calculating TPP concentrations on NPs, this was considered. All in all, to synthesize targeted empty NPs containing 10% and 20% TT80 by weight as a targeting agent, the following procedure was employed.

For the synthesis of 10% TT80 by weight containing targeted empty NPs (**10%TT80-PLGA NPs**), PLGA (L:G 50:50, 25 mg, 0.20-0.25 μmol) was dissolved in 800 μL of acetone while TT80 (3.9 mg, 2.18 μmol) was dissolved in 200 μL of ethanol. On the other hand, for the synthesis of 20% TT80 by weight containing targeted empty NPs (**20%TT80-PLGA NPs**), PLGA (L:G 50:50, 25 mg, 0.20-0.25 μmol) was dissolved in 800 μL of acetone while TT80 (7.8 mg, 4.36 μmol) was dissolved in 200 μL of ethanol. The remaining procedure was the same for both of these NPs. 10 μL of Tween80 was added to the 10 mL of slightly heated ddH_2O while stirring at 100 rpm. The mixture was allowed to disperse at 300 rpm for 5 min. After that, the TT80 solution was added to this mixture at 100 rpm. Homogenization of the mixture was performed for a total of 1 min, with 2 second intervals every 10 second. Subsequently, the PLGA solution was added dropwise to this solution at 1100 rpm. The reaction was allowed to proceed for 1h, followed by an additional 1 min of homogenization. The synthesized NPs were then subjected to three rounds of centrifugation against cold ddH_2O for 10 min at 15000 rpm to purify the samples. The

10%TT80-PLGA NPs and 20%TT80-PLGA NPs were eventually resuspended in 10 mL of ddH_2O, and homogenization was applied for 2 min. At the end, NPs were filtered through a 0.45 μm PES syringe filter and stored at -20°C.

In order to synthesize 10% TT80 by weight containing targeted QCT-loaded NPs (**10%TT80-QCT-PLGA NPs**) and 20% TT80 by weight containing targeted QCT-loaded NPs (**20%TT80-QCT-PLGA NPs**), almost the same approach was utilized with a minor alteration. The main difference was that QCT (2.5 mg, 8.27 μmol) and PLGA (L:G 50:50, 25 mg, 0.20-0.25 μmol) were dissolved simultaneously in 800 μL of acetone. The subsequent procedures were followed.

Targeted NP synthesis using PPT

In addition to the usage of TT80, PPT was also used as another mitochondrial targeting agent within the scope of this project. The objective was to compare the effectiveness of different targeting agents as well as varying amounts of these agents to identify the most promising results. It is clearly reported in the literature that the critical concentration for cationic TPP molecule is 10 μM. Above this value, it has some hazardous effects including the proton leakage and mitochondrial membrane depolarization (27). For this reason, while calculating TPP concentrations that will be conjugated on NPs, this was strictly considered. All in all, the following procedure was utilized to synthesize targeted empty NPs incorporating 1.25% and 2.50% PPT by weight as a targeting agent. TPP amount found in 1.25% and 2.50% PPT-conjugated NPs were the equivalents of the TPP amount found in 10% and 20% TT80-conjugated NPs, respectively.

In order to synthesize 1.25% PPT by weight containing targeted empty NPs (**1.25%PPT-PLGA NPs**), PLGA (L:G 50:50, 25 mg, 0.20-0.25 μmol) and PPT (17.8

mg, 0.28 μmol) were dissolved in 1 mL of acetone. Similarly, for the preparation of 2.50% PPT by weight containing targeted empty NPs (**2.50%PPT-PLGA NPs**), PLGA (L:G 50:50, 25 mg, 0.20-0.25 μmol) and PPT (35.6 mg, 0.57 μmol) were dissolved in 1 mL of acetone. The remaining procedure was the same for both of them. Initially, 10 μL of Tween80 was added to the 10 mL of ddH_2O at 100 rpm and then this mixture was homogenized for 1 min. After that, the prepared solution containing PLGA and PPT was added dropwise to this mixture at 1100 rpm and the reaction continued for 1h. After the completion of the reaction, the resulting NP solution was further homogenized for an additional 1 min. To eliminate impurities, it was centrifuged three times at 15000 rpm for 10 min against cold ddH_2O. At the end, prepared NPs were resuspended in 10 mL of ddH_2O and homogenized for 2 min. Then, the NPs were filtered using a 0.45 μm PES syringe filter to obtain nanocarriers within the desired size range. Finally, the filtered NPs were stored at -20°C.

Almost the same procedure was followed for the synthesis of 1.25% PPT by weight containing targeted QCT-loaded NPs (**1.25%PPT-QCT-PLGA NPs**) and 2.50% PPT by weight containing targeted QCT-loaded NPs (**2.50%PPT-QCT-PLGA NPs**). In this case, QCT (2.5 mg, 8.27 μmol) as the drug molecule was dissolved together with PLGA (L:G 50:50, 25 mg, 0.20-0.25 μmol) and PPT (35.6 mg, 0.57 μmol) in 1 mL of acetone. The remaining steps of the procedure remained unchanged and were carried out as described previously.

3.2.3.5. Characterization of NPs

Within the scope of this project, DLS and zeta potential analysis were conducted for all of the synthesized NPs as it was explained in Section 3.2.1.7 in detail. Also, some other characterization studies were carried out as follows.

Morphological Analysis: The morphologies of non-targeted PLGA NPs, QCT-PLGA NPs, 10%TT80-QCT-PLGA NPs, and 2.50%PPT-QCT-PLGA NPs were analysed using SEM as it was explained in Section 3.2.1.7. In addition, 10%TT80-QCT-PLGA NPs, 20%TT80-QCT-PLGA NPs, 1.25%PPT-QCT-PLGA NPs, and 2.50%PPT-QCT-PLGA NPs were analysed with TEM to observe the dimensions and structure of NPs. The analysis was carried out by using lacey carbon film supported copper TEM grids as it was explained in Section 3.2.1.7. 20 μL of NP solutions were dropped on grids and were waited to dry for almost 2 days before conducting the analysis.

Stability Analysis: The stability analysis was conducted on both the non-targeted PLGA NPs and QCT-PLGA NPs. The NPs were subjected to incubation in 1M pH 7.4 PBS at two different temperatures, 25˚C and 37˚C. At specific time intervals (0h, 0.25h, 0.5h, 0.75h, 1h, 2h, 3h, 4h, 5h, 6h, 24h, 48h, 72h, 96h, 168h, 216h, and longer), the hydrodynamic diameter of NPs was measured using DLS with three repetitions. This analysis aimed to evaluate the stability of the NPs under various environmental conditions and determine their ability to maintain their initial structure over time.

Total QCT Amount Determination: In the synthesis of non-targeted and targeted drug-loaded NPs, the amount of QCT used was previously mentioned in Section 3.2.3.1 and Section 3.2.3.4. To measure the amount of QCT encapsulated inside the NPs, LC/MS-MS analysis was employed, and the results were reported in terms of μg/mL. Also, EE of QCT was calculated as a percentage using eq.1, which takes into account the amount of QCT encapsulated in the NPs relative to the initial amount of QCT used in the synthesis. To actualize this, bursting was employed. The NPs were subjected to a 1:1 volume ratio of acetone, which caused the NPs to rupture and release the encapsulated QCT to the environment. Different concentrations of QCT solutions were prepared, and a calibration curve was constructed using LC/MS-MS. This calibration curve, as depicted in Figure 3.9, served as a reference for quantifying the overall drug concentration present in the NPs.

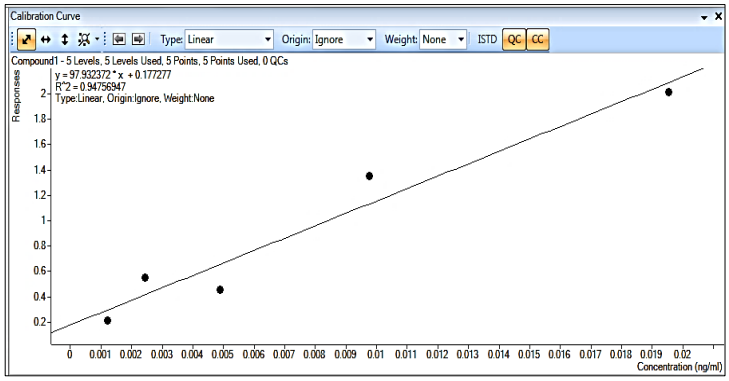

Figure 3. 9. Calibration curve prepared for QCT.

Measurement of Drug Release Profiles from NPs: The release rate of QCT from the QCT-PLGA NPs was investigated using 1M pH 7.4 PBS and pH 5.5 acetate buffer solution as a release media. The procedure described in Section 3.2.1.7 of the study was followed for the experiment. At specified time intervals (0h, 0.25h, 0.5h, 0.75h, 1h, 2h, 3h, 4h, 5h, 6h, 7h, 24h, and longer), samples were collected from the release medium. These samples were then analysed using an LC/MS-MS device and a calibration curve in Figure 3.9. By measuring the concentration of QCT in the collected samples and referring to the calibration curve, the release profile of QCT from the NPs over time could be determined. This analysis provided information about the release profiles and behaviour of QCT from QCT-PLGA NPs.

3.2.4.6. In vitro evaluation of NPs

In vitro cytotoxicity assay

Mouse skin fibroblast L-929 (ATCC CCL-1) cell lines were incubated with complete growth medium in an incubator at 37°C, 5% CO_2 and about 95% relative humidity. The complete growth medium consisted of DMEM/F-12 which was supplemented with 10% FBS and 1% Penicillin-Streptomycin antibiotic solution. When there was around 90% confluency, the culture medium in the T75 flask was

discarded, and cells were washed with 2 mL of DPBS. After that, 2 mL of 0.25% Trypsin-EDTA solution was added to the flask and cells were incubated at 37°C for 5 min until the cells were detached from the surface of flask. After 5 min, the cells were observed with light microscope and after ensuring the cells were detached, trypsin was deactivated by adding 6 mL of complete growth medium to the flask. The detached cells were collected and centrifuged at 800 rpm for 5 min. Then, the supernatant was removed carefully, and the cell pellet was resuspended with complete DMEM/F-12. For cell counting, 10 µL of cell suspension was taken and 10 µL of trypan blue dye was added on it. 10 µL was taken from this mixture and dropped on the Thoma cell counting chamber. In this way, the cells were counted with haemocytometer with the help of light microscope.

To evaluate the *in vitro* cytotoxicity of free QCT, QCT-PLGA NPs, 10%TT80-QCT-PLGA NPs, 20%TT80-QCT-PLGA NPs, 1.25%PPT-QCT-PLGA NPs, and 2.50%PPT-QCT-PLGA NPs, a CCK-8 assay was performed following the protocol outlined in the assay's booklet. First, 100 µL of cell suspension (10000 cells/well) were seeded in a flat-bottom 96-well plate. The 96-well plate was incubated at 37°C and 5% CO_2 for 24h for cell attachment. In the next day, the serial dilutions of QCT, QCT-PLGA NPs, 10%TT80-QCT-PLGA NPs, 20%TT80-QCT-PLGA NPs, 1.25%PPT-QCT-PLGA NPs, and 2.50%PPT-QCT-PLGA NPs containing 1 µM, 5 µM, 10 µM, 25 µM, 50 µM, 75 µM, 100 µM, 150 µM, 200 µM, 300 µM, and 375 µM drug molecule were prepared. 100 µL of various concentrations of substances were added to the wells. Moreover, as a positive control, L-929 cells containing only complete medium was used while 100 µL of complete medium was used as negative control. All measurements were performed in triplicate. Then, the 96-well plate was again incubated at 37°C and 5% CO_2 for 24h. At the end of 24h, 10 µL of CCK-8 solution was added to each well and the plate was incubated at 37°C and 5% CO_2 for 2h. After 2h of incubation, the absorbance was measured at 450 nm to determine the toxicity of samples on cells by using a microplate reader.

ROS assay

Mouse microglial EOC 20 (ATCC CRL-2469) cell lines were incubated in a complete growth medium consisting of DMEM/F-12 which was supplemented with 10% FBS and 1% Penicillin-Streptomycin antibiotic solution. These cells were placed in an incubator which functioned at 37°C, 5% CO_2 and about 95% relative humidity. The medium was renewed every 2 to 3 days. When confluency reached approximately 80%, the cells were subcultured. To actualize this, they were removed from the incubator and 75% of the old culture medium was discarded. After that, the cells were scraped using cell scraper and centrifuged at 140 g for 5 min. The supernatant was removed and the pellet consisting of cells was resuspended with fresh complete DMEM/F-12 medium without phenol red. For cell counting, 10 µL of cell suspension was added on 10 µL of trypan blue dye. After that, 10 µL of this mixture was taken and dropped on the Thoma cell counting chamber. In this way, the resuspended cells were counted with haemocytometer using light microscope.

In order to analyse the ROS activity of free QCT, QCT-PLGA NPs, 10%TT80-QCT-PLGA NPs, 20%TT80-QCT-PLGA NPs, 1.25%PPT-QCT-PLGA NPs, and 2.50%PPT-QCT-PLGA NPs, DCFDA Cellular ROS Detection Assay Kit was used following the provided protocols. Thanks to the data obtained from CCK-8 assay, the IC25 and IC50 values of samples were determined. The ROS activity of both free drug and NPs was analysed by applying their IC25 and IC50 concentration values on EOC 20 cells. For this purpose, first, 100 µL of cell suspension (25000 cells/well) were seeded in a dark, clear bottom 96-well plate. The cells were allowed to adhere overnight by incubating the 96-well plate at 37°C and 5% CO_2. In the next day, the medium was removed, and the cells were treated with lipopolysaccharide (LPS, 100 ng/mL) for 3h. At the end of 3h, the medium with LPS was removed and the cells were stained by adding 100 µL/well 20 µM DCFDA solution which was previously diluted in medium without phenol red. Then, the cells were incubated for 45 min at 37°C in the dark. At the end of 45 min, DCFDA solution was removed, and the wells were

washed by adding 100 µL/well 1X buffer solution. Then, 100 µL of IC25 and IC50 concentrations of prepared samples were added to the wells properly. Moreover, in order to interpret the results of ROS assay, the cells with both LPS and DCFDA were used as a positive control while medium without cells (blank) and cells with LPS but without DCFDA were used as background controls. All measurements were performed in triplicate. After the addition of samples to be analysed, the 96-well plate was again incubated at 37°C and 5% CO_2 for 4h. After 4h of incubation, the excitation/emission spectra were measured at 485/535 nm using a Varioskan device (Thermo Scientific Varioskan Flash).

JC-1 assay

The handling and subculturing of mouse microglial EOC 20 cell lines were conducted in accordance with the procedures previously explained for the ROS assay in Section 3.2.4.6. In summary, the cells were incubated in a complete DMEM/F-12 medium in an incubator and medium renewal was accomplished every 2 to 3 days. Upon reaching enough confluency, the cells were subcultured using a cell scraper. After centrifugation at 140 g for 5 min, the supernatant was discarded and the pellet consisting of cells was resuspended with fresh complete medium without phenol red. Then, the resuspended cells were counted using a haemocytometer with the help of a light microscope.

In this part of the study, MitoProbe JC-1 Assay Kit was utilized to investigate the changes in the mitochondrial membrane potential of the cells when there was a treatment with free QCT, QCT-PLGA NPs, 10%TT80-QCT-PLGA NPs, 20%TT80-QCT-PLGA NPs, 1.25%PPT-QCT-PLGA NPs, or 2.50%PPT-QCT-PLGA NPs, following the protocols provided in its booklet. For this purpose, three different drug concentration values, which were 5 µM, 10 µM, and 20 µM, were tried on cells for all samples by following the experimental procedure provided by manufacturer with

slight modifications. To interpret and analyse the results of JC-1 assay, the cells without LPS but with carbonyl cyanide 3-chlorophenylhydrazone (CCCP) which is a mitochondrial membrane potential disrupter were used as a positive control. Moreover, the cells with LPS were used as another control to prove the presence of inflammation on the cells when there was not any treatment. In the light of all this information, first, 500 µL of cell suspension (200000 cells/well) were seeded in a clear bottom 24-well plate. Then, the plate was incubated at 37°C and 5% CO_2 for 24h to achieve cell adhesion. At the end of 24h, the culture medium was removed, and the relevant cells were treated with LPS (100 ng/mL) to create inflammation, and they were incubated for 3h. After the completion of 3h, the medium containing LPS was removed and replaced with 500 µL of fresh medium containing either free drug or non-targeted and targeted NPs at a drug concentration of 5 µM, 10 µM, and 20 µM. After the addition of samples to be analysed, the 24-well plate was again incubated at 37°C and 5% CO_2 for 48h. At the end of this process, for positive control wells, the culture medium was removed and replaced with fresh medium containing CCCP with a final concentration of 50 µM. The plate was incubated at 37°C for 5 min. Subsequently, the medium found in all wells were removed and 500 µL of JC-1 solution prepared in fresh medium without phenol red with a final concentration of 2 µM was added to each well in the dark. The cells were incubated for another 20 min. At the end of 20 min, the old medium in each well was removed and wells were washed with 1 mL of PBS by shaking gently. The buffer was removed and 500 µL of cold 4% paraformaldehyde (PFA) was slowly added to wells for cell fixation. The plate was incubated for 10 min with PFA at RT. Then, the PFA was discarded carefully, and the wells were washed with 500 µL of ddH_2O. After that, 100 µL of cold methanol was added to each well and waited for 30 second at RT. Finally, the methanol was removed, and the stained cells were visualized using a fluorescence microscope (Invitrogen™ EVOS™ M5000 Imaging System) at RT under dark conditions.

3.2.4.7. Statistics

Statistical analyses for this project were performed using GraphPad Prism 10, employing two-way ANOVA. The outcomes were given as mean ± standard deviation and a p-value less than 0.05 was considered statistically significant.

4. RESULTS

4.1. Results for Project 1: Macrophage-Targeted NPs

4.1.1. Characterization of S2P peptide and DSPE-PEG-S2P conjugate

First, S2P peptide was synthesized in the laboratory as it was explained in Section 3.2.1.2 and purified using a prep-HPLC device. For this, the peptide was dissolved in the mixture of ddH_2O and ACN and injected into the hydrophobic C18 column. One of the mobile phases was ddH_2O with 0.025% TFA and the other one was ACN with 0.025% TFA. S2P peptide was first run at 100% ddH_2O for 2 min and then increased linearly over 10 min from 0% ACN to 100% ACN. The relevant pure peaks of the peptide, which were indicated in Figure 4.1 as 17^{th}, 18^{th}, and 19^{th} peak, were obtained between 0-1 min in 100% ddH_2O. The samples coming from these peaks were collected and lyophilized for future use after removing the excess ACN using rotary evaporator.

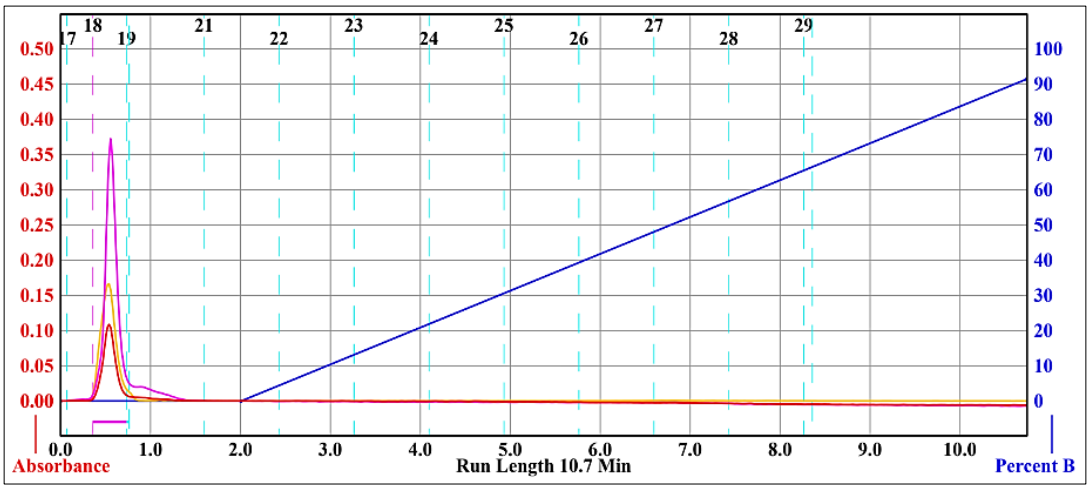

Figure 4. 1. Prep-HPLC analysis of S2P peptide conducted for purification.

The chemical characterization of the synthesized S2P peptide was performed using an LC/MS-MS device. This analysis was carried out by using 50% ACN and 50% ddH_2O as mobile phase, added with 0.05% formic acid. The flow rate was set to 0.5 mL/min. It was previously stated that the MW of S2P peptide is 1078.57 g/mol. In the scan spectrum (Figure 4.2), the molecular ion peak was observed at 1078.20, which closely matched the theoretical MW. Also, since this analysis was carried out in formic acid, +2 and +3 ions were also seen and obtained at 539.60 and 360.10. All in all, this chemical characterization result confirmed the successful synthesis of the peptide.

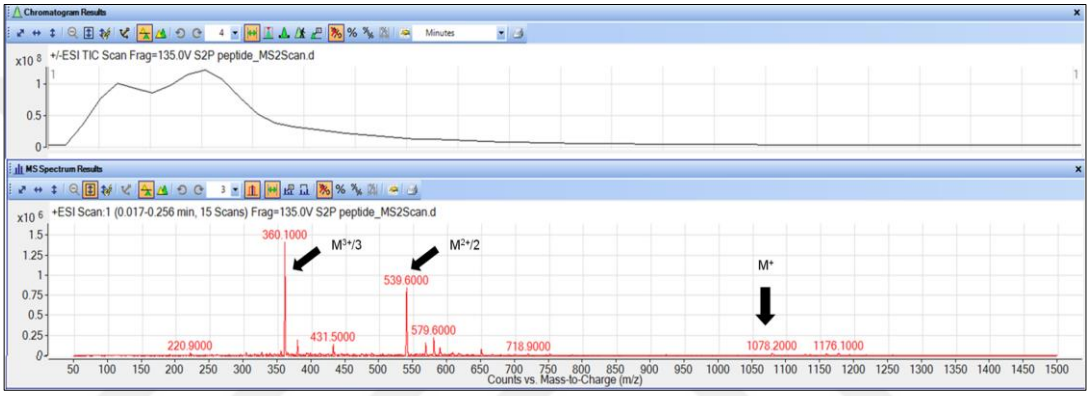

Figure 4. 2. LC/MS-MS analysis of S2P peptide.

After completing the chemical characterization tests of S2P peptide, DSPE-PEG-S2P conjugate was synthesized as it was explained in Section 3.2.1.3. The chemical structure of this conjugate was investigated by ^{1}H NMR spectroscopy in deuterated DMSO. The obtained spectrum was processed as in Figure 4.3. First of all, the -NH amide protons of S2P peptide were observed as a broad multiplet at 7.13-8.21 ppm. Also, the ester protons and -CH_2 protons of PEG polymer can be seen at 4.04-4.19 ppm and 3.19-3.67 ppm, respectively. Moreover, the -CH_2 and -CH_3 protons of both DSPE lipid and S2P peptide were obtained at 0.84-1.53 ppm. In addition to these, the DMSO protons were clearly observed at 2.50 ppm. In conclusion, the presence of the protons of all components, namely DSPE, PEG, and S2P, demonstrated the proper synthesis of DSPE-PEG-S2P conjugate in the laboratory.

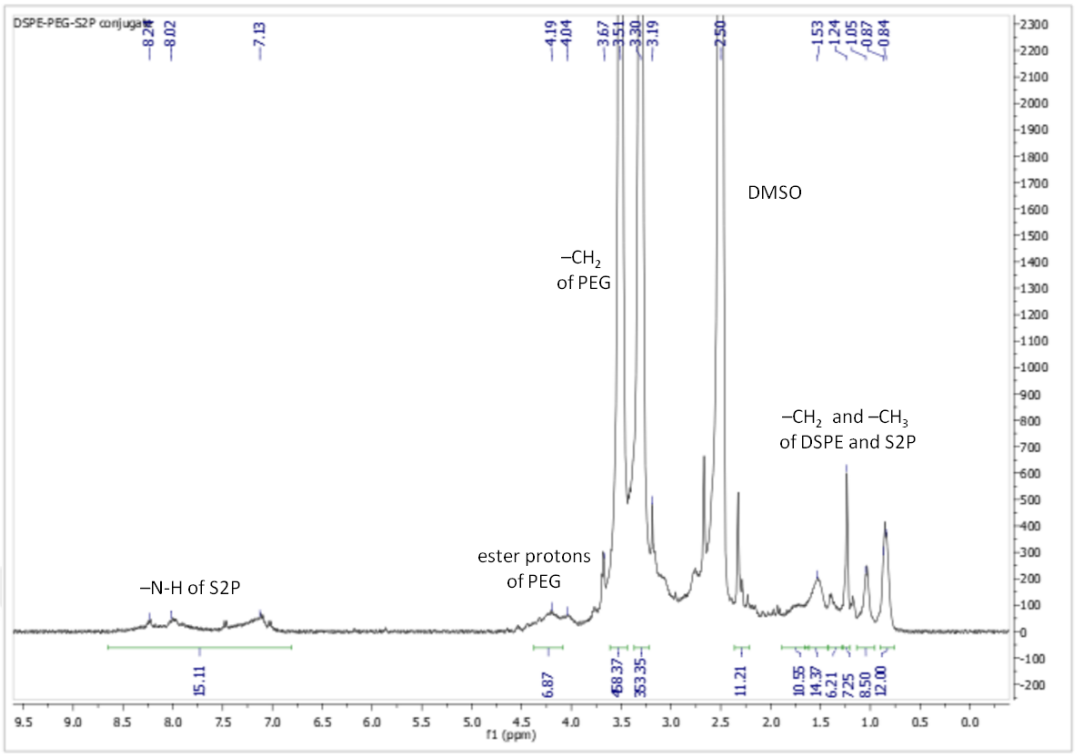

Figure 4. 3. ^{1}H NMR spectrum of the DSPE-PEG-S2P conjugate.

Furthermore, FT-IR analysis was conducted for the DSPE-PEG-Mal, S2P peptide, and DSPE-PEG-S2P conjugate (Figure 4.4). First of all, in the FT-IR spectrum of DSPE-PEG-Mal (Figure 4.4A), peaks corresponding to O-H and N-H bonds were observed at 3398.53 cm^{-1}. However, peaks of the corresponding bonds were obtained at 3266.76 cm^{-1} for the S2P peptide (Figure 4.4B). Following conjugation, the peaks for O-H and N-H bonds shifted to 3273.65 cm^{-1} (Figure 4.4C). Additionally, C-H and C-C stretching bonds were identified at 2850.90 cm^{-1} and 2915.98 cm^{-1} in the FT-IR spectrum of DSPE-PEG-Mal and at 2962.68 cm^{-1} in the FT-IR spectrum of the S2P peptide. After conjugation, this peak was observed at 2881.07 cm^{-1}. The C=O stretching peak coming from the maleimide functional group was seen in the FT-IR spectrum of DSPE-PEG-Mal at 1707.99 cm^{-1}. However, after the conjugation, this peak could not be observed, and this was a sign that proved the formation of DSPE-PEG-S2P conjugate. Last but not least, the P-O and P=O peaks were observed at 1240.02 cm^{-1}, 1279.21 cm^{-1}, 1342.00 cm^{-1}, and 1359.60 cm^{-1} in the FT-IR spectrum of DSPE-PEG-Mal. However, these characteristic bonds were not present in the structure of peptide as it can be seen in Figure 4.4B. After the conjugation, these P-O and P=O

peaks were observed at 1241.09 cm^{-1}, 1279.77 cm^{-1}, 1342.54 cm^{-1}, and 1359.39 cm^{-1} in the FT-IR spectrum of DSPE-PEG-S2P as in Figure 4.4C. All in all, the characteristic functional groups of both DSPE-PEG and S2P peptide were seen in the FT-IR spectrum of DSPE-PEG-S2P conjugate.

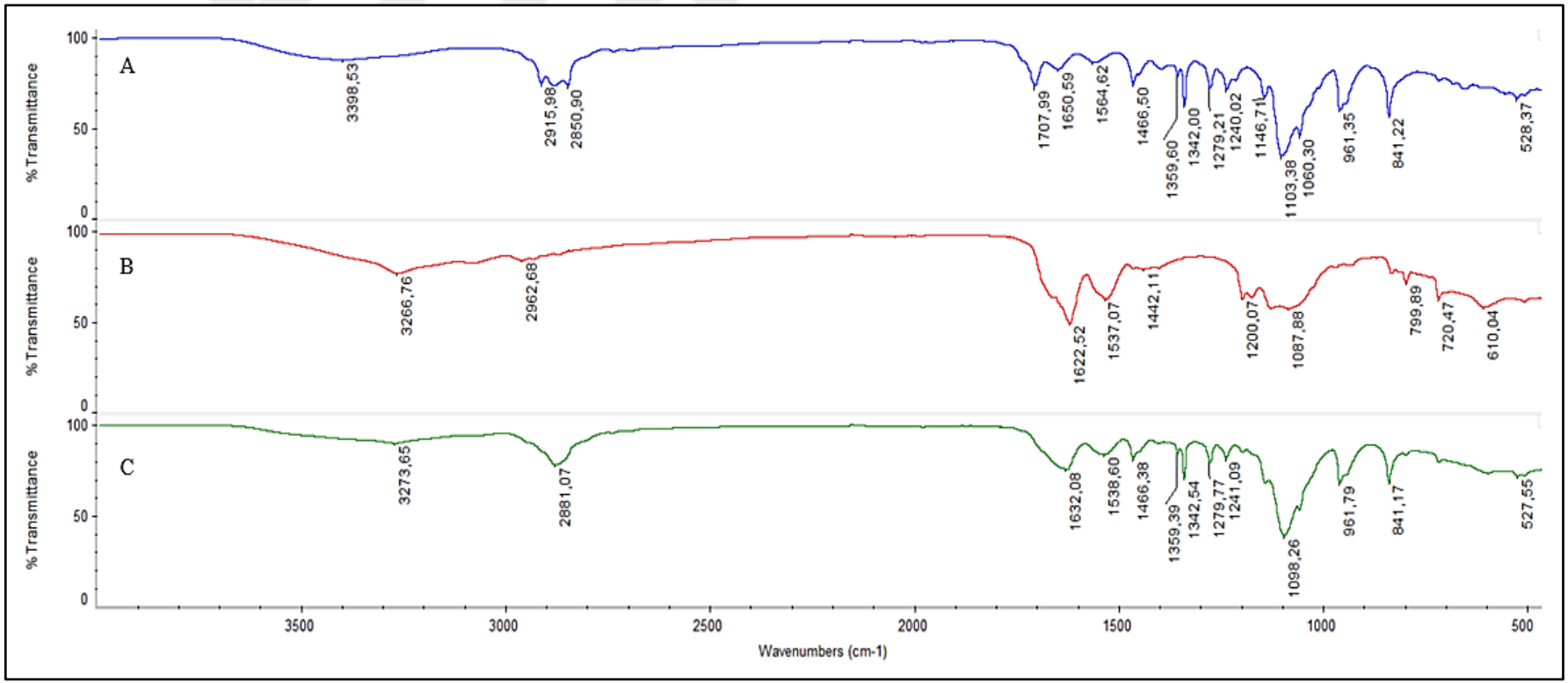

Figure 4. 4. FT-IR spectra of (A) DSPE-PEG-Mal, (B) S2P, (C) DSPE-PEG-S2P.

4.1.2. Characterization of NPs

After the synthesis of NPs, their hydrodynamic diameter and PDI values were analysed using DLS to compare how the coating, targeting, and dye-labelling effects the NP size and size distribution (Figure 4.5, Figure 4.6, Figure 4.7, and Figure 4.8). The hydrodynamic diameter of non-coated NPs was measured as 165.0 nm. However, after the coating, the size of the NPs increased. The hydrodynamic diameter of PLGA NPs, α-13′-COOH PLGA NPs, GA-PLGA NPs were obtained as 234.8 nm, 227.9 nm, and 274.0 nm, respectively. Moreover, PDI values were obtained between 8.9% and 21.3% while α-13′-COOH PLGA NPs had the lowest PDI value (Figure 4.5).

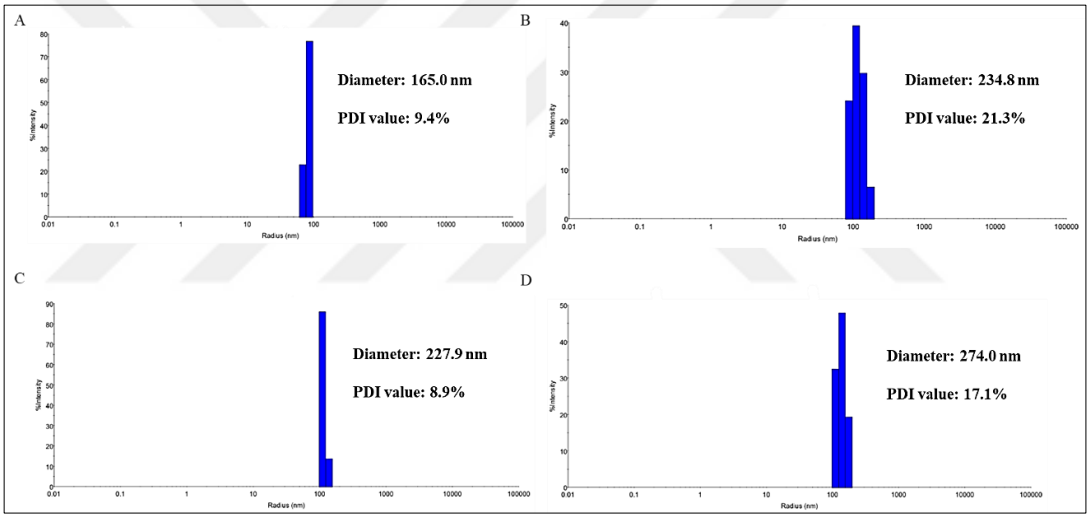

Figure 4. 5. Hydrodynamic diameter and PDI value measurements of non-targeted NPs via DLS (A) non-coated NPs, (B) PLGA NPs, (C) α-13′-COOH PLGA NPs, (D) GA-PLGA NPs.

After the conjugation of S2P peptide, the hydrodynamic diameter of S2P-PLGA NPs and S2P-α-13′-COOH PLGA NPs was obtained as 321.1 nm and 335.4 nm, respectively. These were higher than the hydrodynamic diameter of non-targeted PLGA NPs (Figure 4.5B) and α-13′-COOH PLGA NPs (Figure 4.5C). Furthermore, the PDI values were obtained between 11.5% and 13.6% for the targeted NPs while S2P-PLGA NPs had the lowest PDI value. Moreover, the hydrodynamic diameter of GA-PLGA NPs was measured as 274.0 nm while it was 253.3 nm for S2P-GA-PLGA

NPs. Therefore, the similar increase in the size was not observed for GA-loaded targeted NPs after the conjugation of peptide (Figure 4.6).

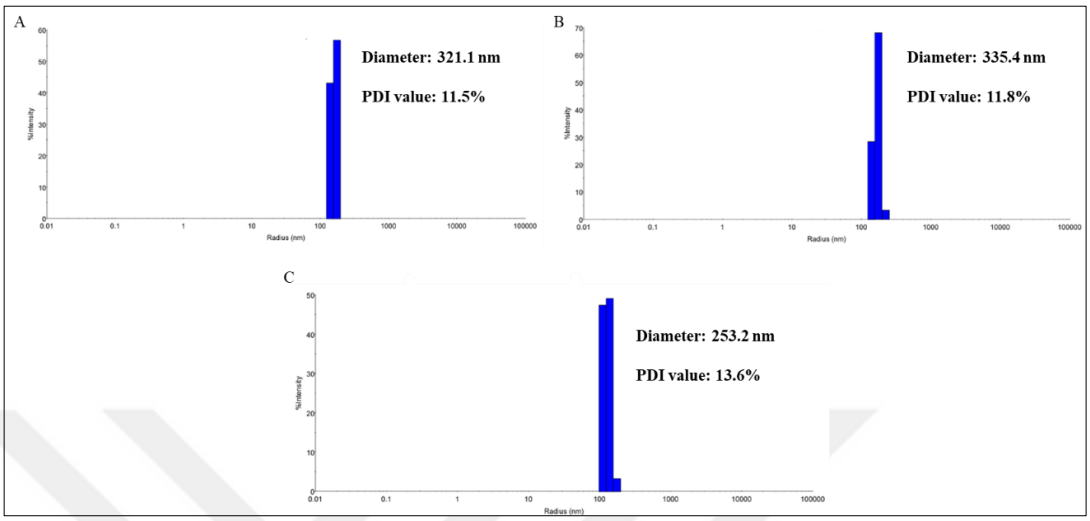

Figure 4. 6. Hydrodynamic diameter and PDI value measurements of targeted NPs via DLS (A) S2P-PLGA NPs, (B) S2P-α-13′-COOH PLGA NPs, (C) S2P-GA-PLGA NPs.

Furthermore, NPs were labelled with FITC and DLS measurements were repeated. FITC-S2P-PLGA NPs (Figure 4.7B) had higher hydrodynamic diameter and lower PDI value compared to non-targeted FITC-PLGA NPs (Figure 4.7A).

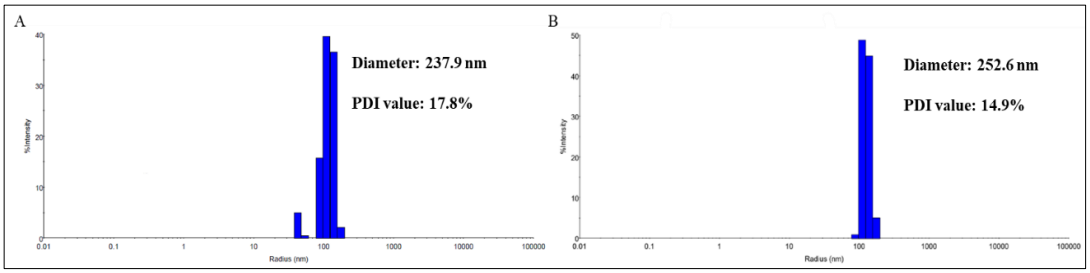

Figure 4. 7. Hydrodynamic diameter and PDI value measurements of FITC-labelled NPs via DLS (A) FITC-PLGA NPs, (B) FITC-S2P-PLGA NPs.

After the conjugation of RhB, DLS measurements were conducted again. The hydrodynamic diameter of RhB-FITC-S2P-PLGA NPs was 270.3 nm with a PDI value of 17.4% while it was 254.5 nm with 11.4% PDI value for RhB-FITC-PLGA NPs. In addition, the hydrodynamic diameter of RhB-FITC-S2P-α-13′-COOH PLGA NPs

were 279.2 nm with a PDI value of 5.1% while it was 269.8 nm with 7.8% PDI value for RhB-FITC-α-13′-COOH PLGA NPs. Therefore, targeted empty and drug-loaded NPs had slightly higher hydrodynamic diameter compared to non-targeted NPs (Figure 4.8).

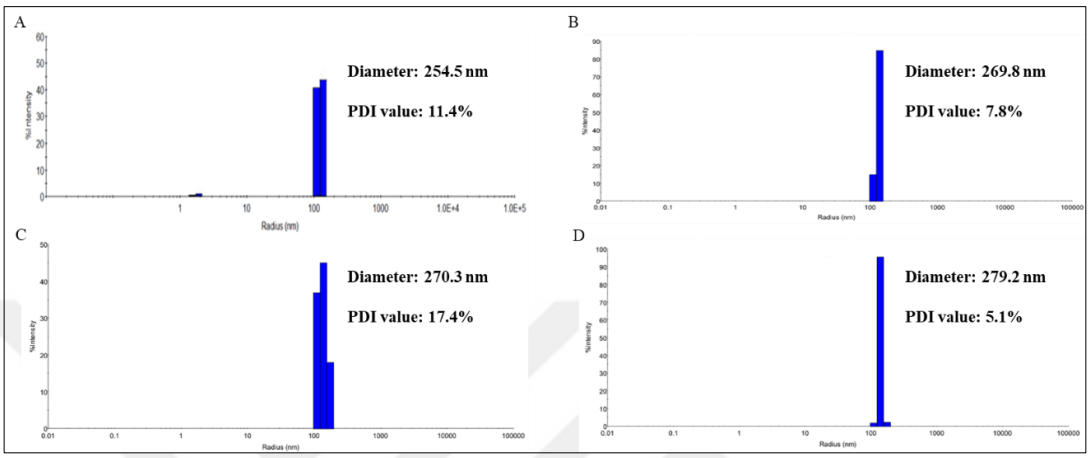

Figure 4. 8. Hydrodynamic diameter and PDI value measurements of RhB-conjugated FITC-labelled NPs via DLS (A) RhB-FITC-PLGA NPs, (B) RhB-FITC-α-13′-COOH PLGA NPs, (C) RhB-FITC-S2P-PLGA NPs, (D) RhB-FITC-S2P-α-13′-COOH PLGA NPs.

Moreover, the surface charge of obtained NPs was measured (Figure 4.9, Figure 4.10, Figure 4.11, and Figure 4.12). The surface charge of non-targeted NPs was obtained as negative which was between -22.7 ± 4.03 mV and -26.9 ± 0.850 mV as in Figure 4.9. However, after the conjugation of positively charged S2P peptide as a targeting agent, the surface charge of targeted NPs was measured again. PLGA NPs had the surface charge of -25.1 ± 3.13 mV while it was -16.7 ± 4.88 mV for S2P-PLGA NPs. α-13′-COOH PLGA NPs had the surface charge of -22.7 ± 4.03 mV while it was -13.6 ± 0.723 mV for S2P-α-13′-COOH PLGA NPs. Similarly, the surface charge of GA-PLGA NPs was -26.9 ± 0.850 mV while it was -20.7 ± 0.503 mV for S2P-GA-PLGA NPs. All in all, the surface charge of NPs shifted towards the positive side (Figure 4.10).

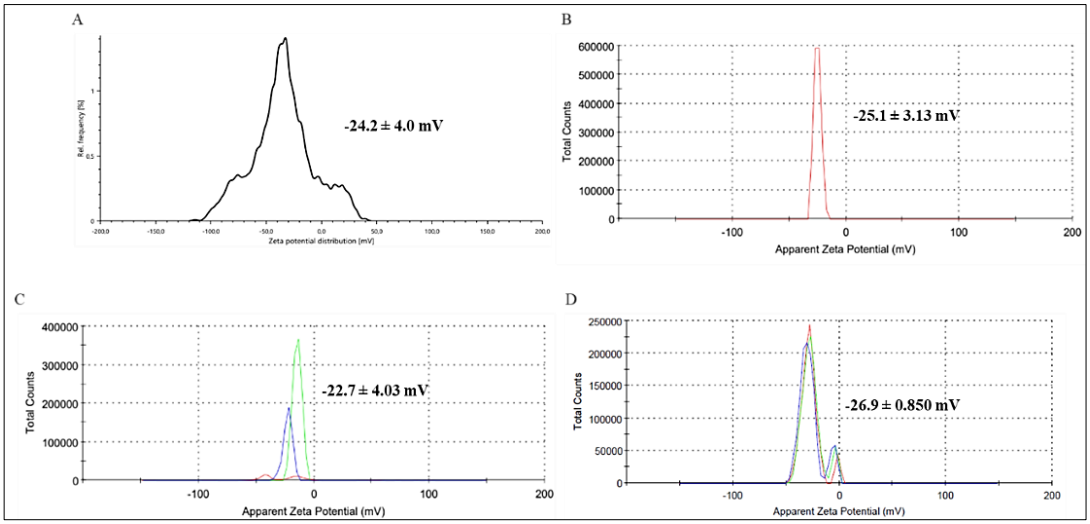

Figure 4. 9. Zeta potential measurements of non-targeted NPs (A) non-coated NPs, (B) PLGA NPs, (C) α-13′-COOH PLGA NPs, (D) GA-PLGA NPs.

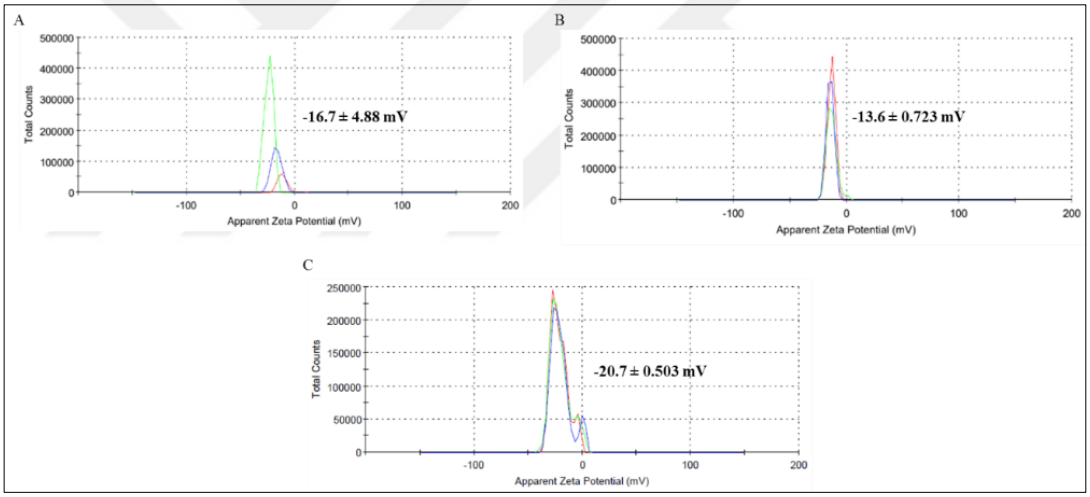

Figure 4. 10. Zeta potential measurements of targeted NPs (A) S2P-PLGA NPs, (B) S2P-α-13′-COOH PLGA NPs, (C) S2P-GA-PLGA NPs.

Furthermore, after the conjugation of S2P peptide, the surface charge of FITC-S2P-PLGA NPs increased from -23.1 ± 1.04 mV to -17.0 ± 0.656 mV (Figure 4.11). Also, after addition of S2P peptide to the surface of NPs, the surface charge of RhB-FITC-S2P-PLGA NPs increased from -22.8 ± 1.50 mV to -14.4 ± 0.777 mV. Similarly, the surface charge of RhB-FITC-S2P-α-13′-COOH PLGA NPs increased from -23.2 ± 0.529 mV to -13.7 ± 2.06 mV. In conclusion, shifting to the positive side was observed in zeta potential values after the conjugation of peptide (Figure 4.12).

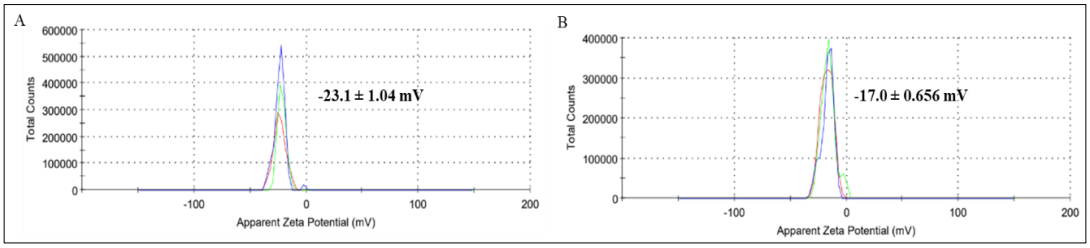

Figure 4. 11. Zeta potential measurements of FITC-labelled NPs (A) FITC-PLGA NPs, (B) FITC-S2P-PLGA NPs.

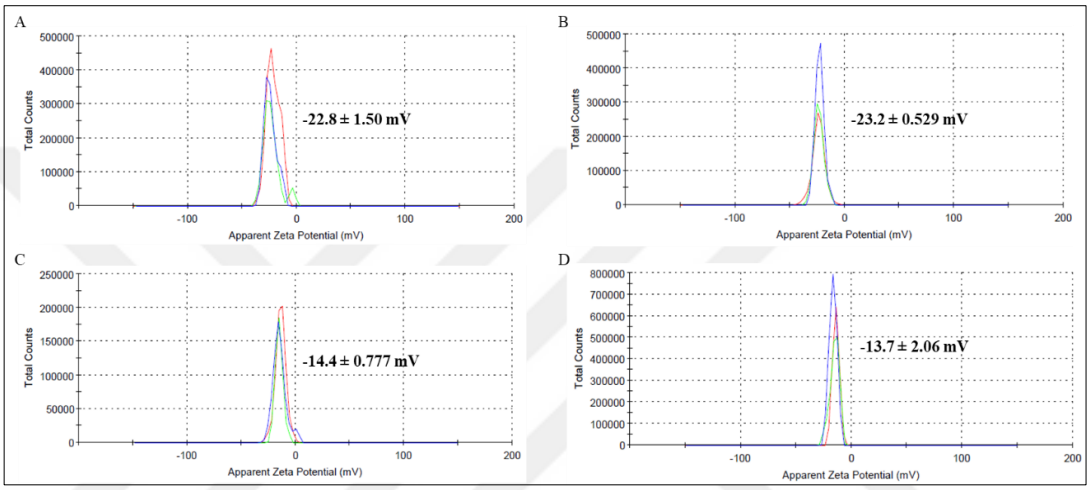

Figure 4. 12. Zeta potential measurements of RhB-conjugated FITC-labelled NPs (A) RhB-FITC-PLGA NPs, (B) RhB-FITC-α-13′-COOH PLGA NPs, (C) RhB-FITC-S2P-PLGA NPs, (D) RhB-FITC-S2P-α-13′-COOH PLGA NPs.

Morphologies of non-targeted and targeted empty and drug-loaded NPs could be seen in Figure 4.13. Smooth and spherical shape of NPs were observed via SEM.

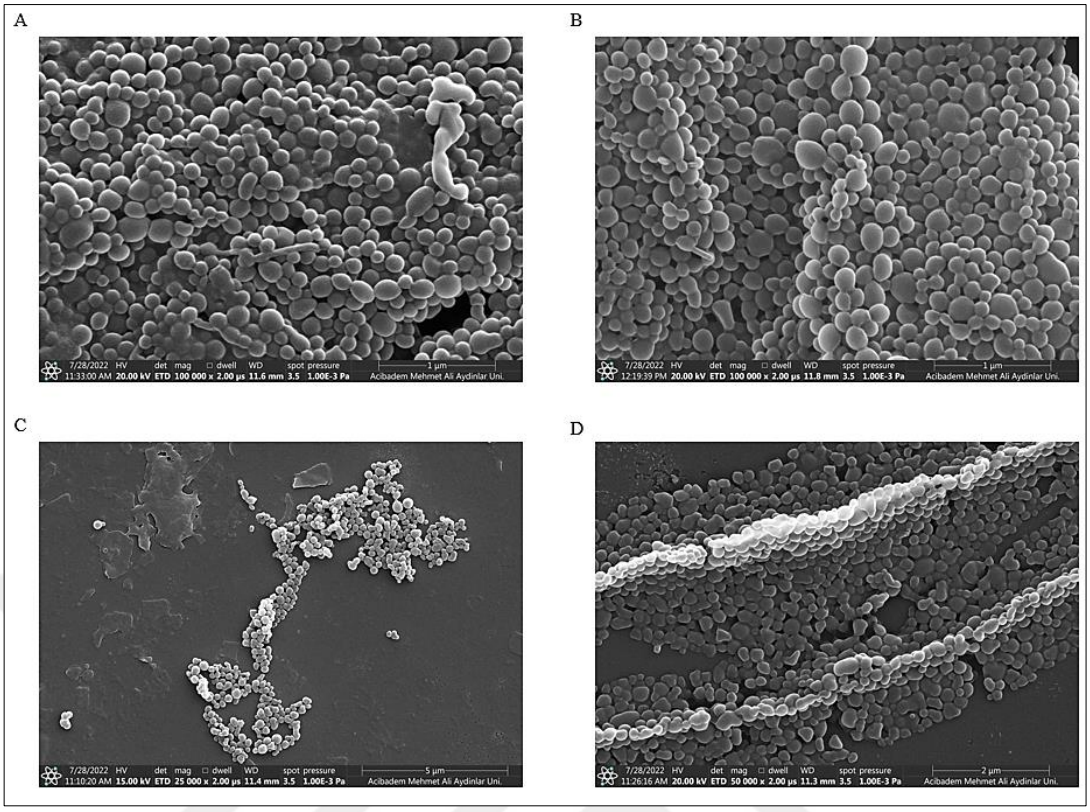

Figure 4. 13. Morphological analysis of NPs via SEM (A) PLGA NPs, (B) α-13′-COOH PLGA NPs, (C) S2P-PLGA NPs, (D) S2P-α-13′-COOH PLGA NPs.

Also, their dimensions and the presence of coating layer on them could be seen in Figure 4.14. The hydrodynamic diameter of PLGA NPs, α-13′-COOH PLGA NPs, S2P-PLGA NPs, and S2P-α-13′-COOH PLGA NPs were measured as 234.8 nm (Figure 4.5B), 227.9 nm (Figure 4.5C), 321.1 nm (Figure 4.6A), and 335.4 nm (Figure 4.6B), respectively by using DLS. However, with TEM, the diameter of PLGA NPs and α-13′-COOH PLGA NPs were obtained as around 174.3 nm (Figure 4.14A), and 220.7 nm (Figure 4.14B), respectively. Moreover, the diameter of S2P-PLGA NPs was measured between 250.5 nm and 256.7 nm as in Figure 4.14C, while the diameter of S2P-α-13′-COOH PLGA NPs was obtained between 217.1 nm and 291.9 nm as in Figure 4.14D. Therefore, the hydrodynamic diameter of NPs that were measured with TEM was smaller compared to the hydrodynamic diameter of NPs that were measured with DLS. In addition, the presence of the coating layer was proved in Figure 4.14 and its thickness was measured as 25.65 nm as in Figure 4.14A.

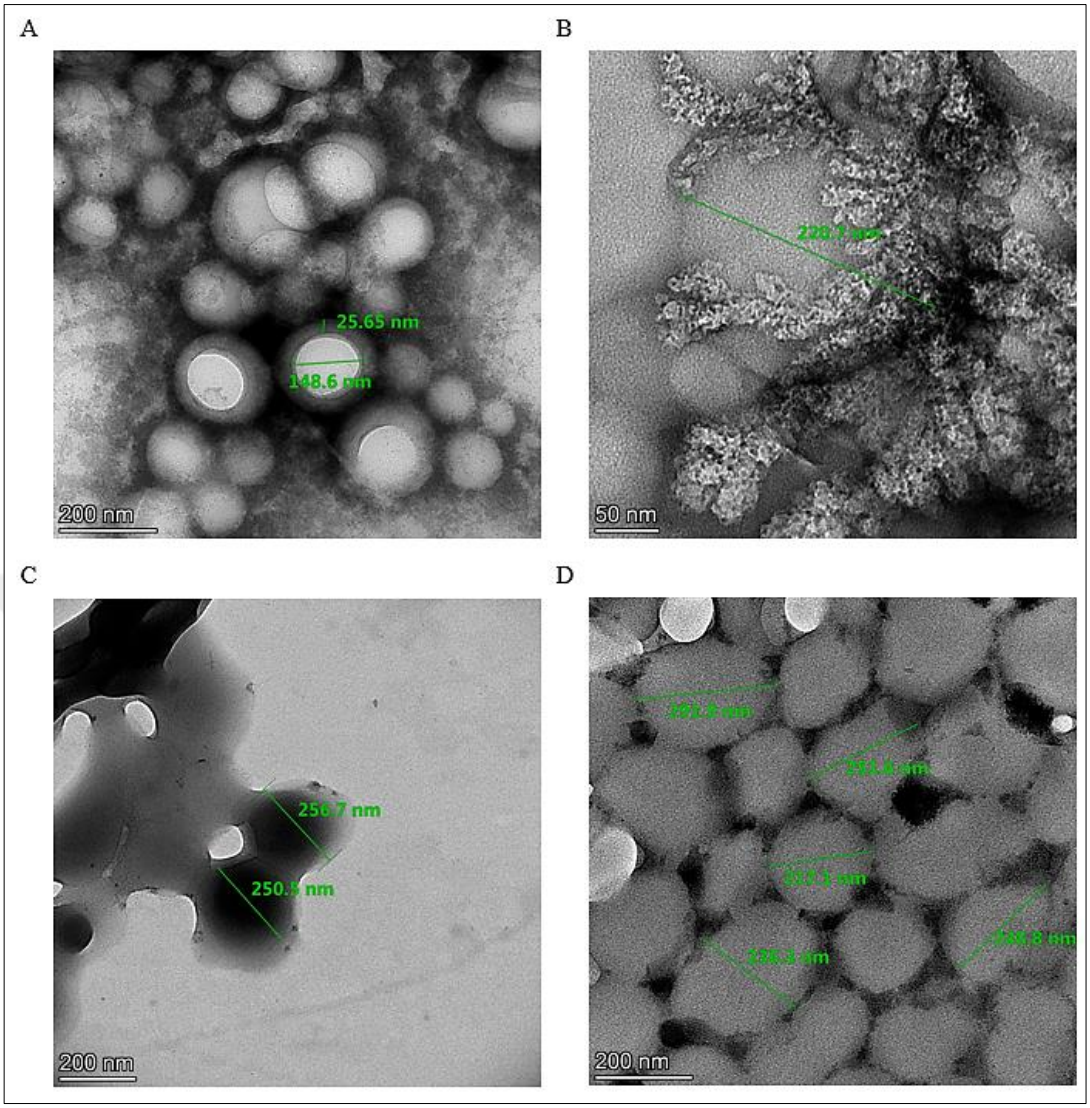

Figure 4. 14. Morphological analysis of NPs via TEM (A) PLGA NPs, (B) α-13′-COOH PLGA NPs, (C) S2P-PLGA NPs, (D) S2P-α-13′-COOH PLGA NPs.

Moreover, FT-IR analysis was conducted for the α-13′-COOH drug molecule, PLGA polymer, non-coated NPs, PLGA NPs, and α-13′-COOH PLGA NPs (Figure 4.15). In the FT-IR spectrum of α-13′-COOH (Figure 4.15A), methyl asymmetric bending peak was seen at 1462.10 cm^{-1} while methyl symmetric bending peak was obtained at 1377.22 cm^{-1}. C-O stretching was seen at 1247.83 cm^{-1} while C-H stretching was observed at 2860.02 cm^{-1} and 2926.03 cm^{-1}. Also, C-O stretching of aliphatic ether group was found at 1086.55 cm^{-1}. In addition to these, the pure PLGA polymer also showed some characteristic peaks as in Figure 4.15B. The peaks observed at 2950.68 cm^{-1} and 2998.06 cm^{-1} were C-H stretching bonds while the peak

at 1746.08 cm^{-1} was the C=O stretching bond. Furthermore, C-O stretching peaks were observed at the 1083.76 cm^{-1}, 1130.64 cm^{-1}, 1159.76 cm^{-1}, and 1268.96 cm^{-1}. In the light of all this information, all characteristic peaks coming from the pure PLGA polymer was observed in the FT-IR spectrum of non-coated NPs (Figure 4.15C). Additionally, in the FT-IR spectrum of PLGA NPs shown in Figure 4.15D, characteristic peaks of the PLGA polymer were also observed. However, after the addition of DSPE-PEG coating, additional C-H stretching peak was observed at 2961.49 cm^{-1}. Finally, some of the characteristic peaks of PLGA polymer, DSPE-PEG coating, and drug molecule were together observed in the FT-IR spectrum of α-13′-COOH PLGA NPs (Figure 4.15E). For instance, peaks observed at 2850.87 cm^{-1}, 2918.62 cm^{-1}, 1460.69 cm^{-1}, and 1379.03 cm^{-1} were attributed to the α-13'-COOH drug molecule, while peaks at 1746.45 cm^{-1} and 1393.31 cm^{-1} originated from the PLGA polymer. Additionally, the peak at 2963.68 cm^{-1} was attributed to the DSPE-PEG coating. These findings collectively demonstrate the presence of the polymer, coating, and drug in the structure of the synthesized α-13′-COOH PLGA NPs.

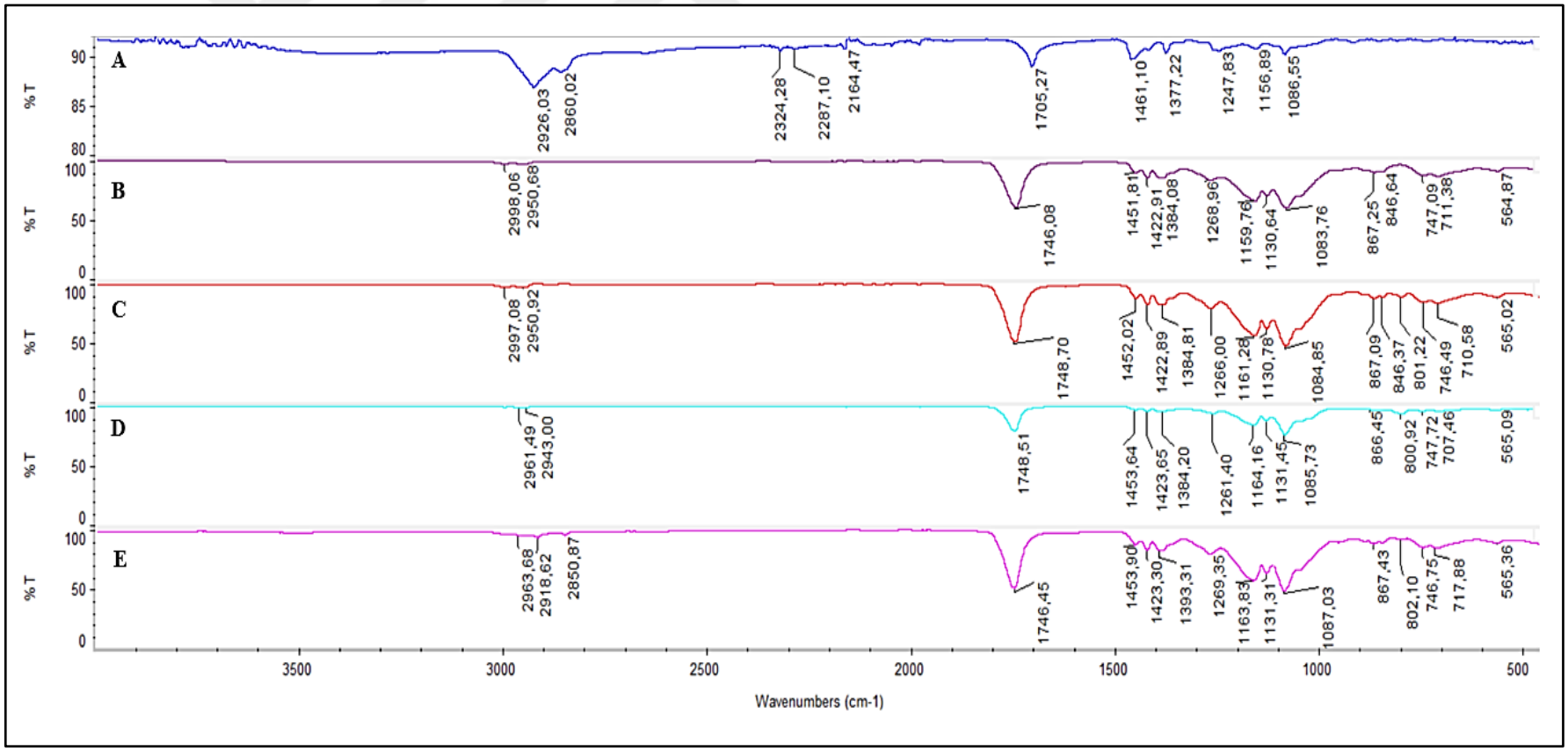

Figure 4. 15. FT-IR spectra of (A) α-13′-COOH drug molecule, (B) PLGA polymer, (C) non-coated NPs, (D) PLGA NPs, (E) α-13′-COOH PLGA NPs.

In addition to all these characterization tests, the stability of PLGA NPs and α-13′-COOH PLGA NPs was analysed by incubating them in 1M pH 7.4 PBS at both 25˚C and 37˚C up to almost 70 days as in Figure 4.16. In the statistical analysis, the p-value was found statistically significant ($p < 0.0001$) for the hydrodynamic diameter of NPs after the 2nd day with respect to their diameter observed during first two days. The hydrodynamic diameter of PLGA NPs and α-13′-COOH PLGA NPs showed some minor fluctuations during the first hours of incubation and after 2 days, the gradual increase in the size was observed. In the long term, around the 15th day and beyond, the sizes of both NPs remained between 600 nm and 700 nm for approximately 8 weeks.

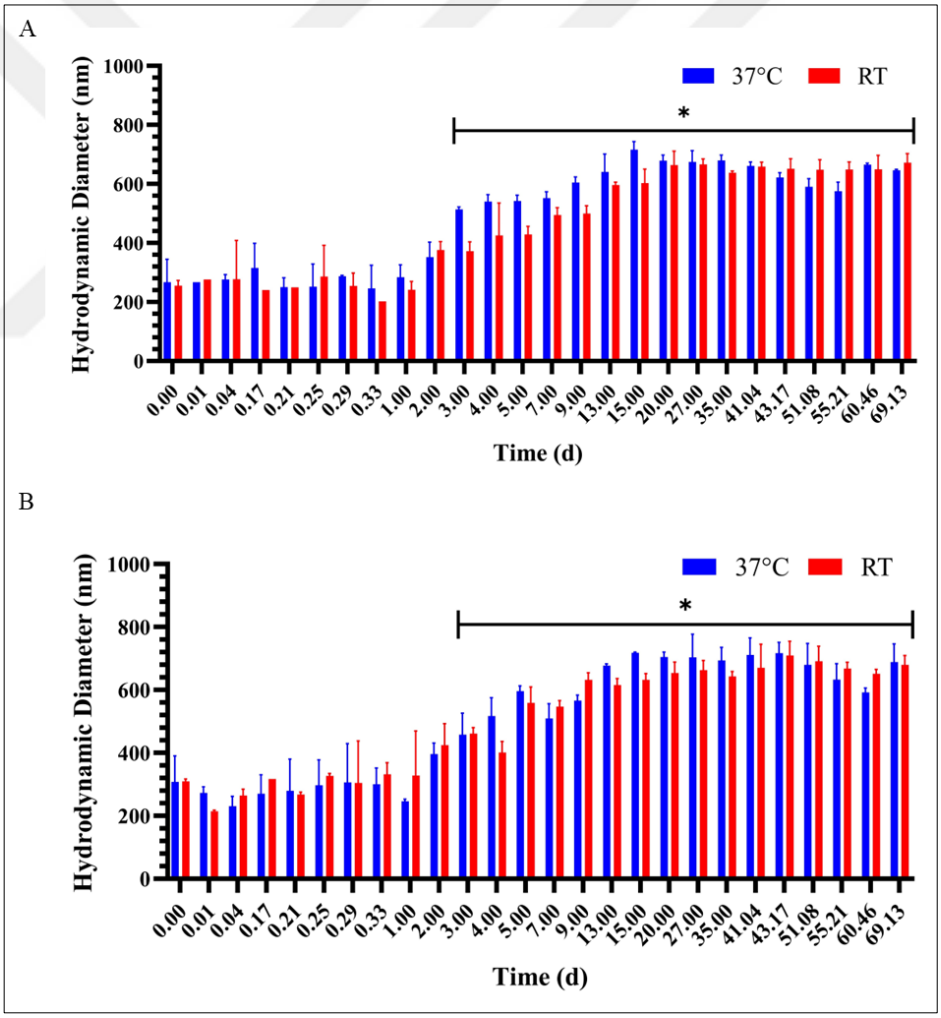

Figure 4. 16. Stability analysis of NPs (A) PLGA NPs, (B) α-13′-COOH PLGA NPs, * $p < 0.0001$ for the hydrodynamic diameter of NPs with respect to their diameter during first 2 days, n = 3.

Furthermore, the stability of GA-PLGA NPs was investigated by incubating them in 1M pH 7.4 PBS at both 25˚C and 37˚C up to 31 days as in Figure 4.17. In statistical analysis, a statistically significant p-value ($p < 0.0001$) was obtained for the hydrodynamic diameter of NPs after the 2nd day compared to their diameter during the initial two days. In other words, the hydrodynamic diameter of GA-PLGA NPs was obtained stable during the first 2 days. The increase in the size was observed at 3rd day and around the 15th day and beyond, the size of GA-PLGA NPs remained between 600 nm and 800 nm for approximately 4 weeks at both RT and 37˚C.

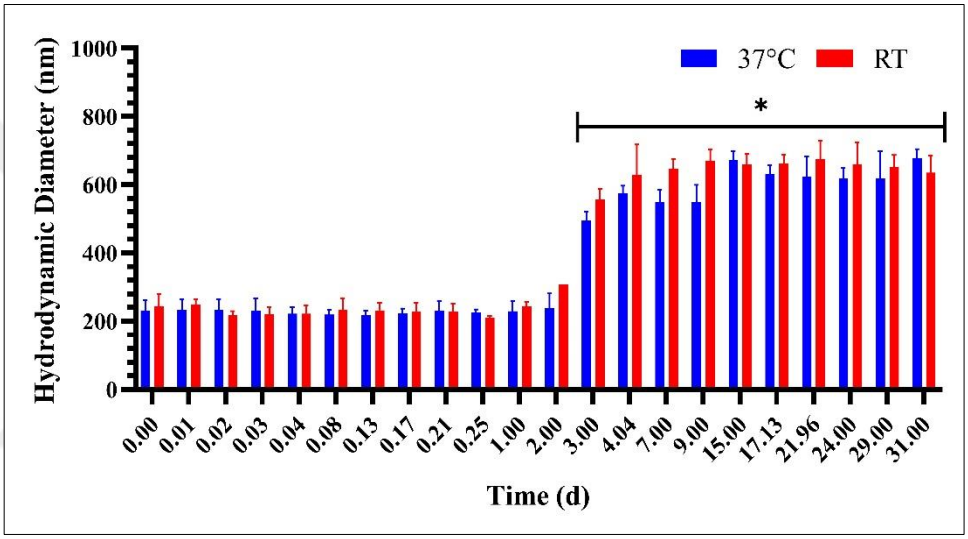

Figure 4. 17. Stability analysis of GA-PLGA NPs, * $p < 0.0001$ for the hydrodynamic diameter of NPs with respect to their diameter during first 2 days, n = 3.

To determine the net protein concentration in targeted NPs, nanodrop analysis was carried out. The absorbance of the S2P peptide was measured at 214 nm and the protein concentration in NPs was calculated. By subtracting the protein concentration of targeted NPs from the protein concentration of non-targeted NPs, the net protein concentration in targeted NPs was calculated as in Table 4.1. All in all, the net protein concentration in S2P-PLGA NPs, S2P-α-13′-COOH PLGA NPs, FITC-S2P-PLGA NPs, RhB-FITC-S2P-PLGA NPs, and RhB-FITC-S2P-α-13′-COOH PLGA NPs was calculated as 17.54 µg/mL, 17.34 µg/mL, 29.09 µg/mL, 13.69 µg/mL, and 15.84 µg/mL, respectively. While the FITC-S2P-PLGA NPs had the highest protein concentration, RhB-FITC-S2P-PLGA NPs had the lowest one. Additionally, the net

protein concentration in S2P-PLGA NPs and S2P-α-13′-COOH PLGA NPs were almost the same with each other. The net protein concentration in RhB-FITC-S2P-PLGA NPs and RhB-FITC-S2P-α-13′-COOH PLGA NPs were also similar to each other.

Table 4. 1. Measured optical density (OD) value, calculated protein concentration, and net protein concentration in NPs.

NPs	OD Value	Calculated Protein Concentration (µg/mL)	Net Protein Concentration (µg/mL)
PLGA NPs	0.10	4.28	-
S2P-PLGA NPs	0.51	21.82	17.54
α-13′-COOH PLGA NPs	0.07	2.99	-
S2P-α-13′-COOH PLGA NPs	0.48	20.33	17.34
FITC-PLGA NPs	0.22	9.29	-
FITC-S2P-PLGA NPs	0.90	38.38	29.09
RhB-FITC-PLGA NPs	0.17	7.28	-
RhB-FITC-S2P-PLGA NPs	0.49	20.97	13.69
RhB-FITC-α-13′-COOH PLGA NPs	0.13	5.56	-
RhB-FITC-S2P-α-13′-COOH PLGA NPs	0.50	21.40	15.84

The amount of α-13′-COOH and GA molecules encapsulated into the non-targeted and targeted NPs were investigated using LC/MS-MS device and total drug concentration and drug EE was calculated as in Table 4.2. Drug EE of non-targeted α-13′-COOH PLGA NPs, RhB-FITC-α-13′-COOH PLGA NPs, and GA-PLGA NPs was calculated as 80.40%, 72.03%, and 20.59%, respectively. After the addition of S2P peptide as a targeting agent, drug EE of S2P-α-13′-COOH PLGA NPs, RhB-FITC-S2P-α-13′-COOH PLGA NPs, and S2P-GA-PLGA NPs was obtained as 80.00%, 75.60%, and 18.82%, respectively as it can be seen in Table 4.2.

Table 4. 2. Total α-13′-COOH and GA concentration and drug EE in NPs.

NPs	Total Drug Concentration (μg/mL)	Drug EE
α-13′-COOH PLGA NPs	201.00	80.40%
S2P-α-13′-COOH PLGA NPs	199.90	80.00%
RhB-FITC-α-13′-COOH PLGA NPs	180.08	72.03%
RhB-FITC-S2P-α-13′-COOH PLGA NPs	188.90	75.60%
GA-PLGA NPs	51.47	20.59%
S2P-GA-PLGA NPs	47.05	18.82%

The release rate of α-13′-COOH from α-13′-COOH PLGA NPs was analysed in both pH 7.4 PBS and pH 5.5 acetate buffer solution. In Figure 4.18, drug release profile from α-13′-COOH PLGA NPs in terms of released drug amount (Figure 4.18A) and drug release percentage (Figure 4.18B) in the range of 0-627h can be seen. Moreover, in order to observe the drug release profile clearly, the release profile in the range of 0-48h was also seen in Figure 4.19. It was observed that drug release percentage from NPs in pH 5.5 solution was higher than the drug release percentage from NPs in pH 7.4 solution. After 48h of incubation, drug release reached almost 60% in pH 5.5 acetate buffer solution while it was around 18% in pH 7.4 PBS solution. Also, after 627h, drug release percentage from NPs was around 75% in pH 5.5 while it was almost 25% in pH 7.4.

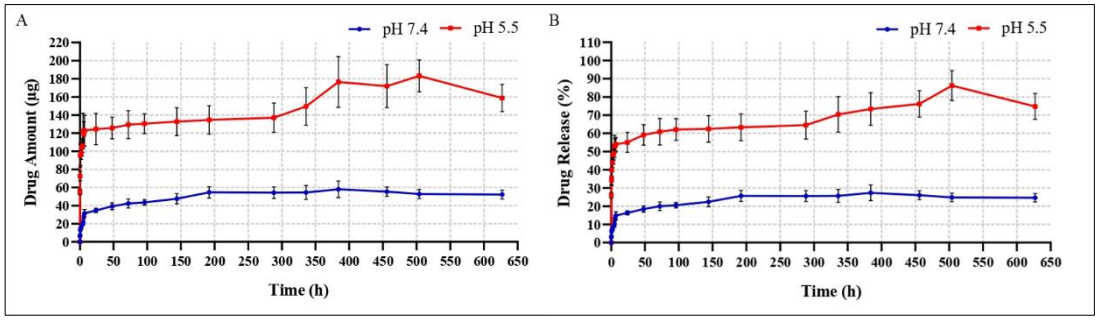

Figure 4. 18. Release profiles after incubation of α-13′-COOH PLGA NPs in pH 7.4 PBS and pH 5.5 acetate buffer solution for certain periods in the range of 0-627h (A) by the amount of drug released, (B) by the percentage of drug released relative to the total amount of drug, n = 3.

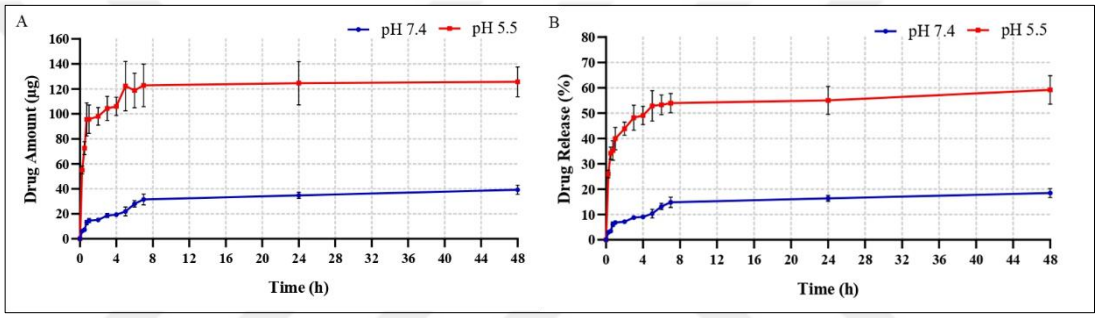

Figure 4. 19. Release profiles after incubation of α-13′-COOH PLGA NPs in pH 7.4 PBS and pH 5.5 acetate buffer solution for certain periods in the range of 0-48h (A) by the amount of drug released, (B) by the percentage of drug released relative to the total amount of drug, n = 3.

Similarly, the release rate of GA from GA-PLGA NPs was analysed in both pH 7.4 PBS and pH 5.5 acetate buffer solution. In Figure 4.20, drug release profile from GA-PLGA NPs in terms of drug release percentage in the range of 0-768h can be seen. It was clear that drug release percentage from NPs in pH 5.5 solution was higher than the one in pH 7.4 solution. At the end of 16th day, drug release was around 64% in pH 5.5 solution while it was around 4% in pH 7.4 solution. Also, after 768h or in other words 32 days, the drug release from GA-PLGA NPs reached almost 77% in pH 5.5 acetate buffer solution. However, at this time, drug release from NPs was around 4% in pH 7.4 PBS solution.

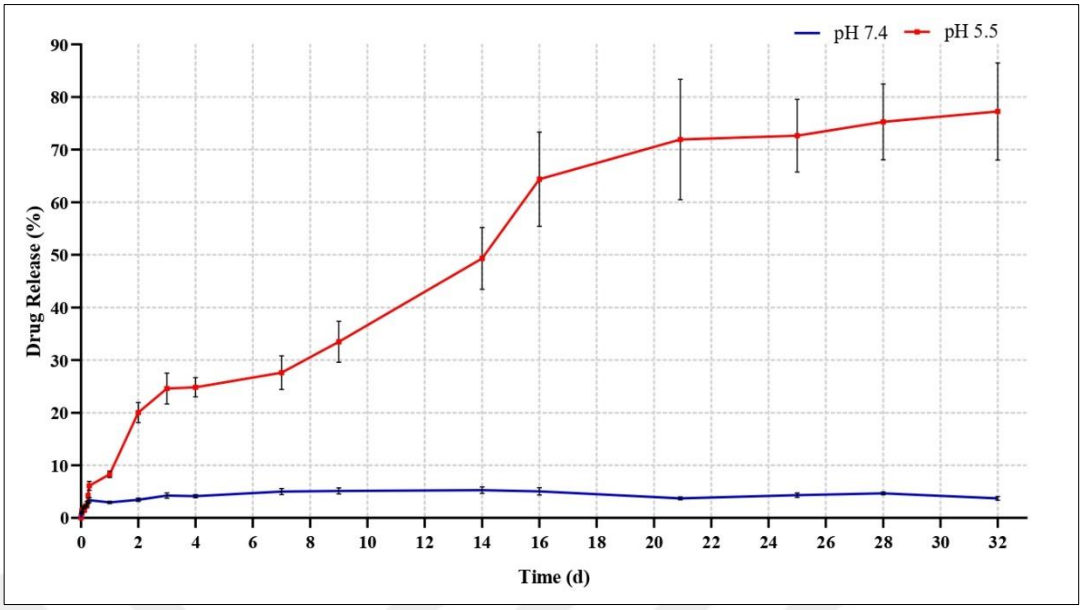

Figure 4. 20. Release profiles after incubation of GA-PLGA NPs in pH 7.4 PBS and pH 5.5 acetate buffer solution for certain periods in the range of 0-32d by the percentage of drug released relative to the total amount of drug, n = 3.

Concentration of FITC fluorescent dye found on the surface of FITC-labelled NPs was investigated by using the calibration curve given in Figure 3.5. The concentration of FITC dye on non-targeted FITC-PLGA NPs, RhB-FITC-PLGA NPs, and RhB-FITC-α-13′-COOH PLGA NPs was calculated as 228.50 µg/mL, 199.33 µg/mL, and 207.67 µg/mL, respectively. However, after the addition of S2P targeting agent, FITC concentration on FITC-S2P-PLGA NPs, RhB-FITC-S2P-PLGA NPs, and RhB-FITC-S2P-α-13′-COOH PLGA NPs was found as 161.83 µg/mL, 182.67 µg/mL, and 170.17 µg/mL, respectively. Although the decrease in the FITC concentration was observed in targeted NPs compared to non-targeted ones, all NPs contained FITC dye with enough amount for visualization.

Table 4. 3. FITC concentration found in NPs.

NPs	Fluorescence Intensity	Concentration (µg/mL)
FITC-PLGA NPs	0.265	228.50
FITC-S2P-PLGA NPs	0.185	161.83
RhB-FITC-PLGA NPs	0.230	199.33
RhB-FITC-S2P-PLGA NPs	0.210	182.67
RhB-FITC-α-13′-COOH PLGA NPs	0.240	207.67
RhB-FITC-S2P-α-13′-COOH PLGA NPs	0.195	170.17

Moreover, RhB was used to synthesize dual-labelled NPs and the concentration of RhB found in NPs was calculated using the calibration curve given in Figure 3.6. The concentration of RhB molecules found in RhB-FITC-PLGA NPs, RhB-FITC-S2P-PLGA NPs, RhB-FITC-α-13′-COOH PLGA NPs, and RhB-FITC-S2P-α-13′-COOH PLGA NPs was calculated as 826.80 µg/mL, 628.80 µg/mL, 718.80 µg/mL, and 646.80 µg/mL, respectively. The decrease was seen in the RhB concentration after the addition of S2P peptide to the NPs.

Table 4. 4. RhB concentration found in NPs.

NPs	Fluorescence Intensity	Concentration (µg/mL)
RhB-FITC-PLGA NPs	0.423	826.80
RhB-FITC-S2P-PLGA NPs	0.324	628.80
RhB-FITC-α-13′-COOH PLGA NPs	0.369	718.80
RhB-FITC-S2P-α-13′-COOH PLGA NPs	0.333	646.80

4.2. Results for Project 2: CS-Coated NPs

4.2.1. Characterization of NPs

After the synthesis of non-coated and coated empty and drug-loaded NPs, their hydrodynamic diameter and PDI values were analysed using DLS to compare how the drug-loading and CS coating effects the NP size and size distribution (Figure 4.21 and Figure 4.22). The hydrodynamic diameter of non-coated PLGA NPs was measured as 219.5 nm as in Figure 4.21A. After the loading of drug molecules, the hydrodynamic diameter of NPs was obtained as 231.4 nm and 204.2 nm for CUR-PLGA NPs (Figure 4.21B) and αTCP-PLGA NPs (Figure 4.21C), respectively. The sizes of these NPs were obtained similar to each other. Moreover, PDI values were obtained between 14.3% and 18.6% while αTCP-PLGA NPs had the lowest PDI value (Figure 4.21).

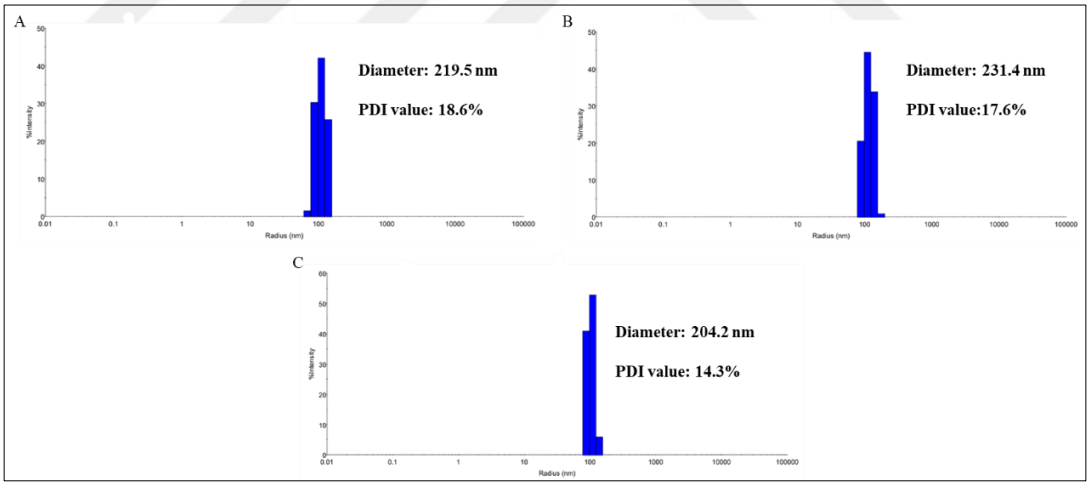

Figure 4. 21. Hydrodynamic diameter and PDI value measurements of non-coated NPs via DLS (A) non-coated PLGA NPs, (B) CUR-PLGA NPs, (C) αTCP-PLGA NPs.

After the CS coating, the hydrodynamic diameter and PDI value of NPs were measured again to observe the effect of coating on NP size. The size of the CS-PLGA NPs, CS-CUR-PLGA NPs, and CS-αTCP-PLGA NPs were obtained as 336.0 nm, 303.1 nm, and 236.5 nm, respectively as it can be seen in Figure 4.22. Compared to

the hydrodynamic diameter of non-coated NPs given in Figure 4.21, the increase in the size was observed after CS coating. Moreover, the PDI values were obtained between 9.4% and 15.8% while CS-PLGA NPs had the lowest PDI value (Figure 4.22).

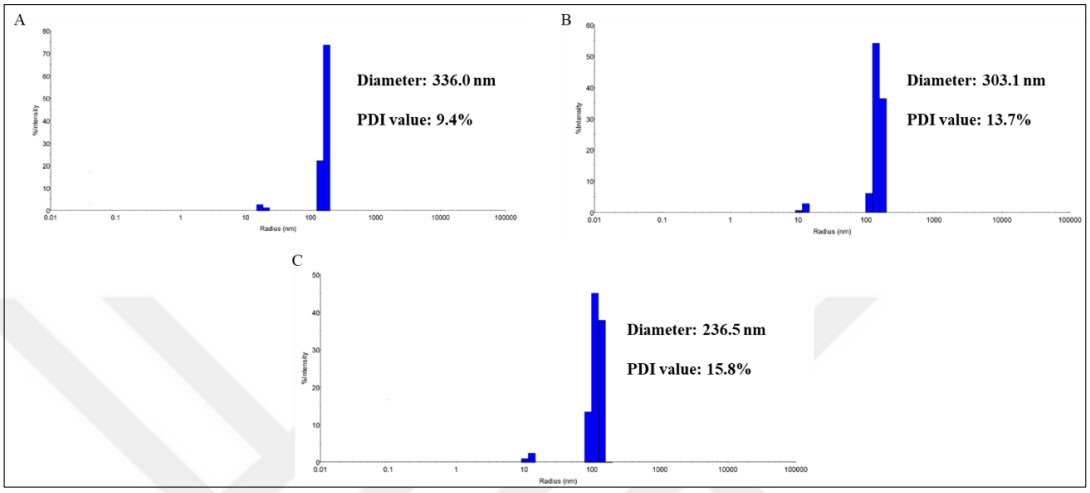

Figure 4. 22. Hydrodynamic diameter and PDI value measurements of CS-coated NPs via DLS (A) CS-PLGA NPs, (B) CS-CUR-PLGA NPs, (C) CS-αTCP-PLGA NPs.

Furthermore, the surface charge of non-coated and CS-coated NPs was measured as in Figure 4.23 and Figure 4.24, respectively. The surface charges of non-coated NPs were obtained as negative which was between -4.80 ± 0.59 mV and -7.11 ± 1.79 mV (Figure 4.23). However, after the coating with CS, the surface charge of NPs was analysed again. The surface charge of non-coated PLGA NPs was -7.11 ± 1.79 mV while it was 6.57 ± 2.8 mV for CS-PLGA NPs. Similarly, the zeta potential value for non-coated CUR-PLGA NPs and αTCP-PLGA NPs was -4.80 ± 0.59 mV and -6.50 ± 0.232 mV, respectively. However, after the coating with positively charged CS, the surface charges of CS-CUR-PLGA NPs and CS-αTCP-PLGA NPs were obtained as 18.8 ± 1.64 mV and 13.2 ± 1.54 mV, respectively. In conclusion, the surface charge of NPs shifted towards positive side (Figure 4.24).

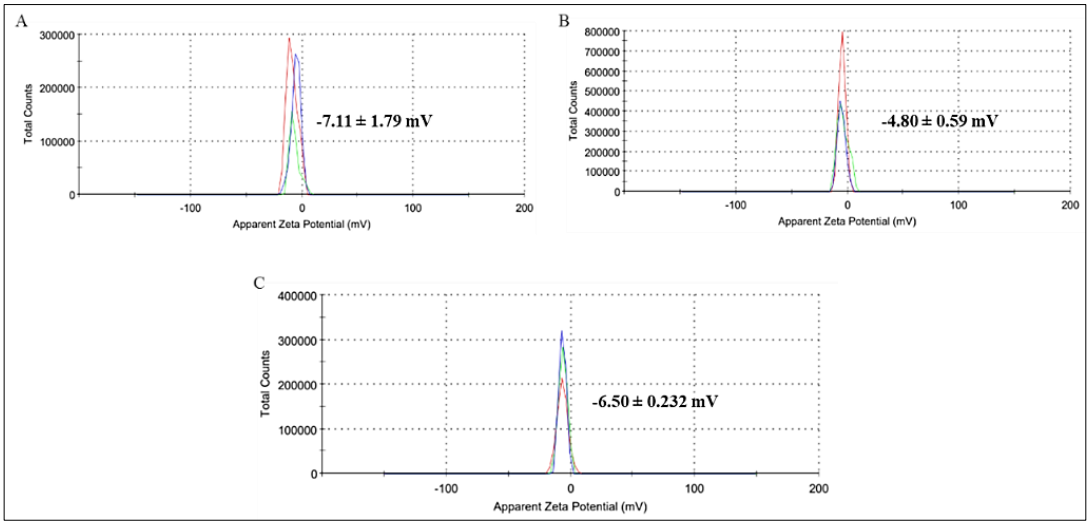

Figure 4. 23. Zeta potential measurements of non-coated NPs (A) non-coated PLGA NPs, (B) CUR-PLGA NPs, (C) αTCP-PLGA NPs.

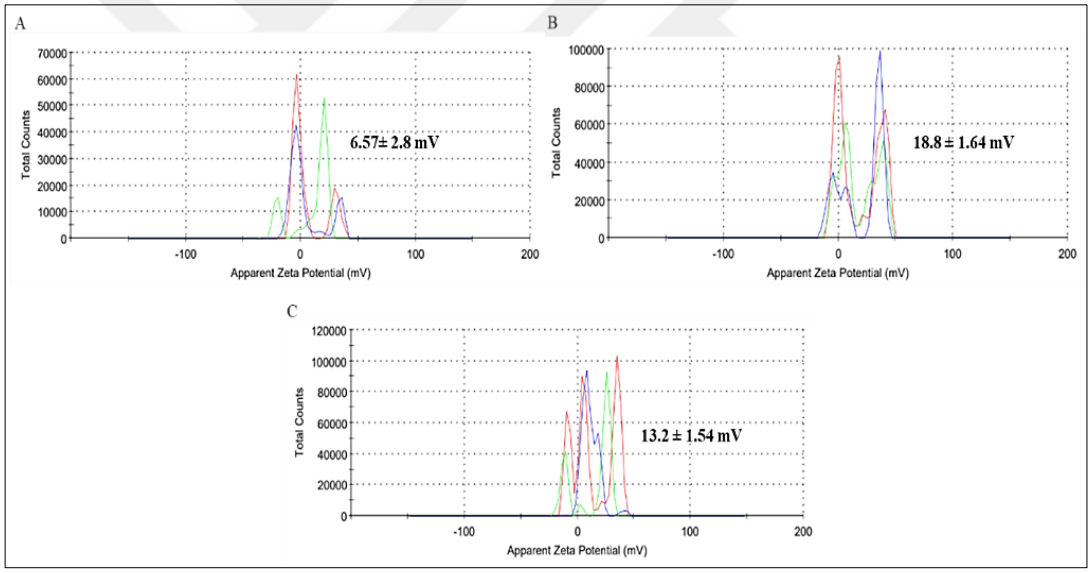

Figure 4. 24. Zeta potential measurements of CS-coated NPs (A) CS-PLGA NPs, (B) CS-CUR-PLGA NPs, (C) CS-αTCP-PLGA NPs.

The surface morphologies of both non-coated and CS-coated empty and drug-loaded NPs were analysed using SEM and the results can be seen in Figure 4.25. The NPs exhibited a surface characterized by its smooth and spherical morphology.

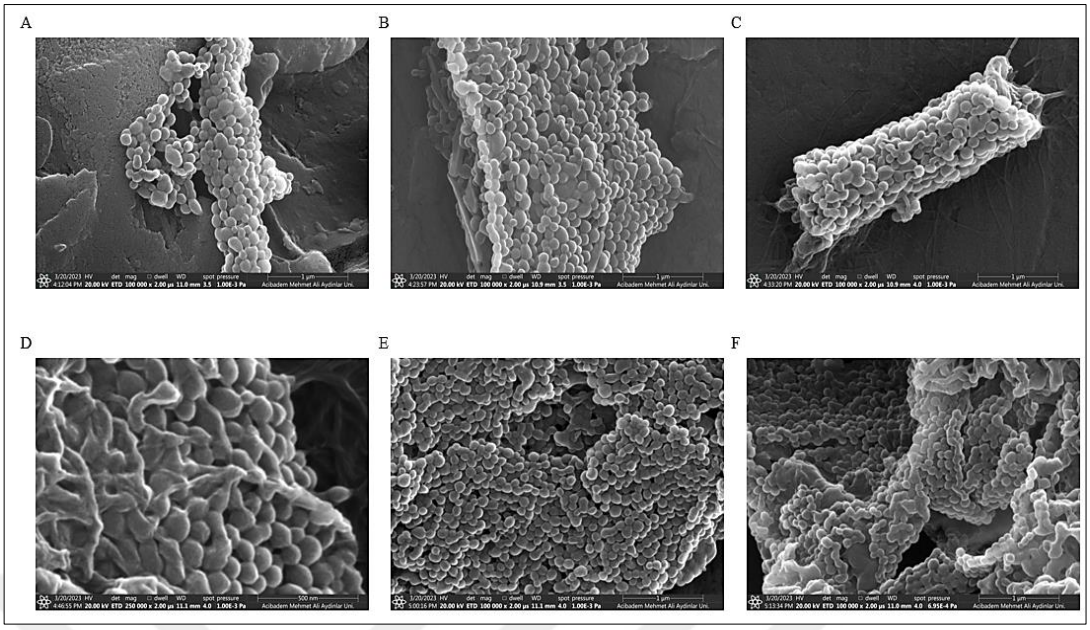

Figure 4. 25. Morphological analysis of NPs via SEM (A) non-coated PLGA NPs, (B) CUR-PLGA NPs, (C) αTCP-PLGA NPs, (D) CS-PLGA NPs, (E) CS-CUR-PLGA NPs, (F) CS-αTCP-PLGA NPs.

Together with all these characterization tests, the stability of non-coated and CS-coated NPs was investigated by incubating them in 1M pH 7.4 PBS at both RT and 37˚C up to several weeks as can be seen in Figure 4.26, Figure 4.27, and Figure 4.28. For all graphs, non-significant p-value ($p > 0.05$) was statistically obtained. First, the results of the stability analysis of non-coated PLGA NPs and CS-PLGA NPs were given in Figure 4.26A and Figure 4.26B, respectively. The hydrodynamic diameter of non-coated PLGA NPs showed some fluctuations during the first 15 min of incubation at both RT and 37˚C. In the long term, the size of non-coated PLGA NPs increased compared to their initial size. Similar fluctuations were observed during the first 15 min of incubation for CS-PLGA NPs. Also, in the long term, the size of CS-PLGA NPs increased compared to their initial size and this was more obvious at RT. At 1.13^{th} day, the increase in the size was observed at RT for CS-PLGA NPs while the increase was observed at 0.17^{th} day at RT for non-coated PLGA NPs. Moreover, the increase in the size was seen at 4^{th} day at 37˚C for CS-PLGA NPs while the increase in the size was observed at 1.13^{th} day at 37˚C for non-coated PLGA NPs. All in all, compared to non-coated PLGA NPs, CS-PLGA NPs showed less fluctuations in their

hydrodynamic diameter measurements, and they were more stable during the incubation, especially at 37˚C compared to non-coated NPs.

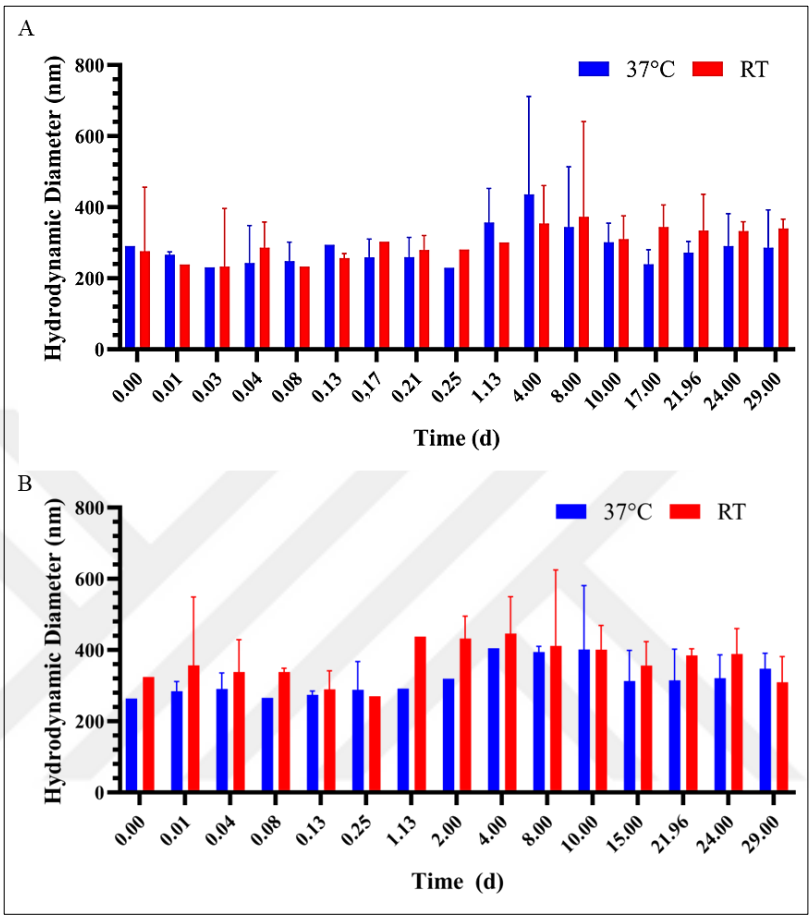

Figure 4. 26. Stability analysis of (A) non-coated PLGA NPs, (B) CS-PLGA NPs, n = 3.

In the same manner, the stability experiments were also conducted for CUR-PLGA NPs and CS-CUR-PLGA NPs as in Figure 4.27A and Figure 4.27B, respectively. For CUR-PLGA NPs, some fluctuations were observed during the first hour of incubation. At 11.13th day, the increase in the size was observed at RT while their hydrodynamic diameter was more stable until 21st day at 37˚C. After 21st day, the decrease in the size was observed. On the other hand, the size of CS-CUR-PLGA NPs were more stable during the first hours of incubation compared to CUR-PLGA NPs. The hydrodynamic diameter values were close to each other even at 28th day at 37˚C. Some fluctuations were seen at RT in the size of CS-CUR-PLGA NPs after 14th day.

All in all, compared to non-coated CUR-PLGA NPs, it was observed that the CS coating improved the stability of CS-CUR-PLGA NPs in the long term.

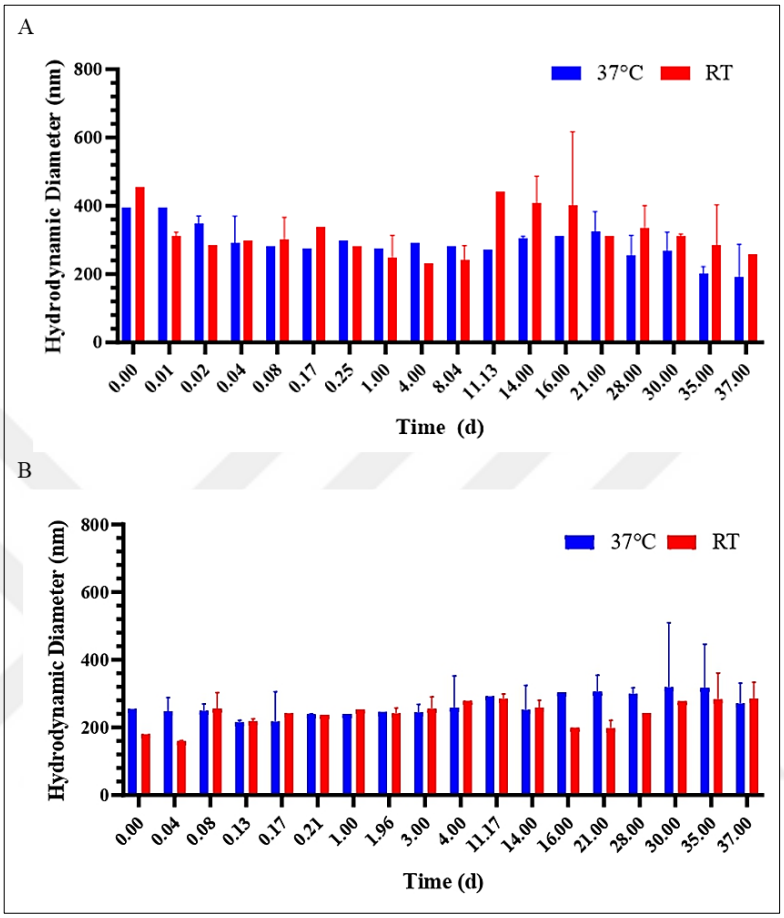

Figure 4. 27. Stability analysis of (A) CUR-PLGA NPs, (B) CS-CUR-PLGA NPs, n = 3.

Finally, the stability analysis was also carried out for αTCP-PLGA NPs and CS-αTCP-PLGA NPs as it can be seen in Figure 4.28A and Figure 4.28B, respectively. For αTCP-PLGA NPs, the hydrodynamic diameter values were similar to each other until 21st day at 37˚C and until 11.13th day at RT. However, for CS-αTCP-PLGA NPs, some fluctuations were observed in the hydrodynamic diameters at RT during first 30 min of incubation. Moreover, the hydrodynamic diameter values were closer to each other until 30th day at 37˚C and until 37th day at RT. Therefore, at the end of this analysis, it was achieved that the CS coating improved the stability of CS-αTCP-PLGA NPs compared to αTCP-PLGA NPs in terms of their hydrodynamic diameters. Also,

drug-loaded CS-CUR-PLGA NPs (Figure 4.27B) and CS-αTCP-PLGA NPs (Figure 4.28B) had enhanced stability in the long term compared to empty CS-PLGA NPs (Figure 4.26B).

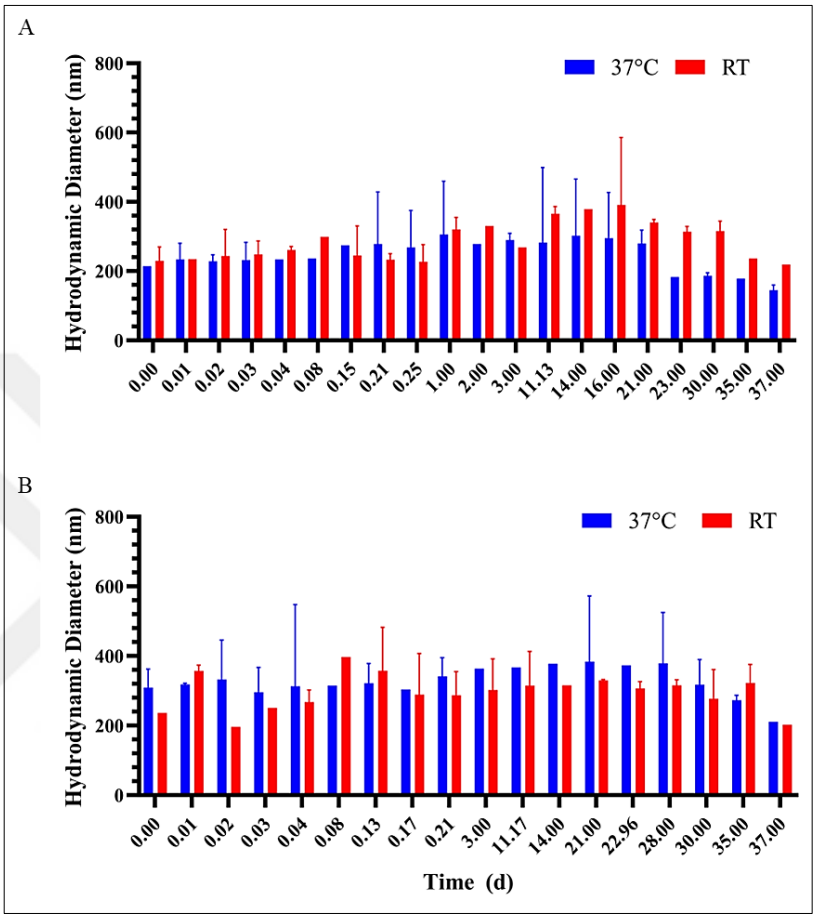

Figure 4. 28. Stability analysis of (A) αTCP-PLGA NPs, (B) CS-αTCP-PLGA NPs, n = 3.

The amount of CUR and αTCP molecules encapsulated into the non-coated and CS-coated NPs were investigated using LC/MS-MS device and total drug concentration and drug EE was calculated as in Table 4.5. Drug EE of CUR-PLGA NPs was calculated as 67.9% and after the coating with CS, the drug EE of CS-CUR-PLGA NPs was obtained as 43.2%. Therefore, the reduction in the EE of CUR was observed after the coating. Moreover, the encapsulation of drug molecules in αTCP-PLGA NPs was found as 78.1% and after the coating with CS, the drug EE of CS-αTCP-PLGA NPs was remained unchanged and obtained as 78.1%.

Table 4. 5. Total CUR and αTCP concentration and drug EE in NPs.

NPs	Total Drug Concentration (μg/mL)	Drug EE
CUR-PLGA NPs	169.7	67.9%
CS-CUR-PLGA NPs	107.9	43.2%
αTCP-PLGA NPs	195.3	78.1%
CS-αTCP-PLGA NPs	195.2	78.1%

The release rate of CUR from CUR-PLGA NPs and CS-CUR-PLGA NPs and the release rate of αTCP from αTCP-PLGA NPs and CS-αTCP-PLGA NPs was analysed in both pH 7.4 PBS and pH 5.5 acetate buffer solution as in Figure 4.29A and Figure 4.29B, respectively. In Figure 4.29, drug release profiles from CUR-loaded NPs and αTCP-loaded NPs were expressed in terms of drug release percentage between 0-110h. At 110^{th} h, almost 100% of CUR was released from CUR-PLGA NPs at pH 5.5 while around 45% of drug was released from these NPs at pH 7.4. Therefore, drug release percentage from CUR-PLGA NPs was faster at pH 5.5 compared to the drug release percentage from those NPs at pH 7.4. Similarly, at 110^{th} h, almost 88% CUR was released from CS-CUR-PLGA NPs at pH 5.5 while around 24% drug was released from these NPs at pH 7.4. In conclusion, drug release from CUR-PLGA NPs and CS-CUR-PLGA NPs was faster at pH 5.5 than the drug release at pH 7.4. Furthermore, considering the drug release percentage at both pH 5.5 and pH 7.4, the release of CUR from CS-coated NPs was slower than the release of CUR from non-coated NPs as in Figure 4.29A. Furthermore, it can be seen from Figure 4.29B that, at 110^{th} h, almost 75% drug was released from αTCP-PLGA NPs at pH 5.5 while around 23% was released from those NPs at pH 7.4. Also, around 60% drug was released from CS-αTCP-PLGA NPs at pH 5.5 while the release percentage was almost 15% for CS-αTCP-PLGA NPs at pH 7.4. Therefore, the release of αTCP from both non-coated and CS-coated NPs was faster at pH 5.5 than its release at pH 7.4. Moreover, considering the drug release percentage at both pH 5.5 and pH 7.4, the release of αTCP from CS-coated NPs was slower than the release of αTCP from non-coated NPs as in Figure

4.29B. All in all, CS coating prolonged the release rate of CUR and αTCP at both pH 7.4 and pH 5.5 compared to non-coated NPs. Also, the drug release at pH 5.5 was faster than the drug release at pH 7.4.

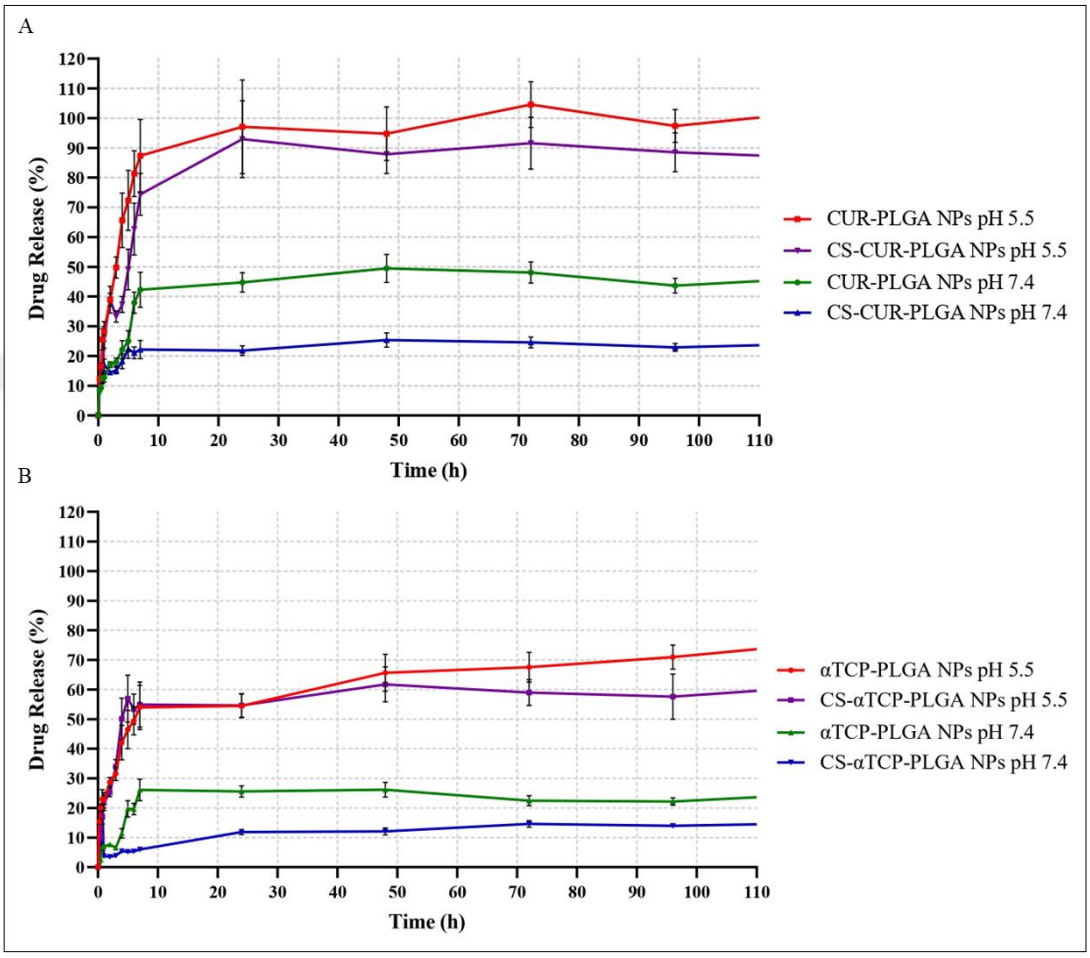

Figure 4. 29. Release profiles of NPs after incubation in pH 7.4 PBS and pH 5.5 acetate buffer solution for certain periods in the range of 0-110h (A) CUR-loaded NPs, (B) αTCP-loaded NPs, n = 3.

4.3. Results for Project 3: Mitochondria-Targeted NPs

4.3.1. Characterization of targeting agents

4.3.1.1. TT80

One of the targeting agents, TT80 conjugate, was synthesized in the laboratory as explained in Section 3.2.3.2. It was purified from impurities using a prep-HPLC device (Figure 4.30). To actualize this, TT80 was dissolved in DMSO and injected into the hydrophobic C18 column. One of the mobile phases was ddH_2O with 0.025% TFA and the other one was ACN with 0.025% TFA. TT80 conjugate was first run at 100% ddH_2O for 2 min and then increased linearly from 0% ACN to 100% ACN. Finally, 100% ACN was applied for last 2 min. The peaks labelled as 15, 16, and 17 were coming from DMSO. However, the peaks that were labelled as 19, 20, 21, 22, 23, and 24 indicated the relevant pure peaks of TT80 conjugate. The samples coming from these peaks were collected and lyophilized for future use as a targeting agent after removing the excess ACN using rotary evaporator.

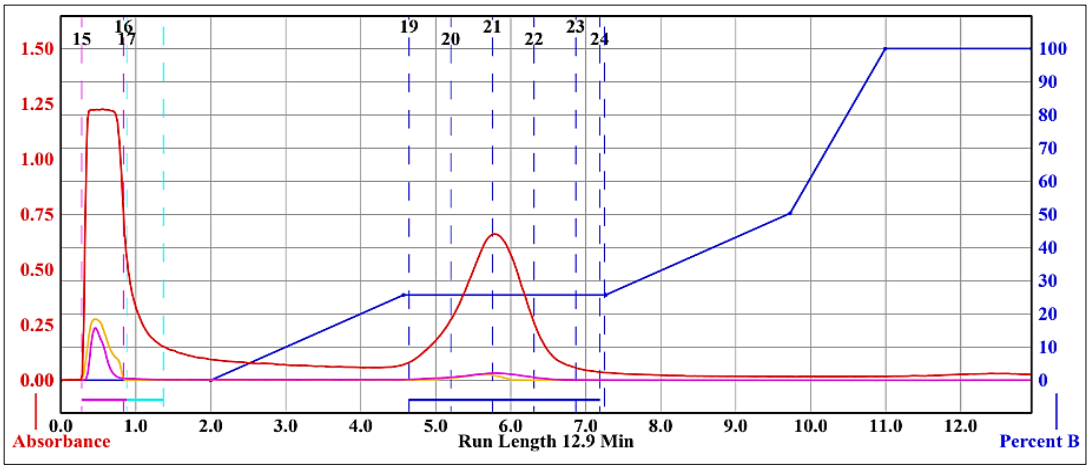

Figure 4. 30. Prep-HPLC analysis of TT80 conjugate conducted for purification.

The chemical characterization of the purified TT80 conjugate was conducted using an LC/MS-MS device. The analysis employed a mobile phase comprising 50% ddH_2O and 50% ACN, with the addition of 0.05% formic acid. The flow rate was adjusted to 0.5 mL/min. Theoretically, the MW of TT80 conjugate was stated as 1703.2 g/mol. In the obtained scan spectrum (Figure 4.31), the molecular ion peak of the TT80 conjugate, along with that of formic acid, was observed at 1409.50. Moreover, due to conducting the assay in formic acid, +2 and +4 ions were also observed at 734.40 and 406.00, respectively. Overall, the close correspondence of these results with expectations indicates the proper synthesis of this conjugate.

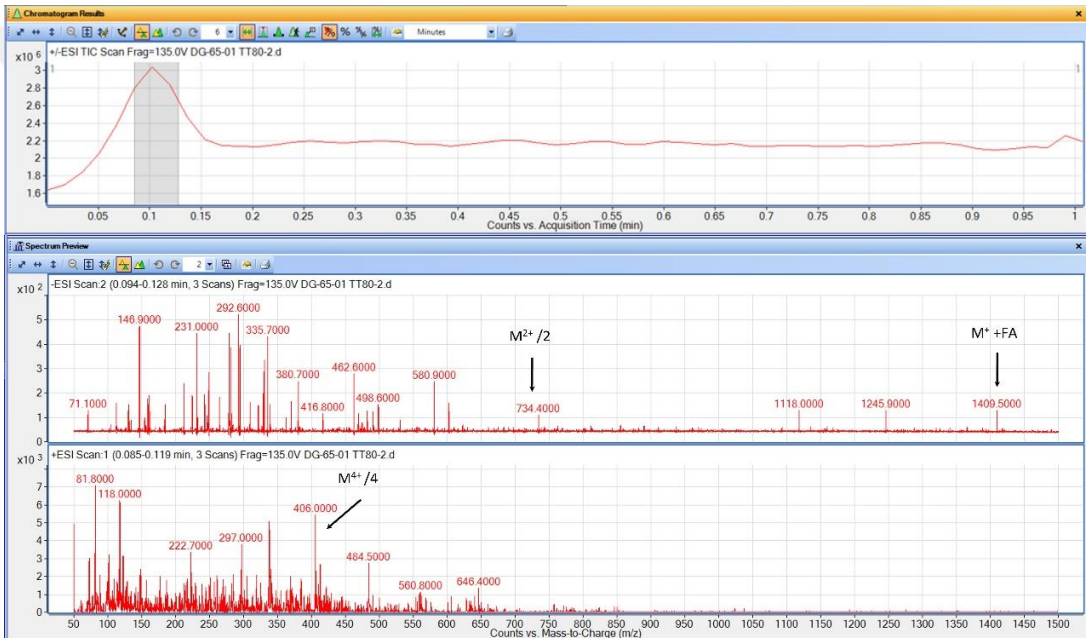

Figure 4. 31. LC/MS-MS analysis of TT80 conjugate.

Moreover, the chemical structure of the TT80 conjugate was characterized using ^{1}H NMR in deuterated chloroform ($CDCl_3$) and the obtained result was depicted in Figure 4.32. The aromatic protons of TPP molecule were seen at 7.67-7.84 ppm, while the -CH_2 protons of PEG polymers found in the structure of Tween80 appeared at 3.56-3.84 ppm. Additionally, the -CH_2 and -CH_3 protons of the aliphatic chains in Tween80 were observed at 1.82-2.28 ppm. Also, the $CDCl_3$ protons were detected at 7.24 ppm. All in all, ^{1}H NMR spectrum of the TT80 conjugate confirmed the presence of both TPP and Tween80 in its structure.

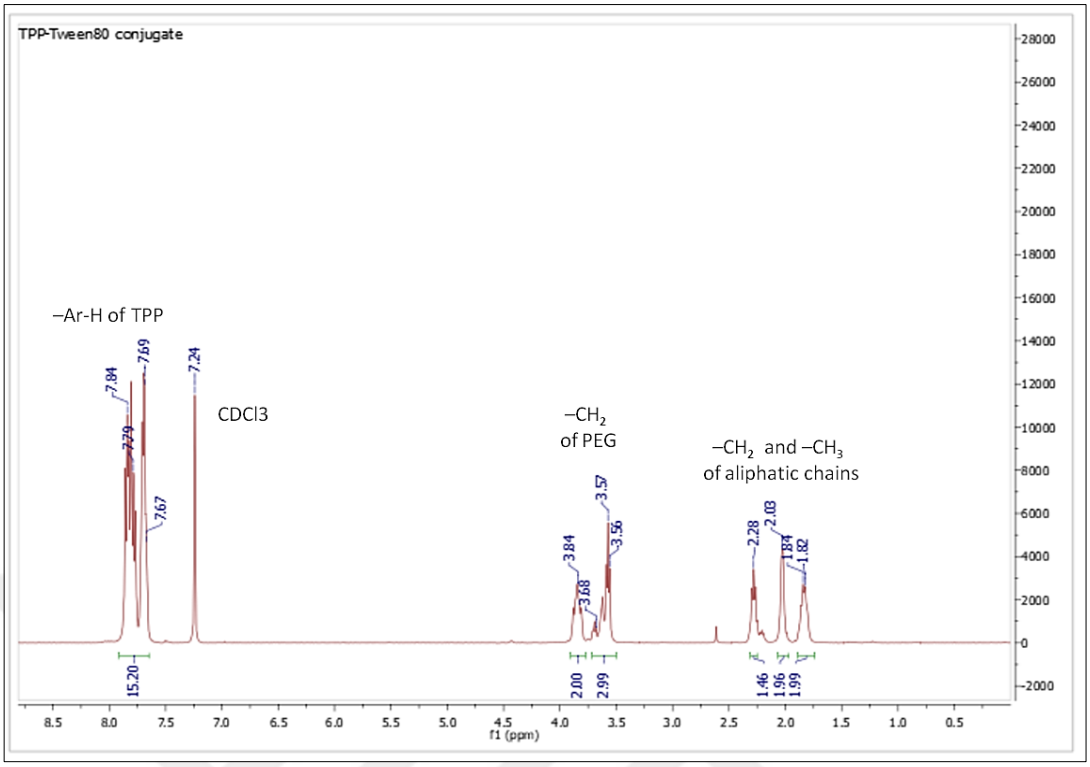

Figure 4. 32. ^{1}H NMR spectrum of the TT80 conjugate.

In order to prove the presence of the characteristic peaks coming from both TPP and Tween80 molecule in TT80 conjugate, the FT-IR analysis was conducted for TPP-Br, Tween80, and TT80 as it can be seen in Figure 4.33A, Figure 4.33B, and Figure 4.33C, respectively. In the FT-IR spectrum of TPP-Br (Figure 4.33A), the C=C stretching peak was observed at 1586.60 cm^{-1} while the P=O stretching peak was observed at 1278.30 cm^{-1}. At 1108.22 cm^{-1}, C-O-C asymmetrical stretching peak was seen. In addition to these, P-O stretching peak was obtained at 983.97 cm^{-1} and 994.40 cm^{-1}. Also, between 688.82 cm^{-1} and 766.98 cm^{-1}, the phenyl ring of TPP was observed. Moreover, in the FT-IR spectrum of Tween80 as in Figure 4.33B, O-H stretching peak was seen at 3843.47 cm^{-1} while the peaks observed at 2856.78 cm^{-1} and 2921.36 cm^{-1} were C-H stretching bonds. Also, a characteristic peak of the Tween80 was seen at 1735.13 cm^{-1} which was assigned to the C=O group. C-H bending peak was observed at 1457.43 cm^{-1} while C-O stretching peaks was seen at 1247.82 cm^{-1} and 1094.43 cm^{-1}. Lastly, the C-O-C symmetrical stretching peak was seen at 946.61 cm^{-1}. In the FT-IR spectrum of TT80 conjugate (Figure 4.33C), the peaks coming from both TPP molecule and Tween80 was observed. The peaks

between 2932.66 cm^{-1} and 2793.01 cm^{-1} were similar to the peaks obtained between 2932.66 cm^{-1} and 2790.52 cm^{-1} for TPP-Br. Also, some other characteristic peaks of TPP such as the C=C stretching peak, P=O stretching peak, and C-O-C asymmetrical stretching peak was obtained at 1586.64 cm^{-1}, 1278.30 cm^{-1}, and 1107.74 cm^{-1}, respectively similar to the those obtained for TPP-Br as in Figure 4.33A. In addition, P-O stretching peak was observed at 984.26 cm^{-1} and 996.21 cm^{-1}. Also, between 688.90 cm^{-1} and 765.42 cm^{-1}, the phenyl ring of TPP was observed. Moreover, some of the characteristic peaks that were coming from the structure of Tween80 was observed in the FT-IR spectrum of TT80. For example, O-H stretching peak and C-O stretching peak was observed at 3395.26 cm^{-1} and 1082.27 cm^{-1}, respectively.

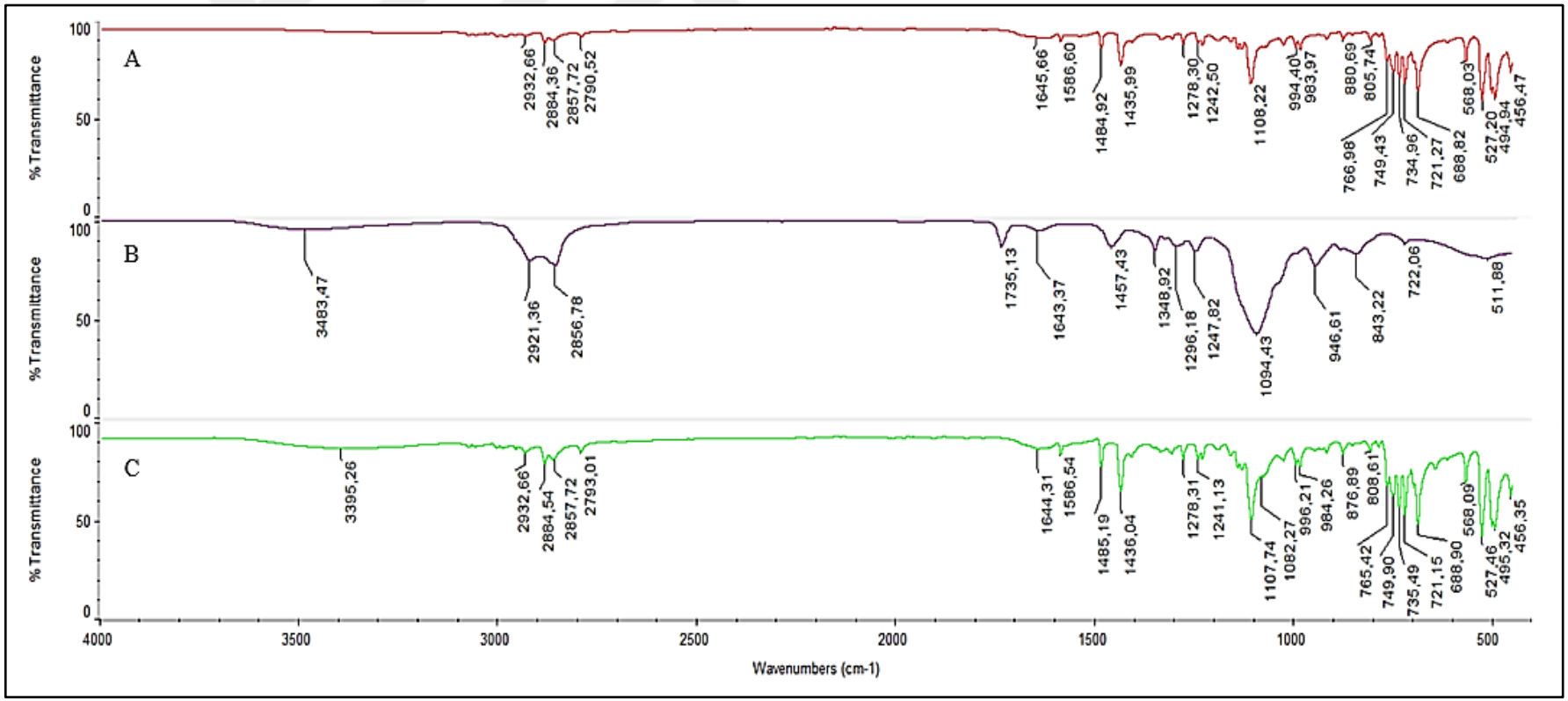

Figure 4. 33. FT-IR spectra of (A) TPP-Br, (B) Tween80, (C) TT80.

4.3.1.2. PPT

As another mitochondrial targeting agent, PPT conjugate was synthesized in the laboratory and some analyses were carried out for its characterization. First of all, before the synthesis of PPT conjugate, PLGA-PEG copolymer was synthesized in the laboratory as it was explained in Section 3.2.3.3. FT-IR analysis was carried out for PLGA-PEG together with its precursor polymers which were PLGA and PEG to understand whether the conjugation was achieved or not as in Figure 4.34. In the FT-IR spectrum of PLGA in Figure 4.34A, O-H stretching peak was obtained at 3507.39 cm^{-1}. The peaks between 2900.56 and 2995.49 belonged to the C-H stretching bonds. Moreover, C=O stretching bond was seen at 1745.47 cm^{-1} and the peak at 1450.74 cm^{-1} attributed to C-H bending. C-O stretching bond was observed between 1048.42 cm^{-1} and 1182.48 cm^{-1}. Furthermore, in the FT-IR spectrum of PEG in Figure 4.34B, the peak at 3411.89 cm^{-1} indicated the O-H stretching bond while the peaks between 2860.25 cm^{-1} and 2948.17 cm^{-1} belonged to the C-H stretching vibrations of the $-CH_2$ group. Also, C-H bending peak was seen at 1466.29 cm^{-1} and 1454.71 cm^{-1}. The C-O stretching bond was observed between and 1059.46 cm^{-1} and 1146.59 cm^{-1}. When the FT-IR spectrum of PLGA-PEG (Figure 4.34C) compared with its precursor molecules, it was observed that the characteristic functional groups of both PLGA and PEG revealed in its spectrum. O-H stretching peak was obtained at 3508.39 cm^{-1} while C-H stretching peak was seen between 2945.58 cm^{-1} and 2995.48 cm^{-1}. As a result of conjugation, slight shift was observed in these peaks compared to pure PLGA and PEG molecules. The C=O stretching bond coming from the PLGA polymer was also seen in the FT-IR spectrum of PLGA-PEG at 1746.74. cm^{-1}. Also, C-H bending peak was observed at 1452.16 cm^{-1} and 1423.88 cm^{-1} similar to both PLGA and PEG. All in all, the characteristic functional groups of PLGA and PEG were both observed in the FT-IR spectrum of PLGA-PEG conjugate. Also, the chemical structure of PLGA-PEG copolymer was characterized using ^1H NMR as depicted in Figure 4.35.

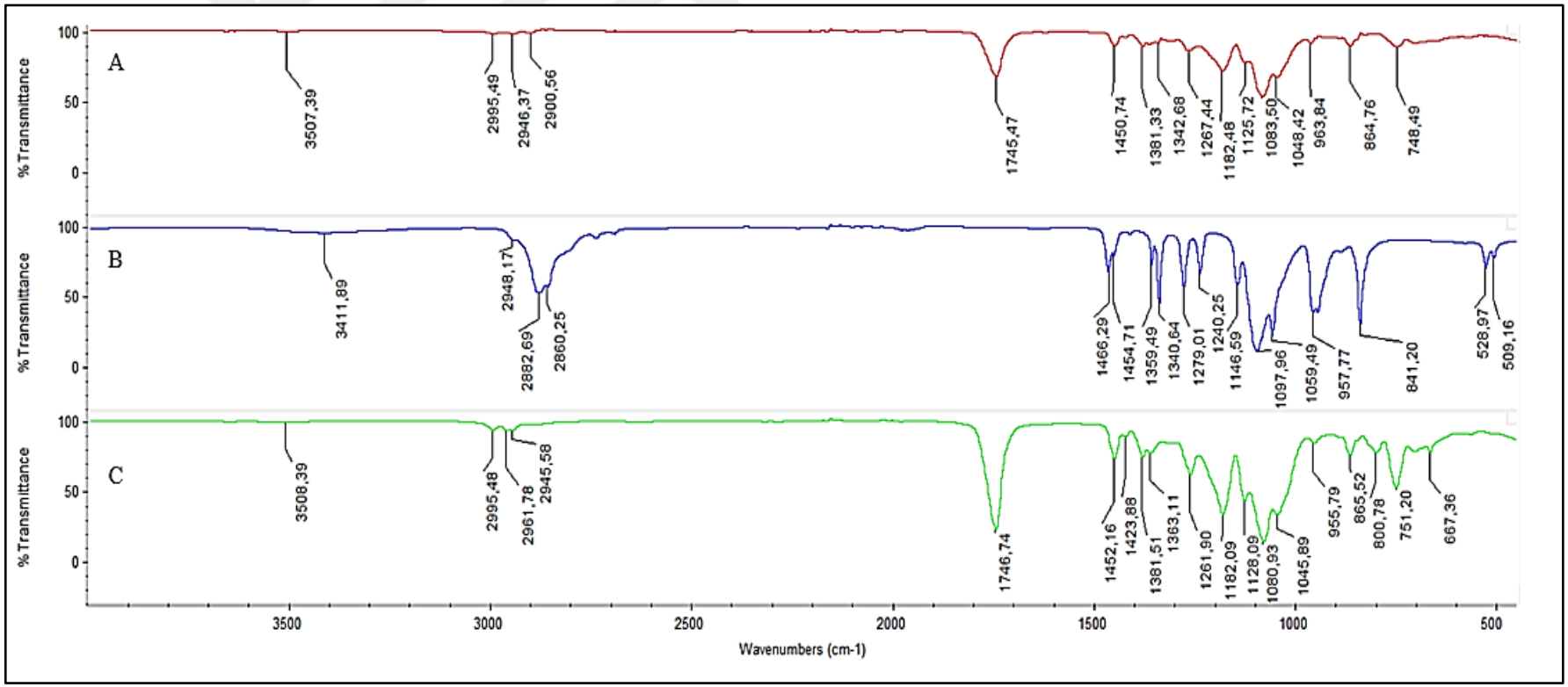

Figure 4. 34. FT-IR spectra of (A) PLGA, (B) PEG, (C) PLGA-PEG.

After that, PPT was synthesized as another mitochondrial targeting agent by using TPP-Br and PLGA-PEG as it was explained in Section 3.2.3.3. The chemical structure of PLGA polymer, PLGA-PEG copolymer, and PPT conjugate was analysed via ^{1}H NMR spectroscopy in $CDCl_3$, and their spectra were depicted in Figure 4.35. First of all, in the ^{1}H NMR spectrum of the PLGA polymer (Figure 4.35A) which has carboxylic acid at the end, -CH and -CH_2 protons and -CH_3 protons of PLGA polymer was obtained around 4.50-5.50 ppm and 1.25-1.75 ppm, respectively. Also, the $CDCl_3$ protons was seen approximately at 7.25 ppm. Furthermore, in the ^{1}H NMR spectrum of the PLGA-PEG copolymer (Figure 4.35B), the relevant protons of the PLGA polymer, namely -CH and -CH_2 and -CH_3 protons, and the protons of $CDCl_3$ were again observed at similar ppm values. However, -CH_2 protons of PEG polymer was additionally seen around 3.25-4.00 ppm. Finally, the chemical structure of synthesized PPT conjugate was analysed by ^{1}H NMR spectroscopy and its spectrum can be seen at Figure 4.35C. The relevant protons of PLGA and PEG polymers found in the spectrum of PLGA-PEG copolymer were obtained at similar ppm values with slight shifts in the ^{1}H NMR spectrum of PPT. For example, the $CDCl_3$ protons was seen around 7.25-7.5 ppm and -CH_2 protons of PEG polymer was obtained around 3.50-4.00 ppm. Together with these, the addition of the TPP molecule resulted in the PPT conjugate exhibiting characteristic protons coming from TPP. For example, the aromatic protons of TPP molecule were seen around 6.50-7.50 ppm and -CH_2 protons found next to TPP was observed around 0.75-1.25 ppm. At the end, the presence of protons coming from all precursor components, including PLGA, PEG, and TPP, confirms the successful synthesis of the PPT conjugate in the laboratory.

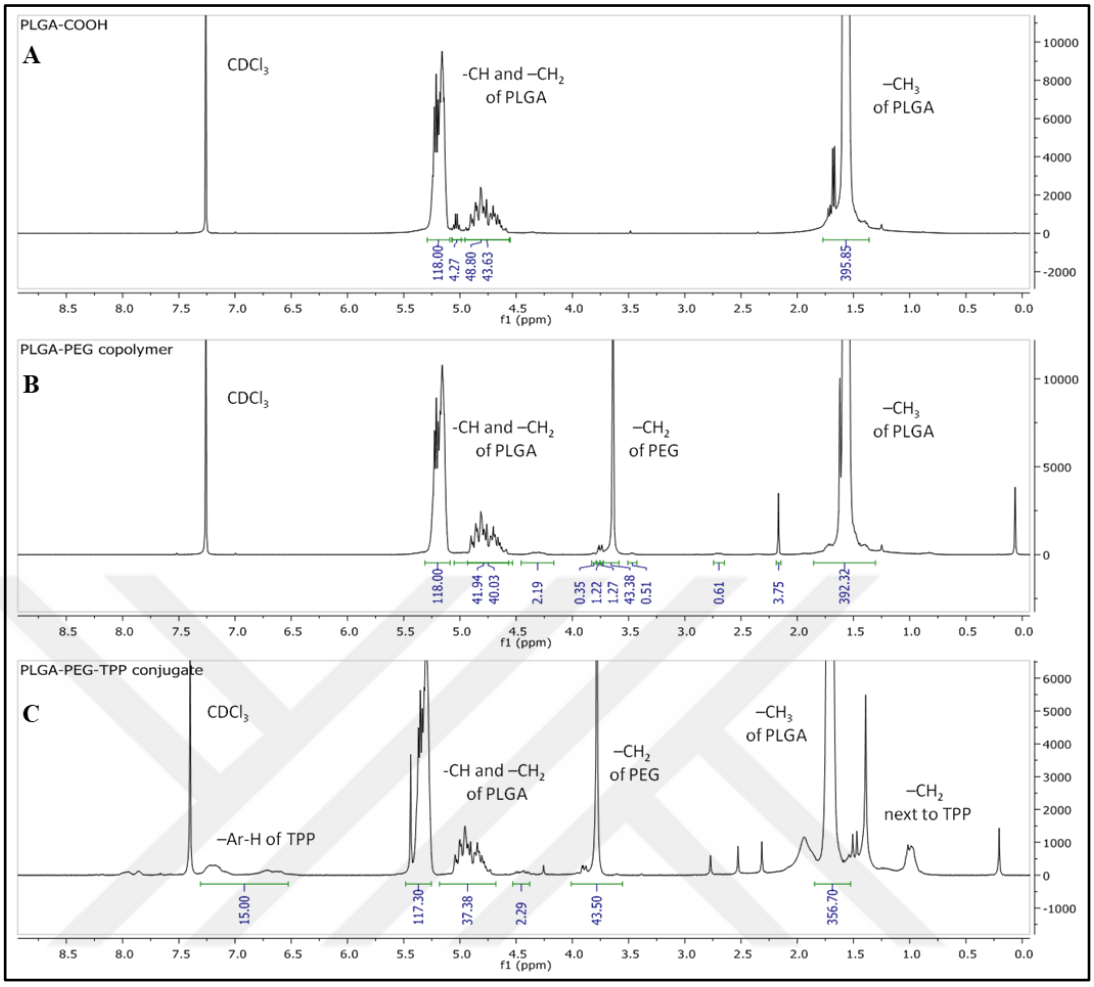

Figure 4. 35. ^{1}H NMR spectrum of the (A) PLGA-COOH, (B) PLGA-PEG copolymer, (C) PPT conjugate.

The FT-IR analysis was conducted for TPP-Br, PLGA-PEG, and PPT conjugate as in Figure 4.36 to prove the presence of the characteristic peaks of precursors in the structure of PPT conjugate. In the FT-IR spectrum of TPP-Br as in Figure 4.36A, the C-H stretching peak was seen at 2790.52 cm^{-1}, 2857.72 cm^{-1}, 2884.36 cm^{-1}, and 2932.66 cm^{-1}. Similarly, in the FT-IR spectrum of PLGA-PEG in Figure 4.36B, the O-H stretching peak was observed at 3508.39 cm^{-1} while C-H stretching peak was seen at 2945.58 cm^{-1}, 2961.78 cm^{-1}, and 2995.48 cm^{-1}. Also, C=O stretching bond was observed at 1746.74 cm^{-1}. Moreover, in the FT-IR spectrum of PPT in Figure 4.36C, the O-H stretching peak coming from the PLGA-PEG conjugate was observed at 3509.19 cm^{-1}. The C-H stretching peaks seen in the FT-IR spectrum of PPT conjugate were coming from both TPP-Br and PLGA-PEG. For example, the C-H stretching

peak observed at 2995.01 cm^{-1} was similar to the ones obtained for PLGA-PEG conjugate at 2995.48 cm^{-1}. Similarly, The C-H stretching peaks at 2853.13 cm^{-1} and 2922.60 cm^{-1} were similar to the peaks observed for TPP-Br at 2857.12 cm^{-1} and 2932.66 cm^{-1}. Finally, the C=O stretching bond seen in the structure of PLGA-PEG conjugate at 1746.74 cm^{-1} was also seen in the structure of PPT conjugate at 1747.11 cm^{-1}. All in all, the characteristic functional groups of TPP and PLGA-PEG were both observed in the FT-IR spectrum of PPT conjugate.

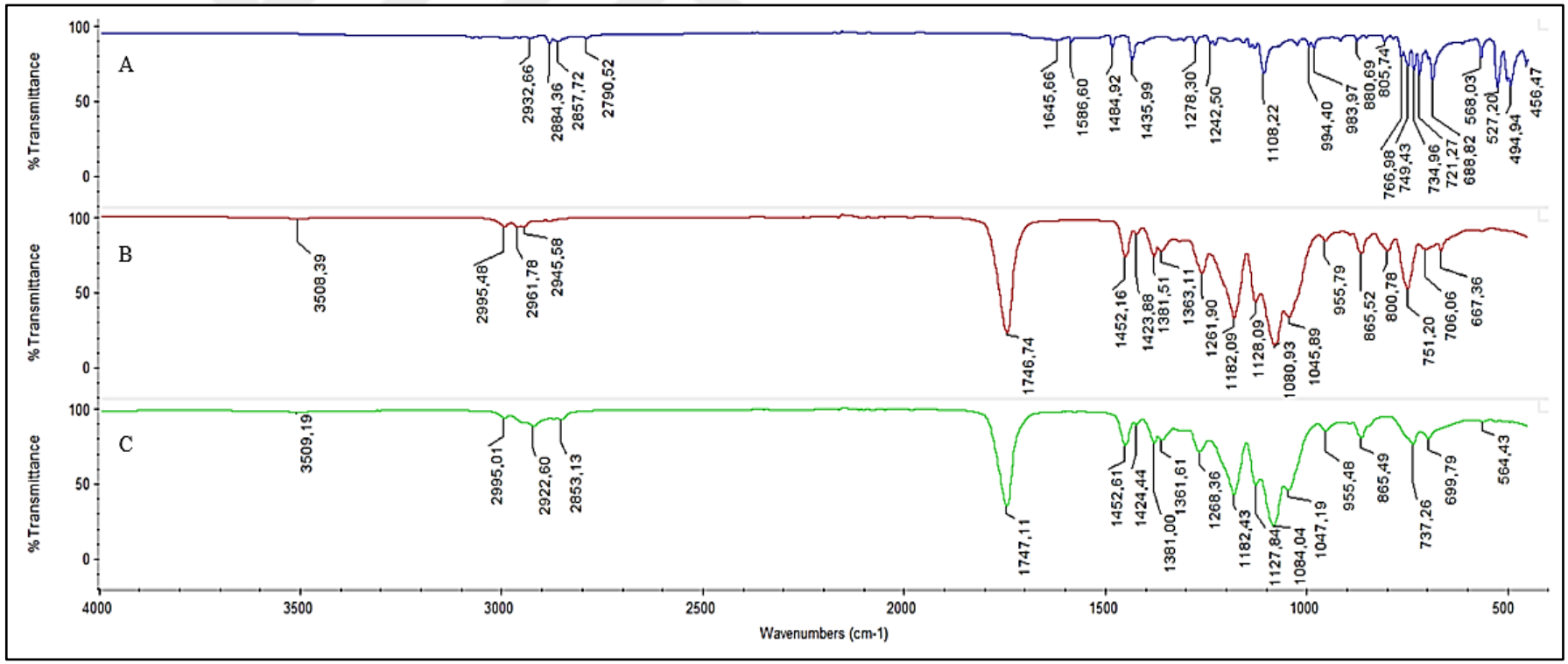

Figure 4. 36. FT-IR spectra of (A) TPP-Br, (B) PLGA-PEG, (C) PPT.

4.3.2. Characterization of NPs

After the synthesis of NPs for the project entitled as "Preparation and *in vitro* evaluation of mitochondria-targeted QCT loaded PLGA NPs for the treatment of oxidative stress-induced inflammation", the hydrodynamic diameter and PDI values of NPs were measured using DLS. First, DLS analysis was conducted for non-targeted NPs as in Figure 4.37. The size of non-targeted PLGA NPs (Figure 4.37A) and OCT-PLGA NPs (Figure 4.37B) was obtained similar to each other and their size were 213.5 nm and 206.5 nm, respectively. Moreover, the PDI value of non-targeted PLGA NPs was obtained as 9.2% which was lower than the PDI value of QCT-PLGA NPs.

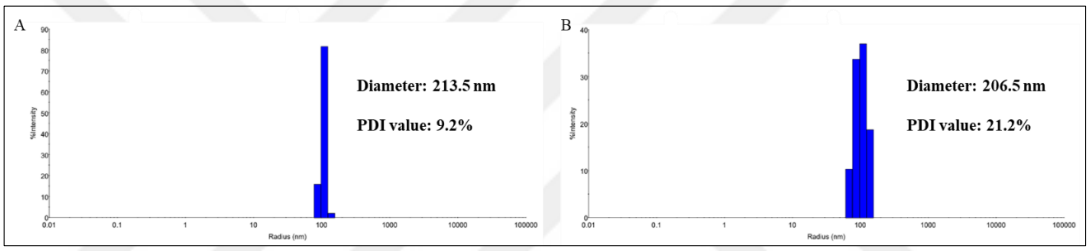

Figure 4. 37. Hydrodynamic diameter and PDI value measurements of non-targeted NPs via DLS (A) non-targeted PLGA NPs, (B) QCT-PLGA NPs.

After the synthesis of non-targeted NPs, targeted empty and QCT-loaded NPs were synthesized using 10% and 20% TT80 by weight as a targeting agent. DLS analysis was also conducted for these NPs as can be seen in Figure 38. The hydrodynamic diameter of 10%TT80-PLGA NPs was measured as 180.2 nm with a PDI value of 9.2% as in Figure 4.38A while the size of 10%TT80-QCT-PLGA NPs was 188.2 nm with a PDI value of 11.9% as it can be seen in Figure 4.38B. All in all, after drug loading, the hydrodynamic diameter and PDI value of 10%TT80-QCT-PLGA NPs were obtained slightly higher than the size and PDI value of 10%TT80-PLGA NPs. For 20%TT80-PLGA NPs and 20%TT80-QCT-PLGA NPs, the hydrodynamic diameter was measured as 204.7 nm and 145.9 nm, respectively. After drug loading, the decrease in the size was observed. However, PDI values of

20%TT80-PLGA NPs and 20%TT80-QCT-PLGA NPs were found as 10.6% and 10.9%, respectively which were almost the same.

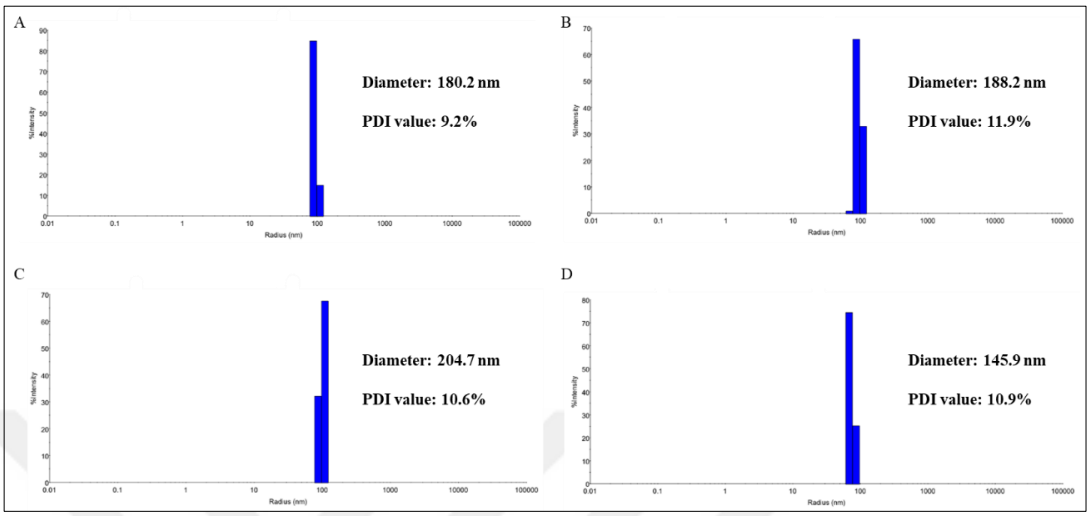

Figure 4. 38. Hydrodynamic diameter and PDI value measurement of targeted NPs via DLS (A) 10%TT80-PLGA NPs, (B) 10%TT80-QCT-PLGA NPs, (C) 20%TT80-PLGA NPs, (D) 20%TT80-QCT-PLGA NPs.

Also, 1.25% and 2.50% PPT by weight was used as a targeting agent and targeted NPs were synthesized using PPT to compare its effects with TT80 that was used as another targeting agent. TPP amount found in 1.25% and 2.50% PPT-conjugated NPs were the equivalents of the TPP amount found in 10% and 20% TT80-conjugated NPs, respectively. First of all, the hydrodynamic diameter of 1.25%PPT-PLGA NPs and 1.25%PPT-QCT-PLGA NPs was measured as 138.5 nm with a PDI value of 9.0% and 149.5 nm with a PDI value of 16.1%, respectively. It can be concluded that a slight increase was observed in the size of the NPs after drug loading while the increase in the PDI value was more obvious. Moreover, the hydrodynamic diameter of 2.50%PPT-PLGA NPs was obtained as 139.5 nm with a PDI value of 7.1%. After drug loading, the size of the 2.50%PPT-QCT-PLGA NPs was measured as 165.7 nm with a PDI value of 19.0%. In this case, drug loading caused an increase in both hydrodynamic diameter and PDI value (Figure 39).

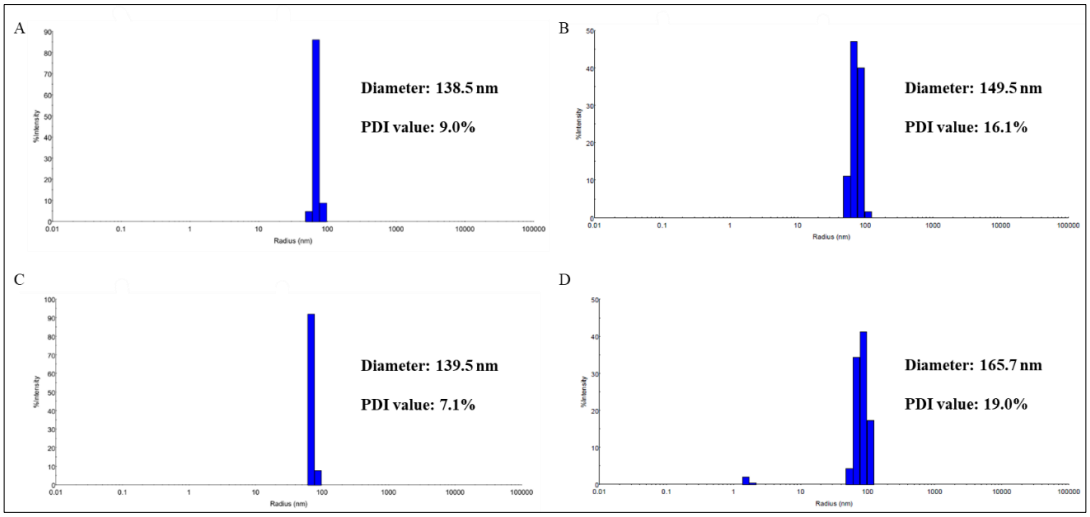

Figure 4. 39. Hydrodynamic diameter and PDI value measurement of targeted NPs via DLS (A) 1.25%PPT-PLGA NPs, (B) 1.25%PPT-QCT-PLGA NPs, (C) 2.50%PPT-PLGA NPs, (D) 2.50%PPT-QCT-PLGA NPs.

Furthermore, the surface charge of NPs was measured as it can be seen in Figure 4.40, Figure 4.41, and Figure 4.42. The zeta potential of non-targeted PLGA NPs was obtained as -13.1 ± 2.12 mV as in Figure 4.40A while the zeta potential of OCT-PLGA NPs was found as -15.1 ± 1.79 mV as in Figure 4.40B. Therefore, the surface charge of non-targeted empty and drug-loaded NPs was obtained negative and similar to each other.

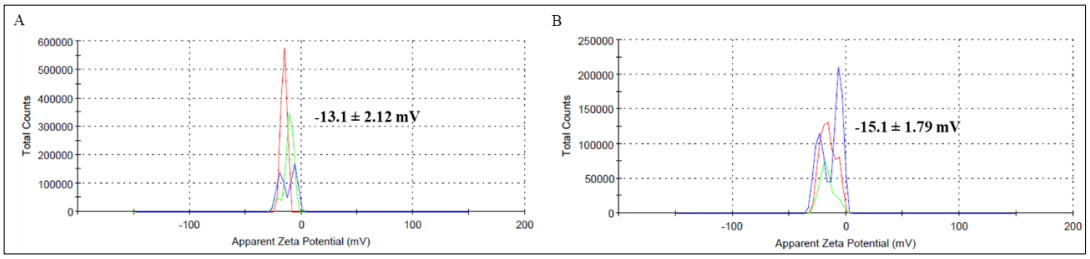

Figure 4. 40. Zeta potential measurements of non-targeted NPs (A) non-targeted PLGA NPs, (B) QCT-PLGA NPs.

After conjugating 10% and 20% TT80 by weight as a targeting agent, zeta potential values of NPs were measured again to determine whether the targeting was achieved or not as it can be seen in Figure 4.41. After conjugating positively charged TPP molecule, the surface charge of 10%TT80-PLGA NPs and 20%TT80-PLGA NPs

was found as -5.22 ± 0.581 mV and -2.99 ± 1.19 mV, respectively while the non-targeted PLGA NPs had a surface charge of -13.1 ± 2.12 mV (Figure 4.40A). Moreover, after encapsulating QCT as a drug molecule, the zeta potential of 10%TT80-QCT-PLGA NPs and 20%TT80-QCT-PLGA NPs was measured as -2.34 ± 0.35 mV and -11.8 ± 2.48 mV, respectively while the surface charge of QCT-PLGA NPs was -15.1 ± 1.79 mV (Figure 4.40B). All in all, the shift was observed in the surface charge values of TT80 targeted NPs through the positive side compared to non-targeted NPs.

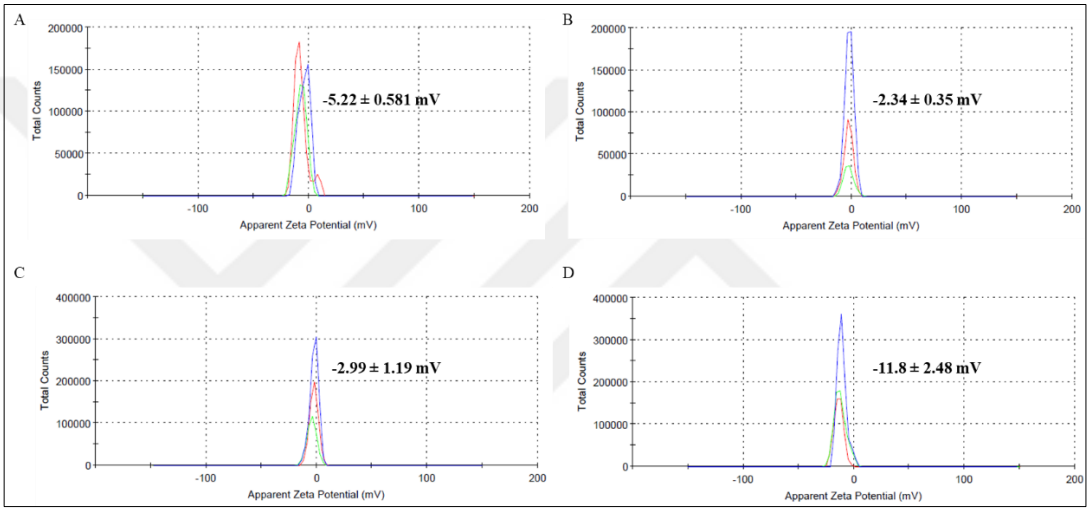

Figure 4. 41. Zeta potential measurements of targeted NPs containing TT80 as a targeting agent (A) 10%TT80-PLGA NPs, (B) 10%TT80-QCT-PLGA NPs, (C) 20%TT80-PLGA NPs, (D) 20%TT80-QCT-PLGA NPs.

Furthermore, after conjugating 1.25% and 2.50% PPT by weight as a targeting agent, the surface charge of NPs was analysed again as in Figure 4.42. The zeta potential values of 1.25%PPT-PLGA NPs and 2.50%PPT-PLGA NPs was found as -4.76 ± 1.12 mV and -4.28 ± 1.15 mV, respectively while the non-targeted PLGA NPs had a surface charge of -13.1 ± 2.12 mV (Figure 4.40A). Also, the surface charge of 1.25%PPT-QCT-PLGA NPs and 2.50%PPT-QCT-PLGA NPs was measured as 6.92 ± 0.619 mV and 3.11 ± 0.619 mV, respectively while the surface charge of QCT-PLGA NPs was -15.1 ± 1.79 mV (Figure 4.40B). Therefore, the surface charge values of targeted NPs shifted towards the positive side compared to non-targeted NPs. Also, after the drug loading, positive surface charge was obtained for 1.25%PPT-QCT-

PLGA NPs and 2.50%PPT-QCT-PLGA NPs as in Figure 4.42B and Figure 4.42D, respectively.

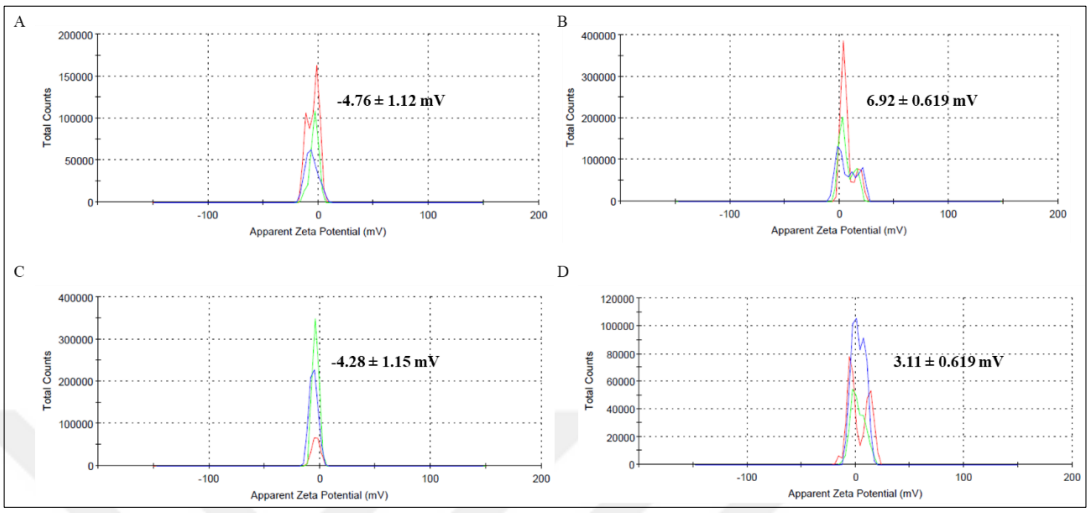

Figure 4. 42. Zeta potential measurements of targeted NPs containing PPT as a targeting agent (A) 1.25%PPT-PLGA NPs, (B) 1.25%PPT-QCT-PLGA NPs, (C) 2.50%PPT-PLGA NPs, (D) 2.50%PPT-QCT-PLGA NPs.

The surface morphology of non-targeted PLGA NPs, QCT-PLGA NPs, 10%TT80-QCT-PLGA NPs, and also 2.50%PPT-QCT-PLGA NPs was analysed using SEM as in Figure 4.43A, Figure 4.43B, Figure 4.43C, and Figure 4.43D, respectively. Moreover, the diameter of some of these NPs was determined. Smooth and spherical morphology was observed for NPs. Moreover, the hydrodynamic diameter of non-targeted PLGA NPs, QCT-PLGA NPs, and 2.50%PPT-QCT-PLGA NPs was obtained as 213.5 nm, 206.5 nm, and 165.7 nm, respectively using DLS device. However, with SEM, the measured diameters of these non-targeted PLGA NPs, QCT-PLGA NPs, and 2.50%PPT-QCT-PLGA NPs were found smaller than these values as it can be seen in Figure 4.43.

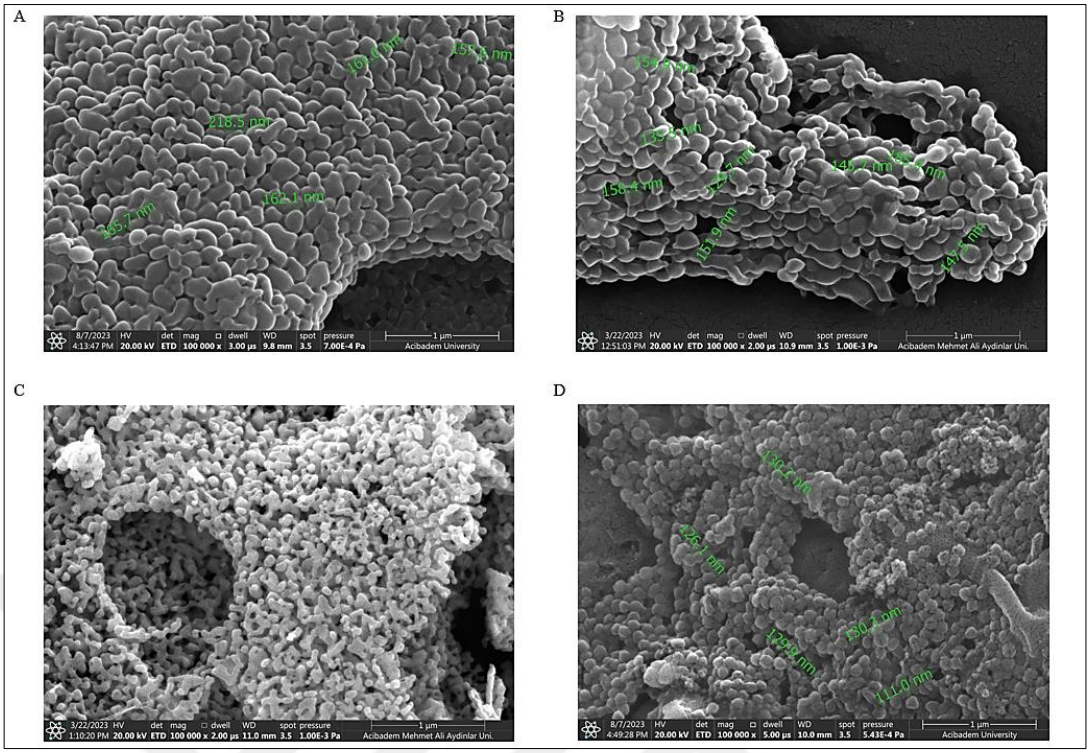

Figure 4. 43. Morphological analysis of NPs via SEM (A) non-targeted PLGA NPs, (B) QCT-PLGA NPs, (C) 10%TT80-QCT-PLGA NPs, (D) 2.50%PPT-QCT-PLGA NPs.

Furthermore, the dimensions and the structure of NPs were examined using TEM as in Figure 4.44. As it was stated previously, the hydrodynamic diameter of 10%TT80-QCT-PLGA NPs, 20%TT80-QCT-PLGA NPs, 1.25%PPT-QCT-PLGA NPs, and 2.50%PPT-QCT-PLGA NPs were measured as 188.2 nm (Figure 4.38B), 145.9 nm (Figure 4.38D), 149.5 nm (Figure 4.39B), and 165.7 nm (Figure 4.39D), respectively by using DLS device. However, with TEM, the hydrodynamic diameters were found smaller compared to the ones measured with DLS. In addition to these, spherical shape of targeted and drug-loaded NPs was observed.

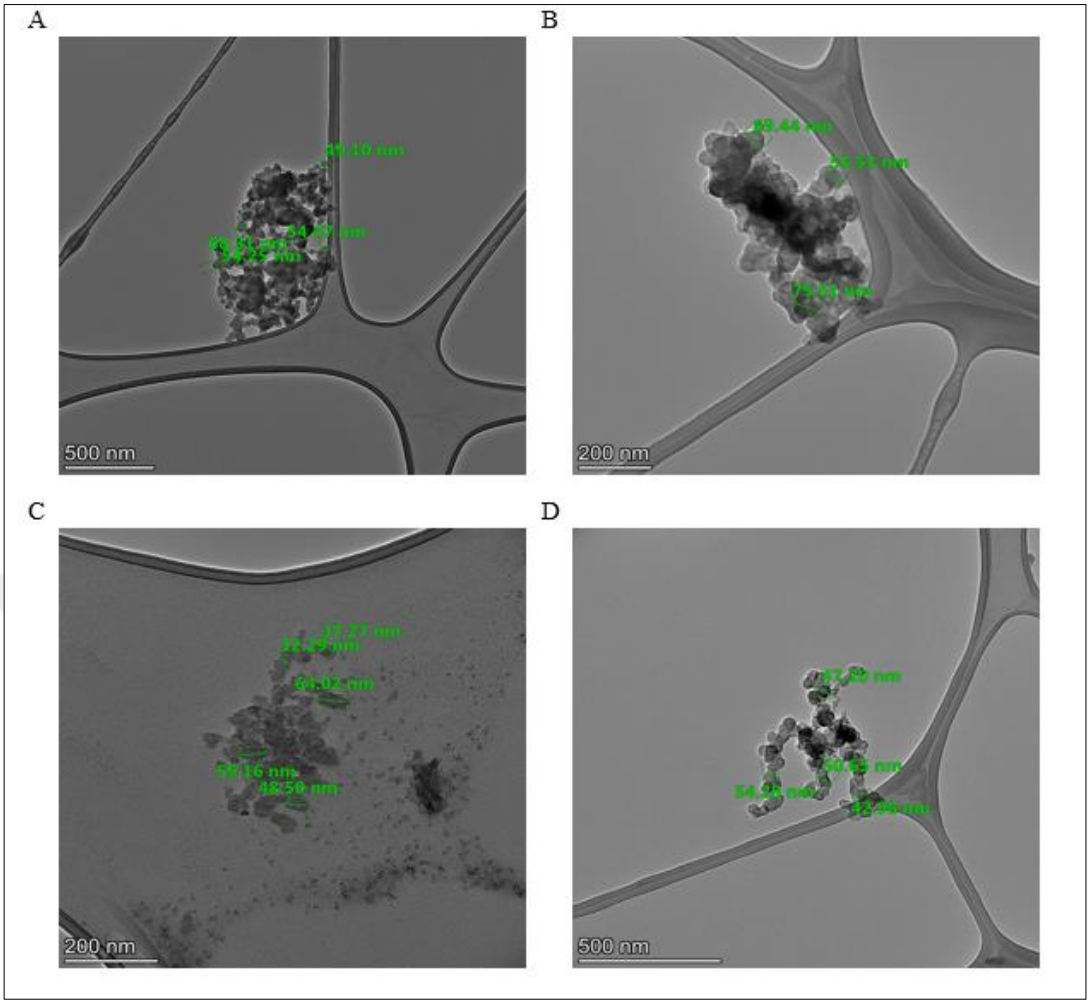

Figure 4. 44. Morphological analysis of NPs via TEM (A) 10%TT80-QCT-PLGA NPs, (B) 20%TT80-QCT-PLGA NPs, (C) 1.25%PPT-QCT-PLGA NPs, (D) 2.50%PPT-QCT-PLGA NPs.

The stability of non-targeted PLGA NPs and QCT-PLGA NPs was investigated as in Figure 4.45A and Figure 4.45B, respectively by incubating them in 1M pH 7.4 PBS at both 25˚C and 37˚C up to almost 30 days. The hydrodynamic diameter of both non-targeted PLGA NPs and QCT-PLGA NPs was found closer to each other during first 9 days. However, after this point, some fluctuations in the size were seen and an increase in the NP size was observed in the long term. In the statistical analysis, the p-value was found statistically significant ($p < 0.0001$) for the hydrodynamic diameter of NPs after the 9th day with respect to their diameter observed during first 9 days.

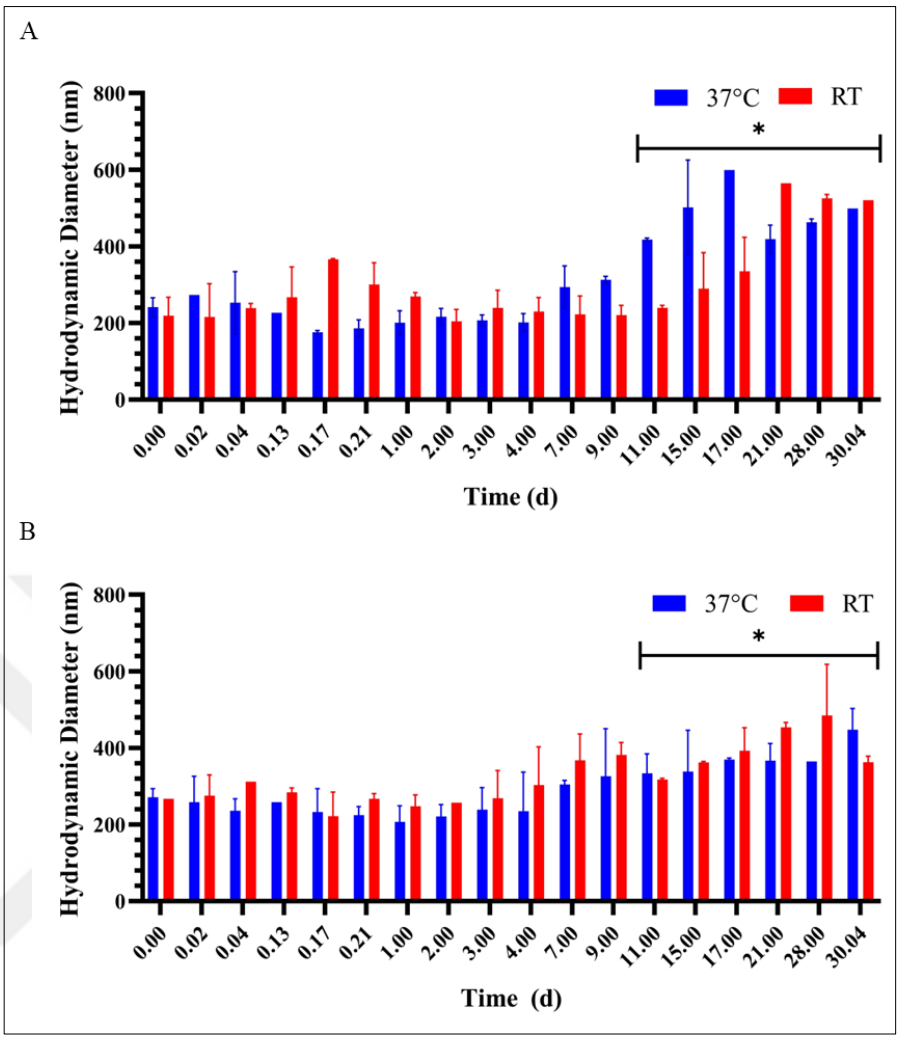

Figure 4. 45. Stability analysis of NPs (A) non-targeted PLGA NPs, (B) QCT-PLGA NPs, * $p < 0.0001$ for the hydrodynamic diameter of NPs with respect to their diameter during first 9 days, n = 3.

The amount of QCT molecule encapsulated into the non-targeted and targeted NPs was determined using LC/MS-MS device and total drug concentration and drug EE was calculated as in Table 4.6. The drug EE of QCT-PLGA NPs was found as 56.88%. After addition of TT80 as a targeting agent, the drug EE of 10%TT80-QCT-PLGA NPs and 20%TT80-QCT-PLGA NPs was obtained as 53.60% and 60.20%, respectively. In addition, after targeting with PPT, the drug EE of 1.25%PPT-QCT-PLGA NPs and 2.50%PPT-QCT-PLGA NPs was calculated as 54.64% and 47.96%, respectively. All in all, total drug concentration in both non-targeted and targeted NPs was found close to each other.

Table 4. 6. Total QCT concentration and drug EE in NPs.

NPs	Total Drug Concentration (µg/mL)	Drug EE
QCT-PLGA NPs	142.20	56.88%
10%TT80-QCT-PLGA NPs	134.09	53.60%
20%TT80-QCT-PLGA NPs	150.49	60.20%
1.25%PPT-QCT-PLGA NPs	136.60	54.64%
2.50%PPT-QCT-PLGA NPs	119.90	47.96%

Furthermore, the release rate of QCT from QCT-PLGA NPs was analysed in two different environments which were pH 7.4 PBS and pH 5.5 acetate buffer solution as in Figure 4.46. The drug release percentage from NPs was notably higher in pH 5.5 solution compared to pH 7.4 solution. At the end of 11th day, drug release from QCT-PLGA NPs reached to almost 95% at pH 5.5 acetate buffer solution while it was only around 35% in pH 7.4 PBS solution.

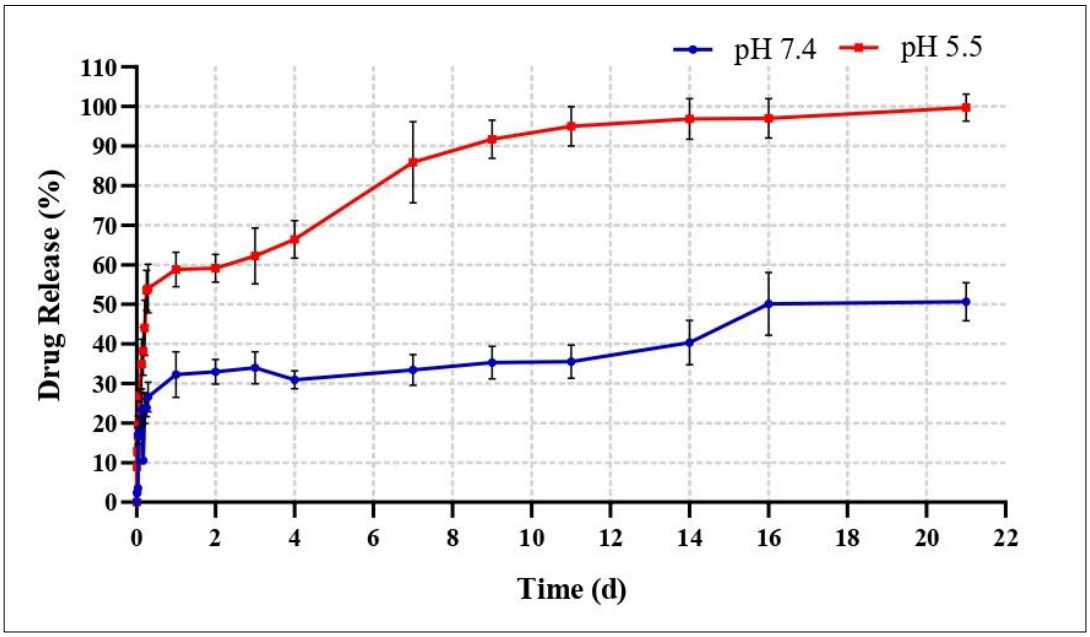

Figure 4. 46. Release profiles of QCT-PLGA NPs after incubation in pH 7.4 PBS and pH 5.5 acetate buffer solution for certain periods in the range of 0-21d, n = 3.

After the characterization of NPs, *in vitro* evaluation of them was carried out. First of all, *in vitro* cytotoxicity of NPs was investigated via CCK-8 assay. Different concentrations of samples were prepared such that they included the 1 µM, 5 µM, 10 µM, 25 µM, 50 µM, 75 µM, 100 µM, 150 µM, 200 µM, 300 µM, and 375 µM concentration of drug molecule. The cell viability graph with respect to different concentration values was obtained in terms of percentage as in Figure 4.47, Figure 4.49, and Figure 4.51. Furthermore, in order to find the IC50 value for these samples, the nonlinear regression curves were drawn using GraphPad Prism as in Figure 4.48, Figure 4.50, and Figure 4.52.

The change in the percentage of cell viability with respect to the increase in the concentration values was given in Figure 4.47 for QCT and QCT-PLGA NPs. P-value was obtained statistically significant ($p < 0.0001$) for QCT-PLGA NPs with respect to QCT. It was observed that the cell viability was around 100% between the concentration values of 1 µM and 10 µM for QCT while it was around 100% between 1 µM and 50 µM for QCT-PLGA NPs. After these points, the decrease in the cell viability was observed as the concentration increased for both samples. However, this decrease occurred more gradually in QCT-PLGA NPs compared to QCT. Also, between 25 µM and 200 µM, the viability of cells was higher when they were treated with QCT-PLGA NPs rather than QCT.

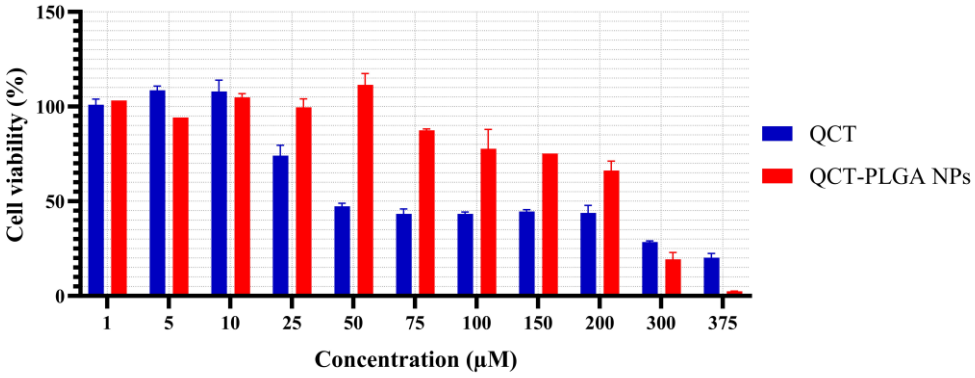

Figure 4. 47. Cell viability (%) vs. concentration (µM) graph for QCT and QCT-PLGA NPs, $p < 0.0001$ for QCT-PLGA NPs with respect to QCT, $n = 3$.

Also, in Figure 4.48, it was observed that the decrease in the cell viability started from the lower concentration values when the cells were treated with QCT instead of QCT-PLGA NPs.

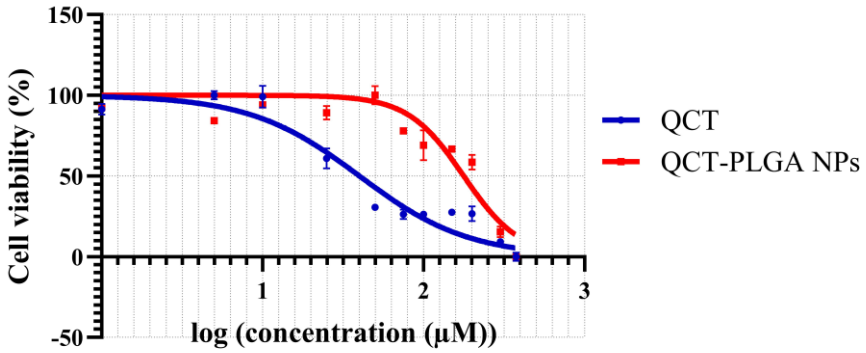

Figure 4. 48. Cell viability results obtained by CCK-8 assay for QCT and QCT-PLGA NPs, n = 3.

The cell viability of 10%TT80-QCT-PLGA NPs and 20%TT80-QCT-PLGA NPs with respect to different concentrations was given in Figure 4.49. P-value was obtained statistically significant ($p < 0.0001$) for TT80-conjugated NPs with respect to QCT. It was observed that, between 25 µM and 200 µM, the viability of cells was higher in the presence of NPs compared to QCT. Also, the cell viability was found between 95% and 100% even at 100 µM drug concentration for 10%TT80-QCT-PLGA NPs. After this point, the gradual decrease in the viability was observed as the concentration increased. However, the cell viability was around 71% and 80% between 1 µM and 100 µM for 20%TT80-QCT-PLGA NPs. After this point, the gradual decrease in the viability was observed as the concentration increased. All in all, the cellular viability was higher when there was a treatment with 10%TT80-QCT-PLGA NPs compared to 20%TT80-QCT-PLGA NPs. The increase in the amount of targeting agent caused the decrease in the cell viability.

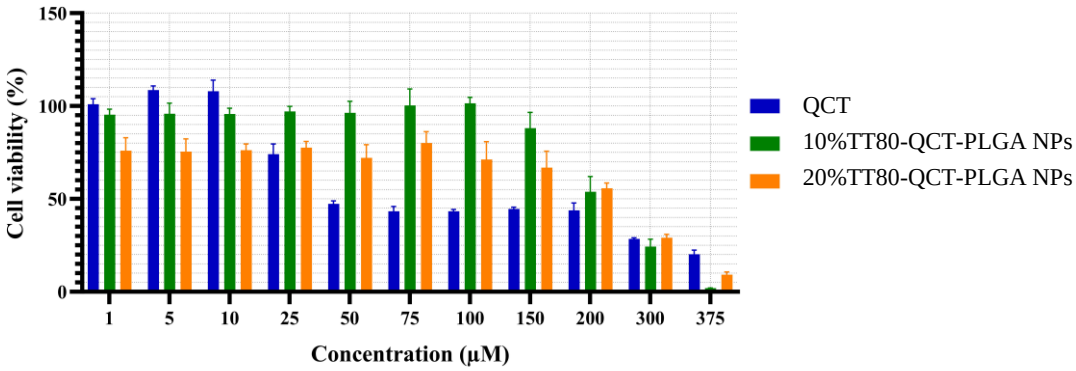

Figure 4. 49. Cell viability (%) vs. concentration (µM) graph for QCT, 10%TT80-QCT-PLGA NPs, and 20%TT80-QCT-PLGA NPs, $p < 0.0001$ for TT80-conjugated NPs with respect to QCT, $n = 3$.

In Figure 4.50, it was seen that the graph obtained for 10%TT80-QCT-PLGA NPs and 20%TT80-QCT-PLGA NPs were almost the same. Also, the decrease in the cell viability was more severe when the cells were treated with QCT compared to TT80-targeted NPs.

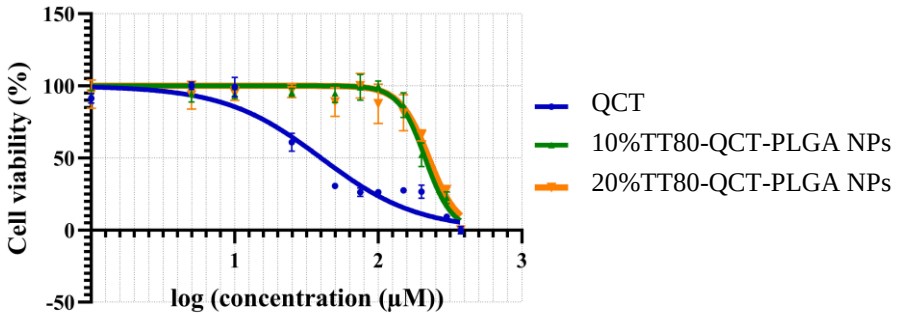

Figure 4. 50. Cell viability results obtained by CCK-8 assay for QCT, 10%TT80-QCT-PLGA NPs, and 20%TT80-QCT-PLGA NPs, $n = 3$.

In Figure 4.51, the cell viability (%) vs. concentration (µM) graph was seen for QCT-loaded and PPT-targeted NPs in comparison with free QCT molecule. P-value was obtained statistically significant ($p < 0.0001$) for PPT-conjugated NPs with respect to QCT. The cell viability was similar and around 100% between 5 µM and 150 µM for 1.25%PPT-QCT-PLGA NPs. After 150 µM, viability of the cells decreased as concentration increased. However, the cell viability was around 100% between 5 µM

and 25 µM for 2.50%PPT-QCT-PLGA NPs and between 50 µM and 100 µM, the cell viability was obtained between 91% and 96%. After this concentration value, the decrease in the cell viability was seen. All in all, it was found that until 300 µM concentration, the cell viability was higher in the presence of NPs compared to QCT. Also, the decrease in the cellular viability was observed when there was an increase in the amount of targeting agent.

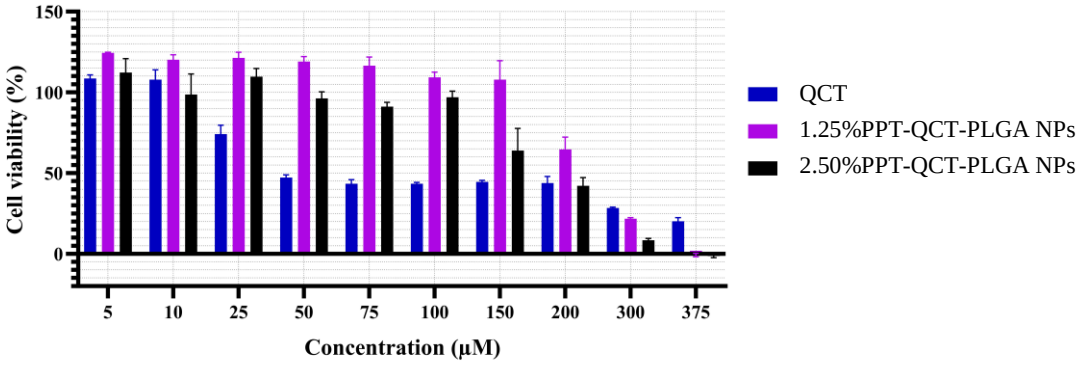

Figure 4. 51. Cell viability (%) vs. concentration (µM) graph for QCT, 1.25%PPT-QCT-PLGA NPs, and 2.50%PPT-QCT-PLGA NPs, $p < 0.0001$ for PPT-conjugated NPs with respect to QCT, n = 3.

In Figure 4.52, it was observed that the decrease in the cell viability occurred at lower concentrations for the cells treated with QCT compared to the ones treated with PPT-targeted NPs. Also, cell viability decreased slower for the cells treated with 1.25%PPT-QCT-PLGA NPs rather than 2.50%PPT-QCT-PLGA NPs.

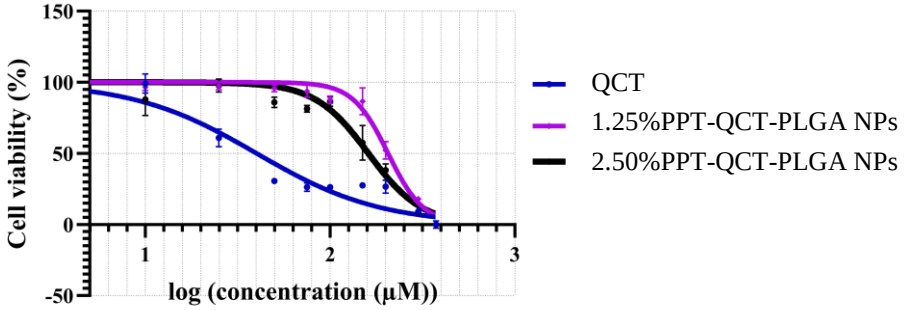

Figure 4. 52. Cell viability results obtained by CCK-8 assay for QCT, 1.25%PPT-QCT-PLGA NPs, and 2.50%PPT-QCT-PLGA NPs, n = 3.

The IC50 values were calculated using the graphs seen in Figure 4.48, Figure 4.50, and Figure 4.52 and they can be seen in Table 4.7. The drug molecule itself had the lowest IC50 value in terms of concentration (μM) compared to all NPs. The IC50 values for 10%TT80-QCT-PLGA NPs, 20%TT80-QCT-PLGA NPs, and 1.25%PPT-QCT-PLGA NPs were found similar to each other while this value was highest for 20%TT80-QCT-PLGA NPs. Compared to QCT-PLGA NPs, 10%TT80-QCT-PLGA NPs, 20%TT80-QCT-PLGA NPs, and 1.25%PPT-QCT-PLGA NPs had higher IC50 values while 2.50%PPT-QCT-PLGA NPs had slightly lower one.

Table 4. 7. IC50 values of free QCT and NPs.

Samples	IC50 value (μM)
QCT	39.9
QCT-PLGA NPs	177.5
10%TT80-QCT-PLGA NPs	211.6
20%TT80-QCT-PLGA NPs	224.5
1.25%PPT-QCT-PLGA NPs	206.1
2.50%PPT-QCT-PLGA NPs	161.2

After the completion of CCK-8 assay, the *in vitro* evaluation of NPs was continued by conducting ROS assay. In this manner, the ROS activity of QCT, QCT-PLGA NPs, 10%TT80-QCT-PLGA NPs, 20%TT80-QCT-PLGA NPs, 1.25%PPT-QCT-PLGA NPs, and 2.50%PPT-QCT-PLGA NPs was analysed by applying their IC25 and IC50 concentration values on mouse microglial cells. At the end, the ROS fluorescence graph with respect to different concentration values was obtained in terms of percentage as in Figure 4.53. P-value was obtained statistically significant ($p < 0.0001$) for QCT with respect to controls; for QCT-PLGA NPs with respect to QCT; and for all targeted NPs with respect to non-targeted QCT-PLGA NPs. It was stated in Section 3.2.4.6 that the cells were treated with LPS to create an inflammatory environment. In this manner, cells with both LPS and DCFDA were used as a positive control. This

showed the maximum ROS production condition of the cells when they were not treated with free drug or any NPs. On the other hand, cells without LPS were used as a background control that showed the basal ROS production of the cells without any treatment. The ROS level was found as almost 72.85% and 35.04% for positive control and background control, respectively. Therefore, in case of an inflammation, the increase in the ROS production was observed. Compared to both positive and background controls, ROS production was found higher for QCT at both IC25 and IC50 values which were almost 99.78% and 91.83%, respectively. However, all NPs including both non-targeted and targeted ones decreased the ROS production compared to both positive control and QCT at two different concentration values. When the results were compared with background control, QCT-PLGA NPs had similar ROS production at both IC25 and IC50 values which were almost 36.38% and 34.72%, respectively. On the other hand, all 10%TT80-QCT-PLGA NPs, 20%TT80-QCT-PLGA NPs, 1.25%PPT-QCT-PLGA NPs, and 2.50%PPT-QCT-PLGA NPs resulted in decreased ROS production compared to both background control and QCT-PLGA NPs at IC25 and IC50 concentration values. The ROS level of 10%TT80-QCT-PLGA NPs, 20%TT80-QCT-PLGA NPs, 1.25%PPT-QCT-PLGA NPs, and 2.50%PPT-QCT-PLGA NPs was obtained as around 9.05%, 7.93%, 25.02%, and 17.07%, respectively at IC25 concentration value. However, they were found as almost 6.5%, 5.30%, 20.79%, and 13.03%, respectively at IC50 concentration value. In addition to these, the measured ROS fluorescence was slightly decreased for QCT when the drug concentration increased while it was almost the same for QCT-PLGA NPs at both IC25 and IC50 values. However, as the drug concentration increases, the measured ROS fluorescence was decreased for all targeted NPs which were 10%TT80-QCT-PLGA NPs, 20%TT80-QCT-PLGA NPs, 1.25%PPT-QCT-PLGA NPs, and 2.50%PPT-QCT-PLGA NPs. In general, compared to 10%TT80-QCT-PLGA NPs, 20%TT80-QCT-PLGA NPs had lower ROS production at both IC25 and IC50 values. Similarly, 2.50%PPT-QCT-PLGA NPs had lower ROS production at both IC25 and IC50 values compared to 1.25%PPT-QCT-PLGA NPs. All in all, the increase in the concentration of targeting agent caused the decrease in the ROS production. Although, statistically significant differences in ROS levels across IC25 and IC50 drug

concentrations were not observed for the samples, the increase in the drug concentration resulted in the slight decrease in the ROS level.

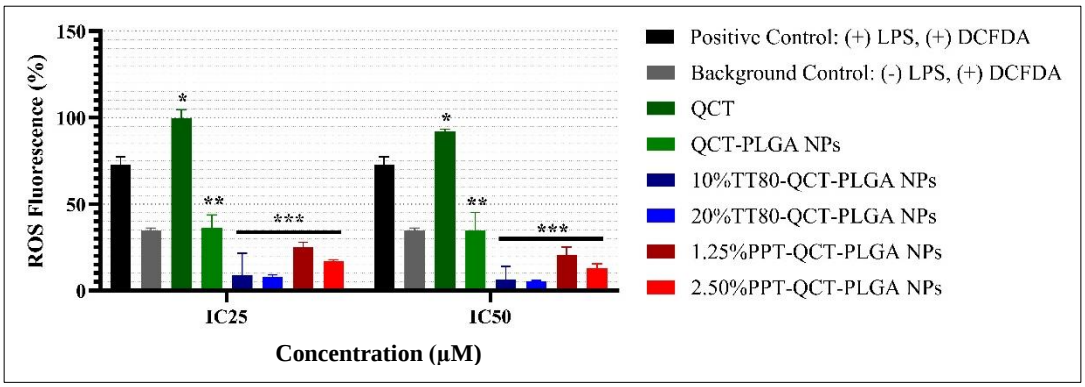

Figure 4. 53. ROS assay results of QCT, QCT-PLGA NPs, 10%TT80-QCT-PLGA NPs, 20%TT80-QCT-PLGA NPs, 1.25%PPT-QCT-PLGA NPs, and 2.50%PPT-QCT-PLGA NPs in comparison with cell controls, * $p < 0.0001$ for QCT with respect to positive and background control; ** $p < 0.0001$ for QCT-PLGA NPs with respect to QCT; *** $p < 0.0001$ for targeted NPs with respect to QCT-PLGA NPs, $n = 3$.

Moreover, JC-1 assay was conducted as a final *in vitro* experiment to assess the mitochondria-targeting efficacy of synthesized targeted NPs compared to non-targeted NPs and free drug. This assay was performed using free QCT, QCT-PLGA NPs, 10%TT80-QCT-PLGA NPs, 20%TT80-QCT-PLGA NPs, 1.25%PPT-QCT-PLGA NPs, and 2.50%PPT-QCT-PLGA NPs. Furthermore, the impact of varying concentration levels of these samples on EOC 20 microglial cells was investigated, including drug concentrations of 5 µM, 10 µM, and 20 µM. Also, two different controls were incorporated into this analysis to evaluate the acquired results. The cells without LPS but with CCCP was used as a positive control since CCCP serves as a mitochondrial membrane disrupter. In addition, the cells with only LPS were used as a cell control to demonstrate both the induction of inflammation upon LPS application on cells and to observe its effect on mitochondrial membrane potential. At the end of this assay, the cells stained in the corresponding wells of the cell culture plate, including both controls and NPs, were observed using a fluorescence microscope at RT in the absence of light. Their images were captured with the scale bar adjusted to 300 µm, as illustrated below.

First, the captured image for controls was presented in Figure 4.54. The images of cells treated with CCCP showed only the formation of green fluorescence, namely JC-1 monomers (J-monomer). In contrast, in the images of the cell control, a minor red fluorescence signal indicating JC-1 aggregates (J-aggregate) was observed alongside clear green signals. This was also evident in the overlay picture.

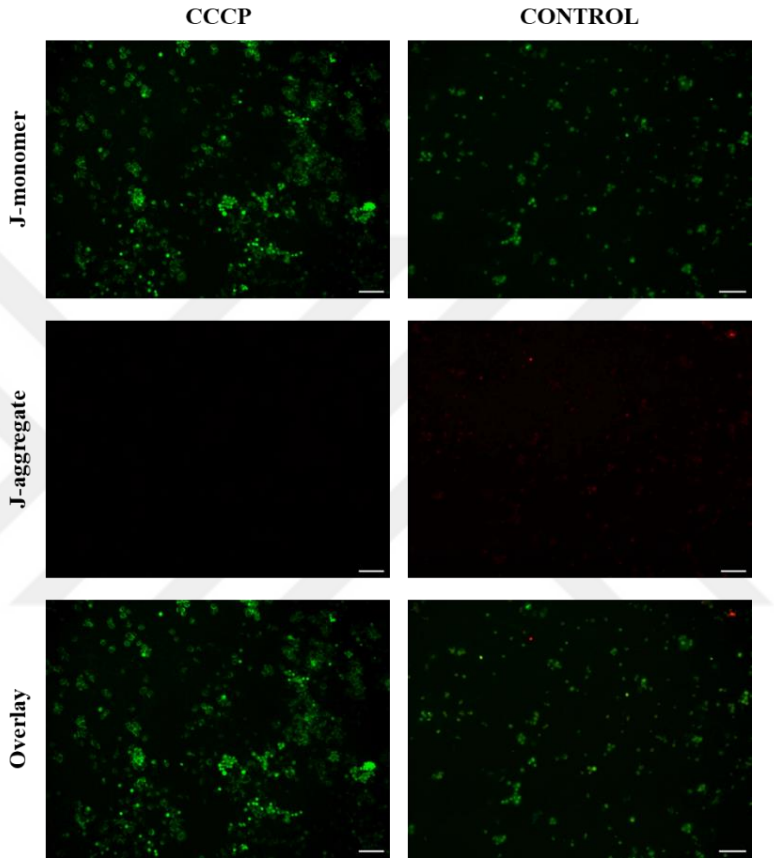

Figure 4. 54. Fluorescence microscopy results of JC-1 assay on EOC 20 cells for CCCP and control.

Furthermore, the fluorescence microscopy images for QCT at different drug concentration values were captured (Figure 4.55). In all concentration values, the intensity of green fluorescence was higher than the red one. However, as the concentration of drug molecule increased from 5 µM to 20 µM, the increase in the red fluorescence was noticed. Therefore, for QCT, it was achieved that as drug concentration increased, the formation of J-aggregates also increased. Moreover,

compared to controls in Figure 4.54, QCT had higher formation of J-aggregates in all concentrations.

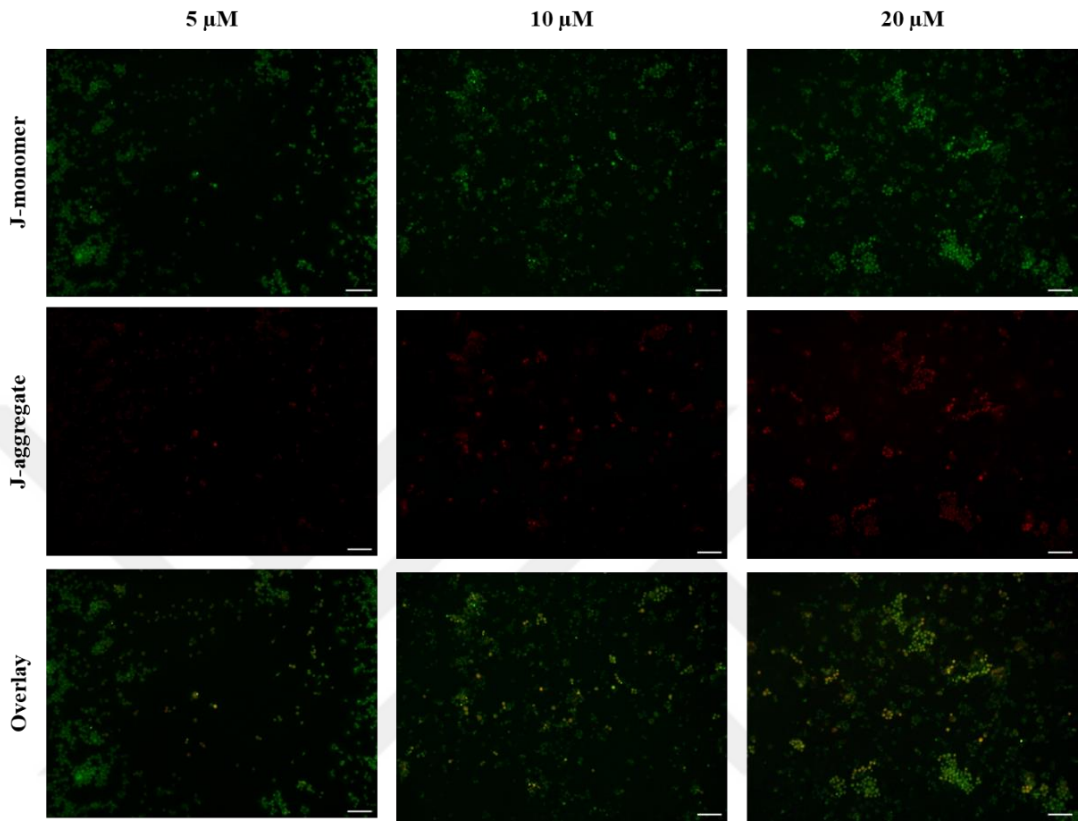

Figure 4. 55. Fluorescence microscopy results of JC-1 assay on EOC 20 cells for QCT at drug concentrations of 5, 10, and 20 µM.

The obtained image for QCT-PLGA NPs at the end of JC-1 assay was presented in Figure 4.56. The increase in the red and the decrease in the green fluorescence were observed while the concentration increased. Furthermore, when compared to both QCT and the controls, the non-targeted QCT-PLGA NPs exhibited a more pronounced formation of J-aggregates and a reduced intensity of the green signal in the overlay image at all concentration values. At all, the usage of NPs enhanced the formation of red J-aggregates compared to both controls and free QCT.

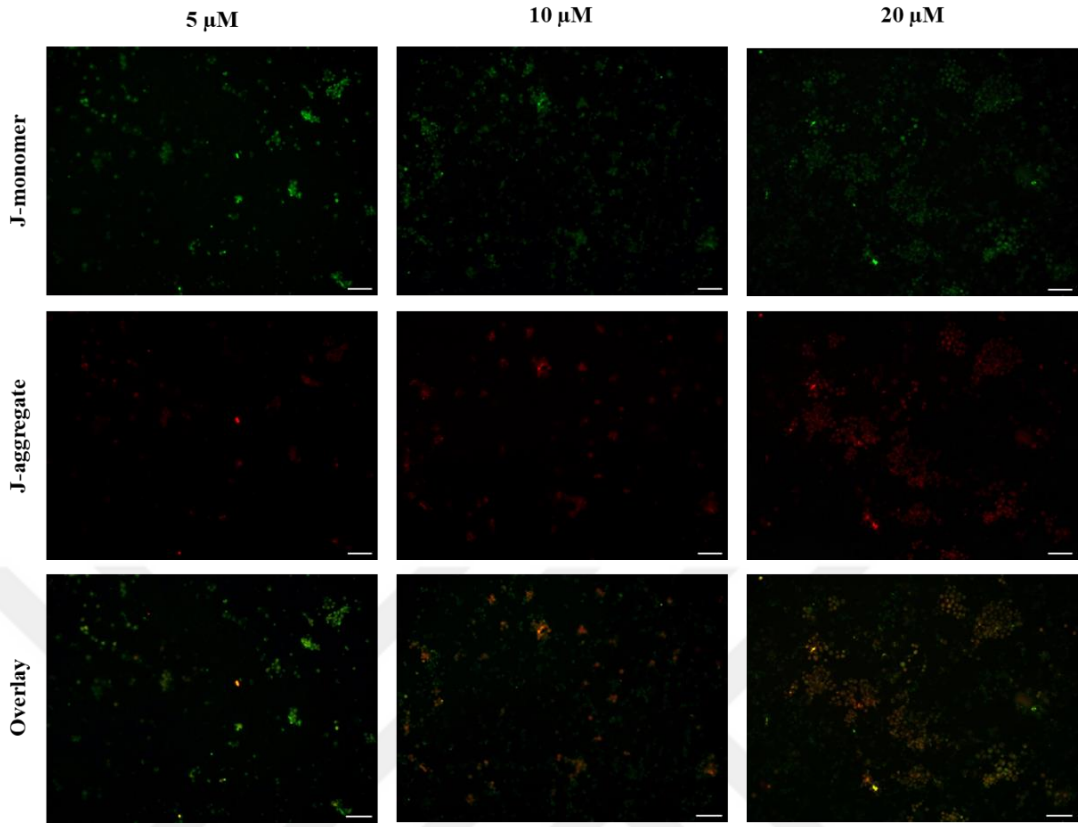

Figure 4. 56. Fluorescence microscopy results of JC-1 assay on EOC 20 cells for QCT-PLGA NPs at drug concentrations of 5, 10, and 20 µM.

Moreover, the images were captured for the cells treated with 10%TT80-QCT-PLGA NPs as in Figure 4.57. It was seen that as concentration increased from 5 µM to 20 µM, there was an increase in the intensity of red fluorescence and a decrease in the intensity of green fluorescence. In addition to this, at all concentration values, the 10%TT80-QCT-PLGA NPs demonstrated a higher formation of J-aggregates and a lower intensity of J-monomers in the overlay image compared to both QCT and QCT-PLGA NPs. All in all, targeting with 10% TT80 resulted in an increased formation of J-aggregates even at the lowest concentration value compared to the results obtained for free drug and non-targeted NPs.

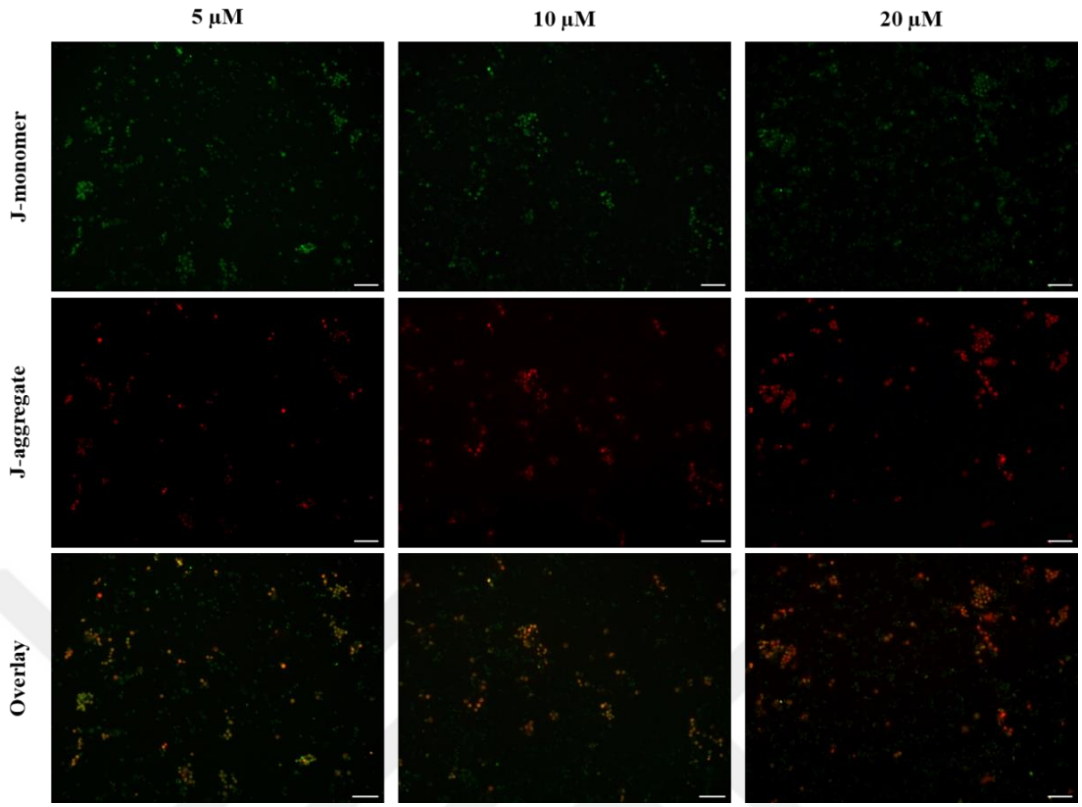

Figure 4. 57. Fluorescence microscopy results of JC-1 assay on EOC 20 cells for 10%TT80-QCT-PLGA NPs at drug concentrations of 5, 10, and 20 μM.

In addition to these, the images for cells subjected to the treatment with 20%TT80-QCT-PLGA NPs can be seen in Figure 4.58. As the concentration value varies from 5 μM to 20 μM, an increase in the brightness of the red signals so in the intensity of J-aggregates were seen, together with the decrease in the J-monomers. Also, when the overlay images of 20%TT80-QCT-PLGA NPs were compared with the 10%TT80-QCT-PLGA NPs, the dose dependent relationship was observed. Specifically, an increase in the dose of the TT80 as a targeting agent led to a proportional increase in the red fluorescence, namely J-aggregates regardless of the drug concentration.

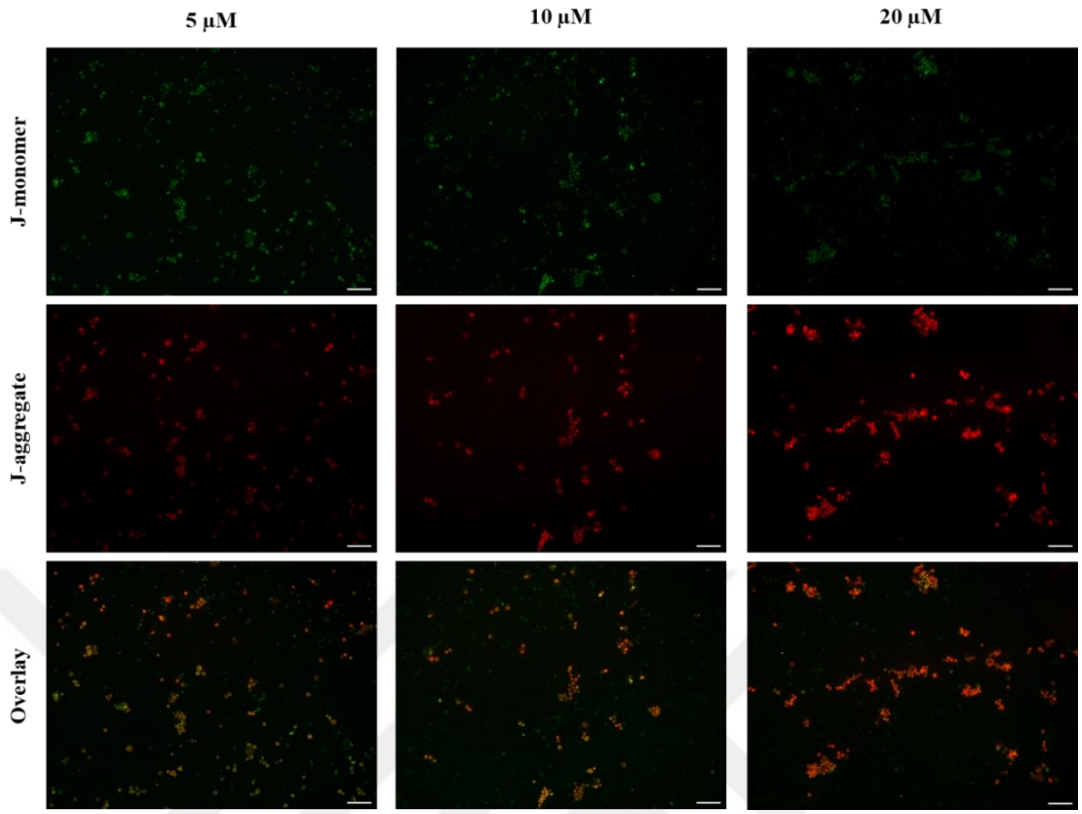

Figure 4. 58. Fluorescence microscopy results of JC-1 assay on EOC 20 cells for 20%TT80-QCT-PLGA NPs at drug concentrations of 5, 10, and 20 µM.

Furthermore, the same assay was conducted for 1.25%PPT-QCT-PLGA NPs and the results were given in Figure 4.59. It was evident that, compared to both 10%TT80-QCT-PLGA NPs and 20%TT80-QCT-PLGA NPs, the brightness and intensity of J-monomers were very high while the intensity of J-aggregates was low at a drug concentration of 5 µM. Yet, with an increase in the concentration, there was a noticeable increase in red fluorescence and a decrease in the brightness of green fluorescence. This indicated that as the drug concentration increased, the formation of J-aggregates also increased. When the overlay images were compared with QCT and QCT-PLGA NPs, it was observed that the addition of PPT as a targeting agent improved the amount of red fluorescence signals even at the lowest drug concentration value.

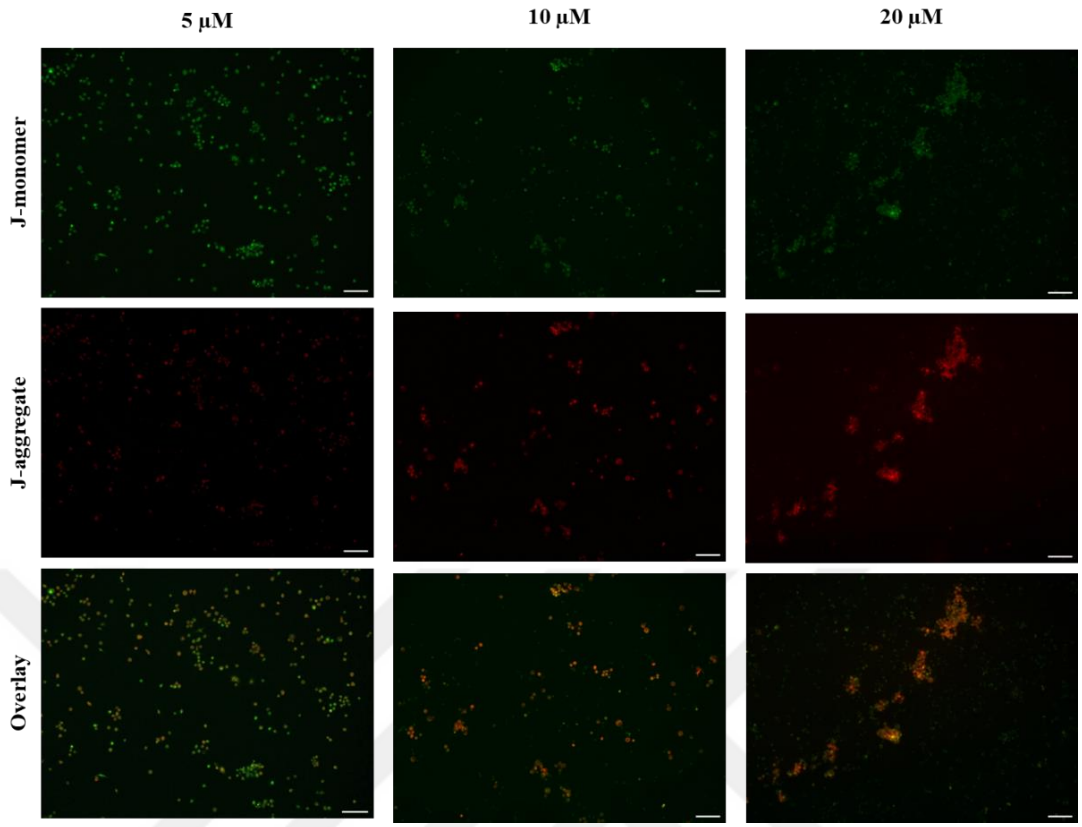

Figure 4. 59. Fluorescence microscopy results of JC-1 assay on EOC 20 cells for 1.25%PPT-QCT-PLGA NPs at drug concentrations of 5, 10, and 20 µM.

Finally, the fluorescence microscopy images of the EOC 20 cells treated with 2.50%PPT-QCT-PLGA NPs can be seen in Figure 4.60. It was observed that as the drug concentration increased, a corresponding increase was also observed in the J-aggregates, similar to the other NPs. As mentioned earlier, a dose dependent relationship was observed when the targeting agent was TT80. In other words, 20% TT80-conjugated NPs exhibited increased red fluorescence compared to the 10% TT80-conjugated ones in all drug concentrations. However, a similar dose dependency was not notably observed when the targeting agent was PPT. When comparing the overlay images of 2.50%PPT-QCT-PLGA NPs with those of 1.25%PPT-QCT-PLGA NPs, it was observed that the amount of red fluorescence signal remained similar, despite an increase in the dose of the targeting agent.

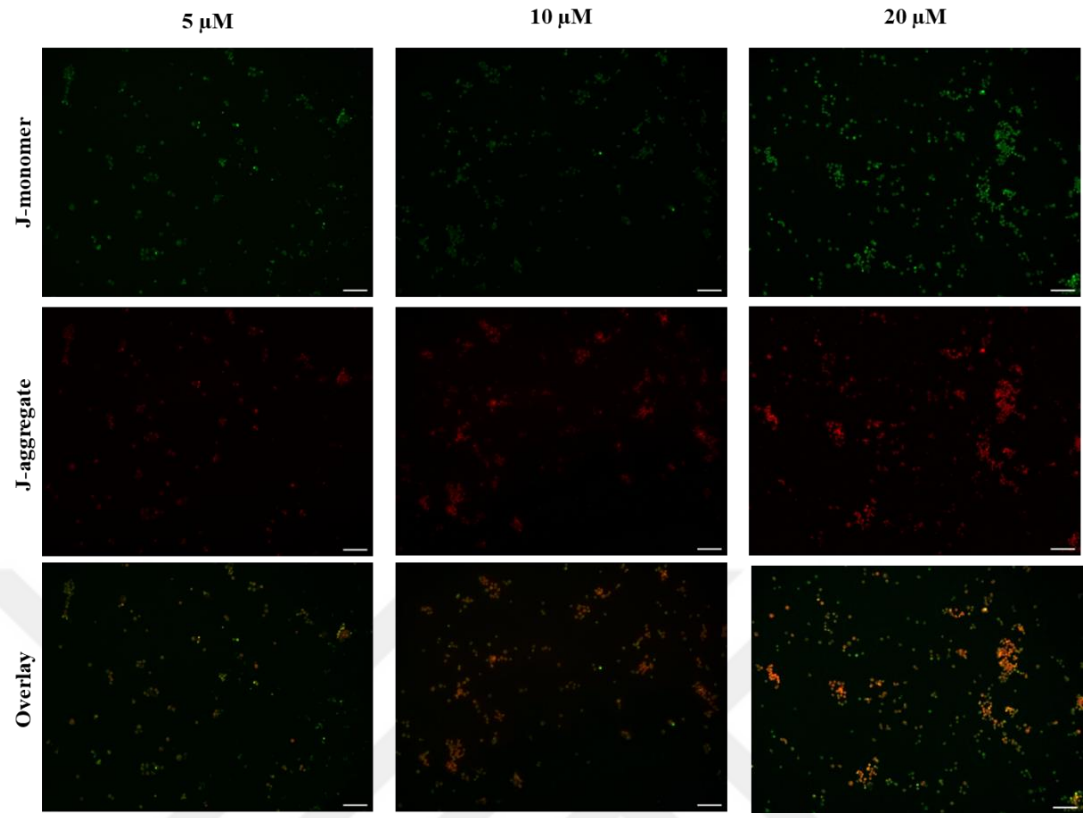

Figure 4. 60. Fluorescence microscopy results of JC-1 assay on EOC 20 cells for 2.50%PPT-QCT-PLGA NPs at drug concentrations of 5, 10, and 20 µM.

5. DISCUSSION

5.1. Discussion for Project 1: Macrophage-Targeted NPs

Inflammatory diseases such as cardiovascular, metabolic, and neurodegenerative diseases often result from increased inflammation and deficiencies that arise during the resolution of inflammation (60,61). AS is one of these chronic inflammatory diseases and its initiation and the progression are greatly affected by the proper functioning of inflammatory cells and factors. For instance, immune cells known as macrophages that are responsible for removing apoptotic cells, play pivotal roles in the resolution of inflammation and the regulation of immune responses (62,63). Therefore, within the scope of this project, these cells were preferred as promising targets for the treatment or prevention of AS. Due to the shortcomings of traditional treatment methods such as high dosage requirements, low therapeutic potency, and inadequate delivery to the target site, novel treatment methodologies have been developed to ensure the proper functioning of these cells and to regulate some anti-inflammatory pathways (2,4). Considering these, macrophage-targeted S2P peptide-conjugated and anti-inflammatory VitE metabolites encapsulated PLGA NPs were developed as a DDS within the scope of this project.

First, non-targeted empty and drug-loaded NPs were synthesized as it was explained in Section 3.2.1.1. After the synthesis of S2P peptide which is specific to the stabilin-2 receptor overexpressed on the surface of macrophages (50,51), its purification was completed via prep-HPLC as in Figure 4.1. Also, the chemical characterization of S2P peptide was confirmed using an LC/MS-MS device, as shown in Figure 4.2. This purified and characterized peptide was linked to DSPE-PEG-Mal and DSPE-PEG-S2P conjugation was accomplished, as described in Section 3.2.1.3. The presence of all components in the conjugate was confirmed by conducting ^{1}H NMR analysis. The spectrum in Figure 4.3 shows the protons of the S2P peptide,

DSPE lipid, and PEG polymer. After that, the FT-IR analysis was conducted for DSPE-PEG-Mal, S2P peptide, and DSPE-PEG-S2P as in Figure 4.4. It was found that the characteristic functional groups of DSPE-PEG and S2P peptide were both seen in the FT-IR spectrum of DSPE-PEG-S2P conjugate. This proved the presence of both of these precursor materials in the structure of conjugate. By using this conjugate, targeted empty and drug-loaded NPs were synthesized as in 3.2.1.4. Also, both FITC-labelled and RhB-conjugated FITC-labelled NPs were synthesized for the visualization of NPs *in vitro*. During all these experimental procedures, the characterization of NPs was conducted and at the end, the NPs were obtained with optimum properties.

After the synthesis of NPs, their hydrodynamic diameter and PDI values were analysed using DLS device. The hydrodynamic diameter of non-targeted empty and drug-loaded NPs were obtained higher compared to non-coated NPs as in Figure 4.5. This increase was due to the coating with PEGylated lipid, namely DSPE-PEG polymer. After the conjugation of S2P targeting peptide, the hydrodynamic diameter of S2P-PLGA NPs and S2P-α-13′-COOH PLGA NPs showed an increase compared to their non-targeted versions as in Figure 4.6. The reason behind this could be the conjugation of S2P peptide to the DSPE-PEG polymer with 1:10 by weight. However, the similar increase in size was not observed for S2P-GA-PLGA NPs compared to non-targeted GA-PLGA NPs. Their hydrodynamic diameter was found close to each other. This could be caused by the additional centrifugation applied on GA-loaded non-targeted and targeted NPs for 2 min at 4000 rpm to remove the aggregates and optimize the NP size. Similarly, FITC-S2P-PLGA NPs, RhB-FITC-S2P-PLGA NPs, and RhB-FITC-S2P-α-13′-COOH PLGA NPs showed slightly higher hydrodynamic diameter compared to FITC-PLGA NPs, RhB-FITC-PLGA NPs, and RhB-FITC-α-13′-COOH PLGA NPs, respectively as seen in Figure 4.7 and Figure 4.8. However, the increase in their size was not highly notable as seen in the size of S2P-PLGA NPs and S2P-α-13′-COOH PLGA NPs. The reason behind this was the additional centrifugation conducted at the end of the synthesis process of these labelled NPs to remove the aggregates and optimize NP size. Furthermore, the PDI values of NPs were

obtained smaller than 0.213 and, in this way, stable, compact, and monodisperse NPs were achieved as in Figure 4.5, Figure 4.6, Figure 4.7, and Figure 4.8. The size of NPs was suitable to circulate through the blood stream and interact with cells.

In addition to DLS analysis, zeta potential of NPs was measured as in Figure 4.9, Figure 4.10, Figure 4.11, and Figure 4.12. It was observed that after the conjugation of positively charged S2P peptide as a targeting agent, the surface charge of NPs shifted towards the positive side. Therefore, this shift in the zeta potential values proved the successful conjugation of macrophage targeting peptide onto the surface of NPs. Moreover, the morphologies of NPs and their diameters were analysed as in Figure 4.13 and Figure 4.14. The presence of coating layer was observed, especially in Figure 4.14A for PLGA NPs. This proved the successful synthesis of DSPE-PEG coated NPs. The hydrodynamic diameter of NPs that were measured with TEM was found smaller compared to the hydrodynamic diameter of NPs that were measured with DLS. The reason behind this was dehydration. As it was stated in the Materials and Methods section, NPs were synthesized and stored in water. However, to conduct SEM and TEM analyses, the NP solutions were dropped on grids, and they were waited to dry for 2 days under sterile conditions. After the water evaporated, the analyses were conducted. For this reason, the reduction in the NP sizes was observed. Furthermore, in the FT-IR spectrum of PLGA NPs in Figure 4.15, all characteristic peaks coming from PLGA polymer and DSPE-PEG coating were observed which proved their presence in the NP structure. Also, some of the characteristic peaks of PLGA polymer, DSPE-PEG coating, and drug molecule were together observed in the FT-IR spectrum of α-13′-COOH PLGA NPs which also proved their presence in the NP structure.

In case of stability analysis, some fluctuations were observed during the first hours of incubation in the size of PLGA NPs and α-13′-COOH PLGA NPs as in Figure 4.16. This rapid change could be caused by the addition of NPs in PBS that contains salt solution. In general, the hydrodynamic diameter of PLGA NPs, α-13′-COOH PLGA NPs, and GA-PLGA NPs was highly stable during first 2 days of incubation and the

gradual increase in the size was observed after this point as in Figure 4.16 and Figure 4.17. This was also statistically confirmed with a significant p-value obtained after the 2nd day, indicating a notable difference in the NP size beyond that point. Around the 15th day and beyond, their diameter remained between 600 nm and 800 nm for weeks. This may indicate that NPs dispersed as they swelled, and polymer chains formed NPs gradually started to move apart from each other after 15 days. Thus, it could be concluded that NPs could maintain their stability for a long time under different environmental conditions. Moreover, the net protein concentrations in targeted NPs were measured via nanodrop device and found between 13.69 µg/mL and 29.09 µg/mL for different NPs as in Table 4.1. Before and after drug loading, the protein concentrations were found close to each other. This proved that there was almost no loss of targeting peptide during drug loading process and all targeted NPs synthesized in this project contained targeting agent on their surface.

Furthermore, drug EE of NPs were analysed as in Table 4.2. Drug EE of non-targeted and targeted NPs were found close to each other. This proved that the addition of targeting peptide did not significantly affect the encapsulation of drug molecules. Also, drug EE was higher in case of α-13′-COOH was used as a drug molecule instead of GA. The reason behind this could be caused by the difference in the chemical structure of drugs. After that, the drug release from NPs were analysed in both pH 7.4 PBS and pH 5.5 acetate buffer solution as in Figure 4.18, Figure 4.19, and Figure 4.20. In case of inflammation, the pH of the environment decreases. Therefore, in this experiment, pH 7.4 represented the healthy body conditions while pH 5.5 environment mimicked the inflammatory case. It was observed that drug release from NPs in pH 5.5 solution was higher than the drug release percentage in pH 7.4 solution. That was a sign that proved the higher drug release in case of inflammation rather than the healthy body fluid. It was observed that after 627h, drug release from α-13′-COOH PLGA NPs was around 75% in pH 5.5 while it was almost 25% in pH 7.4. Also, after 768h, the drug release from GA-PLGA NPs reached almost 77% in pH 5.5 acetate buffer solution while it was around 4% in pH 7.4 PBS solution. Therefore, the sustained and controlled drug release from both α-13′-COOH and GA-loaded NPs was

achieved in pH 5.5 inflammatory environment. In addition to all these characterization tests, the FITC and RhB concentration on dye-labelled non-targeted and targeted NPs was measured as in Table 4.3 and Table 4.4. It was observed that the concentration of dyes found in NPs decreased during the addition process of S2P targeting peptide onto their surface. Despite this decrease in dye concentration, it was achieved that all NPs had enough amount of FITC and RhB dyes for visualization.

At the end of this project, DSPE-PEG coated, macrophage-targeted and anti-inflammatory VitE metabolites containing biocompatible and biodegradable NPs were successfully synthesized in a monodisperse manner and their characterization tests were completed. These NPs showed promising results by providing controlled and sustained drug release against AS-induced inflammation. In the literature, it has been demonstrated that the attachment of the S2P peptide as a biomolecule enables the effective delivery of NPs to macrophages in vivo (50,51). Also, it has been proved that the usage of α-13′-COOH and GA as drug molecules could exhibit promising results in the treatment of inflammatory diseases such as AS thanks to their anti-inflammatory properties (45,46). Although this targeting agent, drug molecules, or polymer itself has been used in the literature, there are no studies available showing the anti-inflammatory effect of α-13′-COOH-loaded S2P-conjugated NPs and GA-loaded S2P-conjugated NPs on macrophages. This contributes to the uniqueness of this project. Also, for the future studies, this project could provide valuable insights into the use of the targeted NPs as carriers in treatment approaches for various diseases where macrophages play a crucial role.

5.2. Discussion for Project 2: CS-Coated NPs

Increased inflammation, imbalances that occur in the process of resolving inflammation, and non-resolution of inflammatory conditions for a long time eventually led to the development of chronic inflammatory diseases (60,61). AS is one

of these diseases that threaten the life of many people for several years (62). Various traditional treatment methodologies are present to find a cure for this disease, but they have some limitations including high dosage requirements and serious side effects. Therefore, novel treatment methodologies using DDS have been studied for years (2,4). In this project, CS-coated CUR and αTCP loaded core-shell PLGA NPs were developed against AS-induced inflammation.

Within the scope of this project, non-coated empty and drug-loaded NPs were synthesized as it was explained in Section 3.2.2.1. After this process, CS-coated empty and drug-loaded NPs were synthesized as in Section 3.2.2.2 and their characterization tests were completed in terms of hydrodynamic diameter, surface charge, morphology, stability, encapsulated total drug amount, and drug release profile. The non-coated and coated versions were compared and at the end, core-shell PLGA NPs with optimum properties were obtained.

First of all, the hydrodynamic diameter and PDI values of NPs were analysed using DLS device. As in Figure 4.21, the size of non-coated empty and drug-loaded NPs were found similar to each other. Therefore, it could be concluded that drug loading did not have a significant effect on hydrodynamic diameter of NPs. Then, CS coating was performed and DLS analysis was conducted again as in Figure 4.22. It was achieved that CS coating caused an increase in the hydrodynamic diameter values of all NPs. However, the increase in the size was smaller for CS-αTCP-PLGA NPs compared to others. The reason behind this could be the centrifugation conducted at the end to remove the aggregates and optimize the NP size. The centrifugation process was longer for CS-αTCP-PLGA NPs compared to CS-PLGA NPs and CS-CUR-PLGA NPs. Therefore, smaller size was obtained for CS-αTCP-PLGA NPs. Finally, the PDI values of NPs were obtained smaller than 0.186 and, in this way, stable, compact, and monodisperse NPs were achieved as in Figure 4.21, and Figure 4.22. All in all, the size of NPs was suitable to circulate through the blood stream and interact with cells.

Moreover, the zeta potential measurements were conducted for both non-coated and CS-coated NPs to observe the effect of coating on NPs as in Figure 4.23 and Figure 4.24. The non-coated NPs showed negative surface potential. However, after the coating with positively charged CS, the surface charge of NPs was found positive. Therefore, this shift in the zeta potential values through the positive side proved the successful coating of CS onto the surface of NPs. In addition, the smooth and spherical shape of all non-coated and CS-coated NPs was observed via SEM analysis as in Figure 4.25.

In case of stability analysis, some fluctuations in the size were observed during the first hour of incubation for both non-coated and CS-coated NPs as in Figure 4.26, Figure 4.27, and Figure 4.28. This could be caused by the instantaneous addition of NPs in PBS solution. However, for all graphs, non-significant p-value ($p > 0.05$) was obtained, indicating that there were no statistically significant changes in the NP size over the period examined under different conditions. This proved the sufficient stability of all these NPs. Moreover, in detail, it was seen at the end that compared to non-coated NPs, all CS-coated NPs showed less fluctuations in their hydrodynamic diameter measurements, and they were more stable during the incubation. The reason behind this was the presence of CS coating. The coating of NPs with natural CS polymer protected the NPs from dispersion and swelling more compared to non-coated ones. Also, drug-loaded CS-CUR-PLGA NPs (Figure 4.27B) and CS-αTCP-PLGA NPs (Figure 4.28B) had enhanced stability in the long term compared to empty CS-PLGA NPs (Figure 4.26B). The loading of NPs with hydrophobic drug molecules increased their stability by providing more compact structure in the hydrophilic environment. Thus, it could be concluded that NPs, especially the CS-coated ones, could maintain their stability for a long time under different environmental conditions. Furthermore, the EE of CUR and αTCP drug molecules were analysed as in Table 4.5 for both non-coated and CS-coated versions. The reduction in the EE of CUR was observed after the coating while the EE of αTCP remained almost the same. This difference in the EE could be caused by the chemical properties of drugs. Both the coating procedure and the additional centrifugations conducted to optimize the NP size

could also be the reasons for the reduction in the EE of CUR inside of NPs. After that, the drug release from NPs were analysed in both pH 7.4 PBS and pH 5.5 acetate buffer solution as in Figure 4.29. In case of inflammation, there is a decrease in the pH level of the surrounding environment. Hence, in this experiment, a pH of 7.4 was employed to simulate healthy body conditions, while a pH of 5.5 was used to mimic an inflammatory environment. The results revealed that the release of the drug from NPs was notably higher in the pH 5.5 solution compared to the drug release percentages observed in the pH 7.4 solution. This situation proved the higher drug release in the presence of inflammation compared to the drug release in a healthy body fluid. Furthermore, it was seen that, both in pH 5.5 and pH 7.4 environment, the release of CUR and αTCP drug molecules from CS-coated NPs was slower than the drug release from their non-coated versions. Therefore, this observation showed that the shell made of CS provided a sustained and slower release by protecting the drug molecule in the PLGA core part. In addition, the release rate of αTCP was slower than the release rate of CUR in both pH 5.5 and pH 7.4. This could occur due to the difference in the chemical structure and properties of drugs. All in all, the sustained and controlled drug release from both CS-CUR-PLGA NPs and CS-αTCP-PLGA NPs was achieved in pH 5.5 inflammatory environment.

As a result of this project, CS-coated, antioxidant and anti-inflammatory CUR and αTCP drug molecules containing, biocompatible and biodegradable core-shell PLGA NPs were synthesized in a monodisperse manner and their characterization tests were completed properly. These NPs showed promising results by providing controlled and sustained drug release against AS-induced inflammation. In the literature, CS, which is one of the natural polymers, has been frequently used for surface coating and modifications. Also, core-shell NPs have been commonly synthesized by using this polymer (57). In most of the studies, CUR and αTCP has been preferred as drug molecules thanks to their superior antioxidant and anti-inflammatory properties (38,41). Although these are widely used in the studies, CUR-loaded and αTCP-loaded, CS-coated core-shell PLGA NPs against AS-induced inflammation are not present in the literature. Their development within the scope of this project adds uniqueness to

this study. Also, with the future studies, this project could enable researchers to compare the efficacy of CS-coated NPs containing different drug molecules on inflammation.

5.3. Discussion for Project 3: Mitochondria-Targeted NPs

Mitochondria are a pivotal cellular organelle that undertake a multitude of vital functions in the body such as the regulation of biosynthesis, metabolism, apoptosis, and cell survival. Also, mitochondria serve as the primary source of ROS and play a key role in the regulation of oxidative stress and immune responses (64). Excessive production of oxidants such as free radicals and ROS in the body results in the formation of oxidative stress, a major contributor to chronic inflammatory diseases (59,65). These chronic inflammatory diseases are fatal and cause several patients to suffer for years. For this reason, it is required to develop novel treatment methodologies against oxidative stress-induced inflammations due to the shortcomings of traditional treatment methods such as high toxicity and insufficient delivery to the target site (2,4). Given the significant impact of oxidative stress on inflammation and its correlation with serious diseases, mitochondria-targeted TPP formulations-conjugated and anti-inflammatory and antioxidant QCT drug molecule loaded PLGA NPs were developed as a DDS within the scope of this project.

First of all, non-targeted empty and drug-loaded NPs were synthesized as it was given in Section 3.2.3.1. After their optimization, TT80 conjugate was prepared to be used as a mitochondrial targeting agent as it was explained in Section 3.2.3.2. The purification of this conjugate was achieved via prep-HPLC, as shown in Figure 4.30. Then, its chemical characterization was accomplished with LC/MS-MS as in Figure 4.31. Furthermore, the chemical structure of TT80 conjugate was confirmed by conducting ^{1}H NMR analysis. The characteristic protons coming from both TPP and Tween80 were observed in its spectrum, as given in Figure 4.32, confirming its

successful synthesis. Also, FT-IR analysis was conducted as in Figure 4.33. It was observed that the characteristic functional groups of both TPP and Tween80 were seen in the FT-IR spectrum of TT80 conjugate. This proved the presence of both precursor materials in the structure of conjugate. In addition, PPT conjugate was synthesized as another mitochondrial targeting agent as it was explained in Section 3.2.3.3. First, PLGA-PEG was synthesized, and its characteristic functional groups were investigated using FT-IR spectroscopy as depicted in Figure 4.34. The FT-IR spectrum of the PLGA-PEG conjugate exhibited the characteristic functional groups of both PLGA and PEG polymers, affirming the successful formation of this conjugate. Subsequently, PPT was synthesized by incorporating both TPP-Br and the synthesized PLGA-PEG. The chemical structure of PLGA polymer, PLGA-PEG copolymer, and PPT conjugate was investigated via ^{1}H NMR analysis as in Figure 4.35. In the spectrum of PLGA-PEG copolymer, the characteristic protons of both PLGA and PEG polymer were observed. Similarly, in the ^{1}H NMR spectrum of PPT conjugate, the protons of PLGA-PEG copolymer and TPP molecule were detected. This indicated the proper synthesis and formation of the PPT conjugate. FT-IR analysis was also carried out for this conjugate as in Figure 4.36 and the presence of the characteristic peaks of precursor TPP and PLGA-PEG molecules was observed in the spectrum of PPT. All in all, TT80 and PPT conjugates were successfully synthesized and chemically characterized within the scope of this project, and they were used as mitochondrial targeting agents. By using these conjugates and their different amounts by weight, targeted empty and drug-loaded NPs were synthesized as it was explained in Section 3.2.3.4. During all these experimental procedures, NPs were characterized, and *in vitro* evaluation of these NPs was completed at the end. All in all, the NPs were obtained with optimum properties to be used in the treatment of oxidative stress-induced inflammation.

Following the synthesis of NPs, their hydrodynamic diameter and PDI values were analysed using DLS device. The size of non-targeted PLGA NPs and QCT-PLGA NPs were found almost the same and they were obtained in a monodisperse manner as in Figure 4.37. This observation demonstrated that drug loading did not have a substantial

impact on the hydrodynamic diameter of non-targeted NPs. After the conjugation of 10% and 20% TT80 by weight as a targeting agent, the DLS analysis was carried out again as in Figure 4.38. The hydrodynamic diameter of empty 10%TT80-PLGA NPs and 20%TT80-PLGA NPs were found as 180.2 nm and 204.7 nm, respectively. After drug loading, the size of 10%TT80-QCT-PLGA NPs and 20%TT80-QCT-PLGA NPs were obtained as 188.2 nm and 145.9 nm, respectively. The minor differences observed in the hydrodynamic diameter values could be caused by the experimental process and conducted homogenizations and filtrations. Moreover, all the targeted NPs obtained using 10% and 20% TT80 by weight as a targeting agent exhibited uniformity in size and were found to be monodisperse, with a PDI value lower than 0.119. In addition to this, targeted NPs were also synthesized by using 1.25% and 2.50% PPT by weight and their hydrodynamic diameter and PDI value measurements were obtained as in Figure 4.39. The amount of TPP found in 1.25% and 2.50% PPT-conjugated NPs were the equivalents of the amount of TPP found in 10% and 20% TT80-conjugated NPs, respectively. The hydrodynamic diameter of empty 1.25%PPT-PLGA NPs and 2.50%PPT-PLGA NPs were measured as 138.5 nm and 139.5 nm, respectively. After drug loading, the size of 1.25%PPT-QCT-PLGA NPs and 2.50%PPT-QCT-PLGA NPs were obtained as 149.5 nm and 165.7 nm, respectively. The minor increase in the size was observed for drug-loaded NPs containing 1.25% and 2.50% PPT by weight compared to empty ones. The slight variations in the hydrodynamic diameter values may be attributed to factors related to the experimental procedures, including the homogenization and filtration processes that were carried out to optimize the NP size. Furthermore, all these targeted NPs, containing 1.25% and 2.50% PPT by weight as a targeting agent, were consistently found to be monodisperse, exhibiting a PDI value lower than 0.190. All in all, after the DLS analysis, it was concluded that stable, compact, and monodisperse, non-targeted and targeted, empty and drug-loaded NPs were obtained. Their size was suitable to circulate through the blood stream and interact with cells in the targeted region.

Moreover, the surface charge of NPs was measured as in Figure 4.40, Figure 4.41, and Figure 4.42. It was observed that the zeta potential values of non-targeted empty

and drug-loaded NPs were negative. After conjugating 10% TT80, 20% TT80, 1.25% PPT, and 2.50% PPT by weight as targeting agents, a shift in the zeta potential values of NPs towards the positive side was observed compared to non-targeted NPs. This shift could be attributed to the attachment of positively charged TPP containing conjugates onto the surface of NPs as a mitochondrial targeting agent. Furthermore, the surface morphology and diameter of non-targeted PLGA NPs, QCT-PLGA NPs, 10%TT80-QCT-PLGA NPs, and also 2.50%PPT-QCT-PLGA NPs were analysed with SEM as it can be seen in Figure 4.43. In the SEM results, the smooth and spherical morphology of non-targeted and targeted NPs was observed. However, the hydrodynamic diameter of NPs that were measured with SEM was found smaller compared to the hydrodynamic diameter of NPs that were measured with DLS. This occurred due to the dehydration. As it was written in the Materials and Methods section, NPs were synthesized and stored in ddH_2O. On the other hand, in order to conduct SEM analysis, the NP solutions were dropped on grids and left to dry for almost 2 days under sterile conditions. After the water evaporated, the NPs were coated with gold and the analysis was conducted under high vacuum. For this reason, the decrease in the NP sizes was observed in the SEM results. Furthermore, the dimensions and structure of 10%TT80-QCT-PLGA NPs, 20%TT80-QCT-PLGA NPs, 1.25%PPT-QCT-PLGA NPs, and 2.50%PPT-QCT-PLGA NPs were investigated with TEM as in Figure 4.44. The spherical shape of targeted and drug-loaded NPs was observed. Compared to the hydrodynamic diameter values measured with DLS device, the decrease in size of NPs was also seen in the TEM results. This decrease could occur due to the dehydration of NPs and the working conditions of the TEM device. Similar to the SEM analysis, NPs that were prepared in ddH_2O were dropped on TEM grids and were waited to dry for almost 2 days under sterile conditions before conducting the experiment. After the water evaporated, the analysis was carried out under high vacuum and low-pressure conditions. Therefore, the decrease in the hydrodynamic diameter of NPs was observed in the TEM results similar to the SEM results.

Following these characterization tests, the stability of both non-targeted PLGA NPs and QCT-PLGA NPs was assessed by incubating them in 1M pH 7.4 PBS at

temperatures of 25˚C and 37˚C for a period of nearly 30 days. As in Figure 4.45, the hydrodynamic diameter of NPs remained relatively consistent during first 9 days under different environmental conditions, with minor fluctuations presumably attributed to the addition of NPs in PBS. Also, statistical analysis revealed a non-significant p-value until the end of 9^{th} day, indicating that there were no significant changes in the hydrodynamic diameter of NPs up to this time. However, after the 9^{th} day, the gradual increase in the NP size was observed for both empty and drug-loaded NPs. Also, a statistically significant p-value smaller than 0.0001 was observed after 9^{th} day, indicating a significant difference in the NP size. This increase in the size could be attributed to the dispersion of NPs since they swelled in PBS solution. The polymer chains which formed the compact NP structure started to move apart from each other so, the hydrodynamic diameter increased gradually. Nevertheless, it can be concluded that the hydrodynamic diameter of both non-targeted PLGA NPs and QCT-PLGA NPs was found highly stable under different environmental conditions up to 9 days. Furthermore, the EE of QCT in NPs were investigated as in Table 4.6. Drug EE of non-targeted and targeted NPs were found close to each other even though there were some minor differences. These minor differences in drug EE could be occurred due to the variations in the experimental conditions, purification processes, and also homogenization and filtration steps performed to achieve monodisperse NPs. At the end, obtained NPs had a drug EE between 47.96% and 60.20%. After that, the release rate of drug molecule from QCT-PLGA NPs was analysed in two different environments which were pH 7.4 PBS and pH 5.5 acetate buffer solution as in Figure 4.46. Theoretically, it is known that if the inflammation occurs, the pH of the environment decreases. Considering this, in this study, a pH of 7.4 was used to simulate a healthy body state, while a pH of 5.5 was employed to mimic inflammatory conditions. At the end, it was clearly observed that the drug release percentage from NPs was significantly higher in pH 5.5 solution compared to pH 7.4 solution. At the end of 11^{th} day, drug release from QCT-PLGA NPs reached to almost 95% at pH 5.5 acetate buffer solution while it was only around 35% in pH 7.4 PBS solution. Therefore, compared to the conventional drug molecules, the sustained and controlled drug release from QCT-PLGA NPs was achieved in pH 5.5 inflammatory environment.

After completion of these characterization tests, *in vitro* evaluation of NPs was conducted to analyse their toxicity, ROS activity, and targeting efficacy. First of all, CCK-8 assay was conducted to investigate *in vitro* cytotoxicity of NPs against various concentration values between 1 μM and 375 μM as it can be seen in Figure 4.47, Figure 4.49, and Figure 4.51. A statistically significant p-value smaller than 0.0001 was observed for all graphs in these figures, indicating that both the drug concentration and the differences in the samples significantly influence cell viability. In detail, it was observed that compared to free drug, the cell viability was higher in the presence of both non-targeted and targeted NPs until 300 μM concentration. Also, the decrease in the cell viability was observed for both free QCT and NPs while the concentration increased. Therefore, it was achieved that the increase in the concentration of drug molecules caused toxic effects on cells after some point. Moreover, the decrease in the cellular viability was observed when there was an increase in the amount of targeting agent. The reason behind this was the increase in the TPP concentration. As it was stated earlier, the critical threshold for the concentration of the cationic TPP molecule is 10 μM. As its concentration increases, it can lead to the development of undesirable side effects, such as proton leakage and depolarization of the mitochondrial membrane (27). Nevertheless, it is evident that, in comparison to free QCT molecule, all NPs exhibited superior cell viability, even at higher drug molecule concentrations. Furthermore, the IC50 values of NPs were investigated by using the nonlinear regression curves as in Figure 4.48, Figure 4.50, and Figure 4.52. It was achieved that compared to all NPs; QCT had the lowest IC50 value in terms of concentration as in Table 4.7. Therefore, it can be concluded that NPs were found more non-toxic to the L-929 mouse skin fibroblast cells compared to free drug.

Furthermore, the ROS activity of NPs was analysed against their IC25 and IC50 concentration values as in Figure 4.53. It was given in Section 2.4.2 that the overproduction of ROS in the body leads to the formation of an oxidative stress that causes severe chronic inflammatory diseases. Therefore, it is crucial to keep the ROS production at an optimum desired level for the proper functioning of the body. Considering this, within the scope of this project, mitochondria-targeted NPs were

developed for the treatment of oxidative stress-induced inflammation, and it had expected them to reduce the ROS production in case of an inflammation. LPS was used during this assay to create an inflammatory condition. In this context, positive cell control was created by applying both LPS and DCFDA on cells to observe the maximum ROS production when the cells were not treated with NPs in case of an inflammation. On the other hand, the background control was obtained by applying only DCFDA on cells to observe the basal ROS production of microglial cells when they were not treated with any NPs. The results clearly proved that in case of an inflammation, ROS production was significantly increased compared to their basal ROS level. Furthermore, the highest ROS production was observed when the cells were treated with free QCT at both IC25 and IC50 concentration values. The statistically significant difference was observed for the ROS level of QCT compared to the ROS level of controls since p-value was obtained smaller than 0.0001. The ROS production of the cells treated with free drug was obtained even higher than the ones depicted as positive control. Therefore, it was achieved that QCT itself did not have a curative effect on ROS production. However, QCT-PLGA NPs significantly lowered the ROS level at both IC25 and IC50 values compared to free drug so that it was similar to the ROS level of background control. This was also demonstrated statistically, and this proved the necessity and efficacy of NPs in decreasing ROS production compared to free drug. On the other hand, it was clearly observed that all targeted NPs, which were 10%TT80-QCT-PLGA NPs, 20%TT80-QCT-PLGA NPs, 1.25%PPT-QCT-PLGA NPs, and 2.50%PPT-QCT-PLGA NPs, significantly reduced the ROS level compared to both QCT and QCT-PLGA NPs at IC25 and IC50 doses. This difference was again proved statistically with a p-value smaller than 0.0001. Therefore, it was achieved that the usage of targeting agents on NPs could have a pivotal role in reducing and regulating ROS level in case of an inflammation. Moreover, for two different doses, it was observed that the increase in the concentration of targeting agent reduced the ROS production. In other words, 20%TT80-QCT-PLGA NPs and 2.50%PPT-QCT-PLGA NPs had lower ROS level than 10%TT80-QCT-PLGA NPs and 1.25%PPT-QCT-PLGA NPs, respectively. This also proved that both TPP and PPT targeting agents could prevent the overproduction of ROS in case of an inflammation since they improved its reduction compared to non-targeted QCT-PLGA NPs and free

drug. Furthermore, slightly lower ROS level for 10%TT80-QCT-PLGA NPs, 20%TT80-QCT-PLGA NPs, 1.25%PPT-QCT-PLGA NPs, and 2.50%PPT-QCT-PLGA NPs was observed at IC50 concentration value than IC25. This showed that the decrease in the ROS production was linearly correlated with the increase in doses when targeted NPs applied. All in all, it can be concluded that targeted NPs could effectively reduce the ROS production compared to free drug and non-targeted NPs and this paved the way for the usage of them in the treatment of oxidative stress-induced inflammations.

In addition to all these experiments, the mitochondrial targeting efficacy of NPs was investigated by conducting JC-1 assay. The principle of this assay mainly depends on the change in the mitochondrial membrane potential. It is mentioned in the literature that JC-1 is able to pass through the cell membrane when the mitochondrial membrane potential is elevated. Under these conditions, it forms aggregates inside the mitochondria, resulting in red fluorescence. On the other hand, when there is a decrease in the membrane potential of mitochondria, JC-1 goes from the mitochondrial matrix to the cytoplasm of the cell, resulting in the formation of monomer with green fluorescent (72). In other words, the JC-1 dyes form red fluorescence or J-aggregates in the healthy mitochondria while they form green fluorescence or J-monomer upon induction of the apoptosis of mitochondria. In this experiment, LPS was employed to create an inflammatory environment, thereby enabling the observation of anti-inflammatory healing effects of both free drug and NPs upon reaching mitochondria. Considering all this information, it was expected to observe higher formation of red fluorescence in the images of cells when synthesized NPs were applied on them. First of all, the cells that were treated with only CCCP and only LPS was analysed as controls (Figure 4.54). Since CCCP acts as a disrupter of mitochondrial membrane potential, it was utilized as a positive control. It was expected to observe the formation intense green fluorescence in the presence of CCCP due to its induction of mitochondrial depolarization. As expected, only J-monomers were seen in the captured images of CCCP-treated cells, with no detection of J-aggregates or red fluorescence. This observation confirmed the proper functioning and reliability of the

assay. In addition, in the images of the cells that were treated with only LPS, intense green fluorescence was observed, along with some minor red fluorescence. This observation confirms the presence of inflammation and the induction of apoptosis in response to inflammation. Furthermore, to better observe the effect of NPs, the cells were also treated with QCT as a free drug, and the JC-1 assay was conducted. Drug concentrations of 5 μM, 10 μM, and 20 μM were applied to the cells. It was observed that the formation of J-aggregates was higher than that obtained for controls regardless of the drug concentration as in Figure 4.55. As drug concentration increased, the increase in the red fluorescence was observed indicating drug-dose dependency. However, the intensity of green fluorescence was also very high and for this reason, J-monomers were highly abundant in the overlay images. Furthermore, the captured images for QCT-PLGA NPs can be seen in Figure 4.56. It was observed that with an increase in drug concentration, there was a corresponding increase in red fluorescence. Compared to QCT alone, the overlay images of QCT-PLGA NPs exhibited more red fluorescence, indicating a higher presence of healthy mitochondria. This also proved the necessity and advantageous feature of the usage of NPs in the treatment of inflammation. Then, the effects of targeting agents on mitochondrial membrane potential and their ability to target mitochondria were analysed at different ratios of the targeting agents. 10%TT80-QCT-PLGA NPs displayed a greater formation of J-aggregates compared to the non-targeted QCT-PLGA NPs, as depicted in Figure 4.57. This observation affirmed that targeting enhanced the healing process in case of an inflammation, leading to a higher occurrence of healthy mitochondria. Also, as the drug dose increased from 5 μM to 20 μM, the decrease in the number of J-monomers and increase in the number and brightness of J-aggregates were observed. This also proved their dose-dependent response and underscored the advantages of employing targeted NPs with TT80 as a targeting agent. When the targeting agent increased to 20% by weight (Figure 4.58), the intensity and amount of red fluorescence significantly increased at all drug concentration values compared to those containing 10% TT80. The decrease in the J-monomers and the increase in the J-aggregates were observed as the concentration increased. In the overlay image, it was evident that there was an increased number of healthy mitochondria when the cells were treated with 20%TT80-QCT-PLGA NPs. Therefore, the targeting ability was found to be linearly

proportional to the ratio of the targeting agent, TT80. When the targeting agent was PPT rather than TT80, the intensity and number of J-aggregates remained similar regardless of the increase in the ratio of the targeting agent from 1.25% PPT (Figure 4.59) to 2.50% PPT (Figure 4.60). Therefore, the targeting ability was not linearly proportional to the ratio of the PPT as a targeting agent. Also, the brightness and the amount of red fluorescence signals were not as pronounced as those observed with TT80-conjugated targeted NPs. This could be attributed to the formation of steric hindrance after conjugating the targeting agent at the end of the polymer, PLGA-PEG. However, as the drug concentration increased, the formation of red fluorescence also increased. Additionally, targeting with PPT still resulted in a higher number of healthy mitochondria compared to QCT and QCT-PLGA NPs. However, due to the steric hindrance, the usage of TT80 provided high mitochondrial membrane potential and increased number of healthy mitochondria compared to PPT. All in all, it can be concluded that the usage of targeted NPs resulted in the formation of more J-aggregates and so provided advantageous results for treating inflammation regardless of the type of targeting agent, compared to both free drug and non-targeted NPs.

In conclusion, biocompatible, biodegradable, and mitochondria-targeted PLGA NPs that were loaded with anti-inflammatory QCT as a drug molecule were successfully synthesized. The necessary characterization tests were completed to obtain NPs with optimized properties in terms of size, surface charge, and morphology. The hydrodynamic diameter of both non-targeted PLGA NPs and QCT-PLGA NPs was found highly stable during first 9 days and QCT-PLGA NPs provided the sustained and controlled drug release at pH 5.5 inflammatory environment. Compared to free drug, all NPs showed higher cell viability even at high concentration values of drug molecule. Moreover, in comparison with free drug and non-targeted NPs, all targeted NPs significantly reduced the ROS production in the presence of an inflammation. Also, the use of targeted NPs enhanced the formation of J-aggregates in JC-1 assay, regardless of the type of targeting agent, thereby providing favourable results for healing inflammation and increasing the number of healthy mitochondria. Therefore, these NPs that were synthesized within the scope of this project exhibited

promising results to be used in the treatment of oxidative stress-induced inflammation compared to conventional treatment methodologies. In the literature, it is stated that the transport of TPP-conjugated NPs from the cytoplasm into mitochondria is facilitated up to a hundred times compared to the transport of non-targeted NPs. Therefore, targeting efficacy of TPP to the mitochondria has been proved (32). Moreover, QCT has been commonly used in the studies thanks to its antioxidant and anti-inflammatory properties. Also, in the literature, it is demonstrated that carrying QCT with NPs enhances its stability, bioavailability, and pharmacokinetic profile while reducing its toxicity to the body (36). Although mitochondrial targeting agent TPP and QCT have been frequently used in the studies separately, there is no study available in the literature that utilizes TPP-conjugated QCT-loaded PLGA NPs for the treatment of oxidative stress-induced inflammation. Also, to compare the effectiveness of targeting agents, two different conjugates containing TPP were synthesized, and their different ratios were conjugated to NPs within the scope of this project. The usage of these conjugates is not also available in the literature. This contributes to the originality of this project. Finally, these optimized mitochondria-targeted anti-inflammatory drug-loaded PLGA NPs have a great potential to serve as an effective DDS for the future studies in the treatment of many chronic inflammatory diseases in which mitochondria play a pivotal role.

6. CONCLUSION

The studies conducted in this thesis consisted of three main projects which included the development of macrophage-targeted NPs, CS-coated NPs, and mitochondria-targeted NPs. In general, all these projects concentrated on the synthesis and evaluation of various PLGA NPs loaded with anti-inflammatory drug molecules to combat inflammation caused by AS or oxidative stress.

In the first project, monodisperse and stable NPs with low PDI values were successfully obtained. The addition of positively charged S2P peptide as a targeting agent onto the NPs was confirmed through zeta potential surface charge measurements. Additionally, the presence of the targeting agent was validated by analysing the net protein concentration found in targeted NPs using a nanodrop device. Moreover, SEM images revealed the smooth and spherical shape of the NPs, while TEM images confirmed the presence of a polymeric coating layer around the NPs. Furthermore, with FT-IR analysis, the presence of chemical functional groups of the drug molecule and coating layer in NPs was confirmed. Drug release studies demonstrated that, after approximately 27 days, the drug release percentage from the NPs was around 75% at pH 5.5, whereas it was approximately 25% at pH 7.4 solution when the drug was α-13′-COOH. Similarly, after approximately 32 days, the drug release from the NPs reached almost 77% at pH 5.5, while it was approximately 4% at pH 7.4 solution when the drug was GA. These findings confirmed the sustained and controlled release of drug molecules in an acidic inflammatory environment. In summary, the successful synthesis of macrophage-targeted PLGA NPs loaded with various VitE metabolites for addressing inflammation induced by AS was achieved.

In the second project, monodisperse NPs with low PDI values were synthesized. After coating the NPs with CS, an increase in size was achieved while maintaining mono-dispersity, enabling safe circulation throughout the blood. The addition of

positively charged CS as a coating layer was confirmed through surface charge measurements. Together with these, their smooth and spherical nature were revealed by SEM images. It was also demonstrated that CS coating improved stability and facilitated sustained and prolonged release of drugs from the NPs. Consequently, the second project of this thesis study was also accomplished properly.

Finally, in the third project, mitochondria-targeted NPs were synthesized using 10% and 20% TT80 and 1.25% and 2.50% PPT by weight as targeting agents, resulting in sizes smaller than 210 nm and exhibiting mono-dispersity. The addition of TT80 or PPT as targeting agents was confirmed by observing a shift in zeta potential values towards the positive side, attributed to TPP being a positively charged small molecule. Their surface morphology, dimensions, and structure were verified through SEM and TEM images. The NPs demonstrated high stability for up to 9 days and provided controlled and prolonged release of QCT in acidic inflammatory environments. Furthermore, *in vitro* characterization assays were conducted to assess the impact of NPs on cell viability, ROS production, and mitochondria-targeting. The synthesized NPs exhibited high cellular viability even at elevated drug concentrations, and all targeted NPs effectively reduced ROS production under inflammatory conditions. Additionally, it was observed from the fluorescence microscope images that targeted NPs promoted the formation of J-aggregates, indicating their ability to prevent mitochondrial apoptosis in the presence of inflammation. This confirmed the efficacy of NPs in targeting mitochondria. In conclusion, optimized mitochondria-targeted NPs loaded with QCT were successfully synthesized and showed a great potential to serve as an effective DDS for treating inflammations induced by oxidative stress.

In the light of all this information, it is evident that all three projects were conducted appropriately, yielding promising results for future studies. Although the PLGA polymer, drug molecules, and targeting agents have been used in the literature for years, their combination as achieved in this thesis study is unique and original. This underscores the potential of the research to enhance the quality of life for patients with

chronic inflammatory disorders. Also, with some variations in targeting agents or drug molecules, it may be possible to extend the application of these studies to treat other severe diseases. Therefore, it can be concluded that the studies conducted within the scope of this thesis will pave the way for numerous future investigations.

7. REFERENCES

1. Jacob J, Haponiuk JT, Thomas S, Gopi S. Biopolymer based nanomaterials in drug delivery systems: A review. Mater Today Chem. 2018;9:43-55.
2. Begines B, Ortiz T, Pérez-Aranda M, Martínez G, Merinero M, Argüelles-Arias F, et al. Polymeric nanoparticles for drug delivery: Recent developments and future prospects. Nanomaterials. 2020;10:1-41.
3. Anselmo AC, Mitragotri S. An overview of clinical and commercial impact of drug delivery systems. J Control Release. 2014;190:15–28.
4. Bhattarai N, Gunn J, Zhang M. Chitosan-based hydrogels for controlled, localized drug delivery. Adv Drug Deliv Rev. 2010;62:83–99.
5. Kumar B, Jalodia K, Kumar P, Gautam HK. Recent advances in nanoparticle-mediated drug delivery. J Drug Deliv Sci Technol. 2017;41:260–8.
6. Singh R, Lillard JW. Nanoparticle-based targeted drug delivery. Exp Mol Pathol. 2009;86:215–23.
7. Yih TC, Al-Fandi M. Engineered nanoparticles as precise drug delivery systems. J Cell Biochem. 2006;97:1184–90.
8. Najahi-Missaoui W, Arnold RD, Cummings BS. Safe nanoparticles: Are we there yet? Int J Mol Sci. 2021 Jan 1;22(1):1–22.
9. Mohanraj VJ, Chen Y. Nanoparticles-A Review. Trop J Pharm Res. 2006;5(1):561-573.
10. Mitchell MJ, Billingsley MM, Haley RM, Wechsler ME, Peppas NA, Langer R. Engineering precision nanoparticles for drug delivery. Nat Rev Drug Discov. 2021;20:101-24.
11. Nagavarma BVN, Yadav H, Ayaz A, Vasudha L, Shivakumar H. Different techniques for preparation of polymeric nanoparticles- A review. Asian J Pharm Clin Res. 2012;5:16-23.
12. Zielińska A, Carreiró F, Oliveira AM, Neves A, Pires B, Venkatesh DN, et al. Polymeric nanoparticles: production, characterization, toxicology and ecotoxicology. Molecules. 2020;25(16):3731.
13. El-Say KM, El-Sawy HS. Polymeric nanoparticles: Promising platform for drug delivery. Int J Pharm. 2017;528:675–91.
14. Sur S, Rathore A, Dave V, Reddy KR, Chouhan RS, Sadhu V. Recent developments in functionalized polymer nanoparticles for efficient drug delivery system. Nano-Struct Nano-Objects. 2019;20:100397.
15. Kumari A, Yadav SK, Yadav SC. Biodegradable polymeric nanoparticles based drug delivery systems. Colloids Surf B Biointerfaces. 2010;75:1–18.
16. Chiu HI, Samad NA, Fang L, Lim V. Cytotoxicity of targeted PLGA nanoparticles: a systematic review. RSC Adv. 2021;11:9433–49.
17. Sharma S, Parmar A, Kori S, Sandhir R. PLGA-based nanoparticles: A new paradigm in biomedical applications. TrAC Trends Anal Chem. 2016;80:30–40.

18. Acharya S, Sahoo SK. PLGA nanoparticles containing various anticancer agents and tumour delivery by EPR effect. Adv Drug Deliv Rev. 2011;63:170–83.

19. Rezvantalab S, Drude NI, Moraveji MK, Güvener N, Koons EK, Shi Y, et al. PLGA-based nanoparticles in cancer treatment. Front Pharmacol. 2018 Nov 2;9:1260.

20. Attia MF, Anton N, Wallyn J, Omran Z, Vandamme TF. An overview of active and passive targeting strategies to improve the nanocarriers efficiency to tumour sites. J Pharm Pharmacol. 2019;71:1185–98.

21. Yoo J, Park C, Yi G, Lee D, Koo H. Active targeting strategies using biological ligands for nanoparticle drug delivery systems. Cancers. 2019 May 1;11(5):640.

22. Yu B, Tai HC, Xue W, Lee LJ, Lee RJ. Receptor-targeted nanocarriers for therapeutic delivery to cancer. Mol Membr Biol. 2010;27:286–98.

23. Peterson KR, Cottam MA, Kennedy AJ, Hasty AH. Macrophage-targeted therapeutics for metabolic disease. Trends Pharmacol Sci. 2018;39:536–46.

24. Ou LC, Zhong S, Ou JS, Tian JW. Application of targeted therapy strategies with nanomedicine delivery for atherosclerosis. Acta Pharmacol Sin. 2021;42:10–7.

25. Song Y, Huang Y, Zhou F, Ding J, Zhou W. Macrophage-targeted nanomedicine for chronic diseases immunotherapy. Chin Chem Lett. 2022 Feb 1;33(2):597–612.

26. Tao W, Yurdagul Jr A, Kong N, Li W, Wang X, Doran AC, et al. siRNA nanoparticles targeting CaMKIIγ in lesional macrophages improve atherosclerotic plaque stability in mice. Sci Transl Med. 2020;12(553).

27. Khan T, Waseem R, Zehra Z, Aiman A, Bhardwaj P, Ansari J, et al. Mitochondrial Dysfunction: Pathophysiology and Mitochondria-Targeted Drug Delivery Approaches. Pharmaceutics. 2022;14(12):2657.

28. Tabish TA, Narayan RJ. Mitochondria-targeted graphene for advanced cancer therapeutics. Acta Biomaterialia. 2021;129:43–56.

29. Ganji C, Muppala V, Khan M, Purnachandra Nagaraju G, Farran B. Mitochondrial-targeted nanoparticles: Delivery and therapeutic agents in cancer. Drug Discov Today. 2023;28(3):103469.

30. Xu J, Shamul JG, Kwizera EA, He X. Recent advancements in mitochondria-targeted nanoparticle drug delivery for cancer therapy. Nanomaterials. 2022 Feb 23;12(5):743.

31. Ren C, Li D, Zhou Q, Hu X. Mitochondria-targeted TPP-MoS2 with dual enzyme activity provides efficient neuroprotection through M1/M2 microglial polarization in an Alzheimer's disease model. Biomaterials. 2020 Feb 1;232:119752.

32. Tabish TA, Hamblin MR. Mitochondria-targeted nanoparticles (mitoNANO): An emerging therapeutic shortcut for cancer. Biomaterials and Biosystems. 2021;3:100023.

33. Lesjak M, Beara I, Simin N, Pintać D, Majkić T, Bekvalac K, et al. Antioxidant and anti-inflammatory activities of quercetin and its derivatives. J Funct Foods. 2018 Jan 1;40:68–75.

34. Li Y, Yao J, Han C, Yang J, Chaudhry MT, Wang S, et al. Quercetin, inflammation and immunity. Nutrients. 2016;8(3):167.

35. Singh Baghel S, Shrivastava N, Singh Baghel R, Agrawal P, Rajput S. A review of quercetin: Antioxidant and anticancer properties. World J Pharm Pharmaceutical Sci. 2012;1:146-160.

36. Sun D, Li N, Zhang W, Yang E, Mou Z, Zhao Z, et al. Quercetin-loaded PLGA nanoparticles: a highly effective antibacterial agent in vitro and anti-infection application in vivo. J Nanopart Res. 2016 Jan 1;18(1):1–21.

37. Hewlings SJ, Kalman DS. Curcumin: A review of its effects on human health. Foods. 2017;6(10):92.

38. Abd El-Hack ME, El-Saadony MT, Swelum AA, Arif M, Abo Ghanima MM, Shukry M, et al. Curcumin, the active substance of turmeric: its effects on health and ways to improve its bioavailability. J Sci Food Agric. 2021;101:5747–62.

39. Sharma RA, Gescher AJ, Steward WP. Curcumin: The story so far. Eur J Cancer. 2005;41(13):1955–68.

40. Colombo ML. An update on vitamin E, tocopherol and tocotrienol-perspectives. Molecules. 2010;15:2103–13.

41. Giusepponi D, Torquato P, Bartolini D, Piroddi M, Birringer M, Lorkowski S, et al. Determination of tocopherols and their metabolites by liquid-chromatography coupled with tandem mass spectrometry in human plasma and serum. Talanta. 2017 Aug 1;170:552–61.

42. Wallert M, Mosig S, Rennert K, Funke H, Ristow M, Pellegrino RM, et al. Long-chain metabolites of α-tocopherol occur in human serum and inhibit macrophage foam cell formation in vitro. Free Radic Biol Med. 2014 Mar;68:43–51.

43. Brigelius- Flohé R, Traber MG. Vitamin E: function and metabolism. FASEB J. 1999 Jul;13(10):1145–55.

44. Hoff J, Karl B, Gerstmeier J, Beekmann U, Schmölz L, Börner F, et al. Controlled release of the α-tocopherol-derived metabolite α-13′-carboxychromanol from bacterial nanocellulose wound cover improves wound healing. Nanomaterials. 2021 Aug 1;11(8):1939.

45. Kluge S, Schubert M, Börmel L, Lorkowski S. The vitamin E long-chain metabolite α-13'-COOH affects macrophage foam cell formation via modulation of the lipoprotein lipase system. Biochim Biophys Acta Mol Cell Biol Lipids. 2021 Apr;1866(4):158875.

46. Wallert M, Bauer J, Kluge S, Schmölz L, Chen YC, Ziegler M, et al. The vitamin E derivative garcinoic acid from Garcinia kola nut seeds attenuates the inflammatory response. Redox Biol. 2019 Jun 1;24:101166.

47. Bartolini D, De Franco F, Torquato P, Marinelli R, Cerra B, Ronchetti R, et al. Garcinoic Acid Is a Natural and Selective Agonist of Pregnane X Receptor. J Med Chem. 2020 Apr 9;63(7):3701–12.

48. Salatin S, Maleki Dizaj S, Yari Khosroushahi A. Effect of the surface modification, size, and shape on cellular uptake of nanoparticles. Cell Biol Int. 2015;39:881–90.

49. Hu X Le, Kwon N, Yan KC, Sedgwick AC, Chen GR, He XP, et al. Bio-Conjugated Advanced Materials for Targeted Disease Theranostics. Adv Funct Mater. 2020;30:1907906.

50. Lee GY, Kim JH, Oh GT, Lee BH, Kwon IC, Kim IS. Molecular targeting of atherosclerotic plaques by a stabilin-2-specific peptide ligand. J Control Release. 2011 Oct 30;155(2):211-7.

51. Gerlach BD, Ampomah PB, Yurdagul A, Liu C, Lauring MC, Wang X, et al. Efferocytosis induces macrophage proliferation to help resolve tissue injury. Cell Metab. 2021 Dec 7;33(12):2445-2463.e8.

52. Marrache S, Dhar S. Engineering of blended nanoparticle platform for delivery of mitochondria-acting therapeutics. Proc Natl Acad Sci U S A. 2012 Oct 2;109(40):16288–93.

53. Al-Nemrawi NK, Okour AR, Dave RH. Surface modification of PLGA nanoparticles using chitosan: Effect of molecular weight, concentration, and degree of deacetylation. Adv Polym Technol. 2018 Dec 1;37(8):3066–75.

54. Alfaifi MY, Shati AA, Elbehairi SEI, Fahmy UA, Alhakamy NA, Md S. Anti-tumor effect of PEG-coated PLGA nanoparticles of febuxostat on A549 non-small cell lung cancer cells. 3 Biotech. 2020 Mar 1;10(3):133.

55. Wang R, Xiao R, Zeng Z, Xu L, Wang J. Application of poly(ethylene glycol)-distearoylphosphatidylethanolamine (PEG-DSPE) block copolymers and their derivatives as nanomaterials in drug delivery. Int J Nanomedicine. 2012;7:4185–98.

56. Li YP, Pei YY, Zhang XY, Gu ZH, Hui Zhou Z b, Yuan WF, et al. PEGylated PLGA nanoparticles as protein carriers: synthesis, preparation and biodistribution in rats. J Control Release. 2001 Apr 2;71(2):203-11.

57. Frank LA, Onzi GR, Morawski AS, Pohlmann AR, Guterres SS, Contri RV. Chitosan as a coating material for nanoparticles intended for biomedical applications. Reactive Funct Polym. 2020;147:104459.

58. Durán-Lobato M, Martín-Banderas L, Gonçalves LMD, Fernández-Arévalo M, Almeida AJ. Comparative study of chitosan- and PEG-coated lipid and PLGA nanoparticles as oral delivery systems for cannabinoids. J Nanopart Res. 2015 Jan 30;17(2):1-17.

59. Hussain T, Tan B, Yin Y, Blachier F, Tossou MCB, Rahu N. Oxidative Stress and Inflammation: What Polyphenols Can Do for Us? Oxid Med Cell Longev. 2016;2016:7432797.

60. Missiroli S, Genovese I, Perrone M, Vezzani B, Vitto VAM, Giorgi C. The role of mitochondria in inflammation: From cancer to neurodegenerative disorders. J Clin Med. 2020 Mar;9(3):740.

61. Nathan C, Ding A. Nonresolving Inflammation. Cell. 2010;140:871–82.

62. Zhu Y, Xian X, Wang Z, Bi Y, Chen Q, Han X, et al. Research progress on the relationship between atherosclerosis and inflammation. Biomolecules. 2018 Aug 23;8(3):80.

63. Linton MF, Fazio S. Macrophages, inflammation, and atherosclerosis. Int J Obes. 2003;27:S35–S40.

64. Chen Y, Zhou Z, Min W. Mitochondria, oxidative stress and innate immunity. Front Physiol. 2018 Oct 18;9:1487.

65. Chatterjee S. Chapter Two - Oxidative Stress, Inflammation, and Disease. In: Dziubla T, Butterfield DA, editors. Oxidative Stress and Biomaterials. Academic Press; 2016: 35-58.

66. Patergnani S, Bouhamida E, Leo S, Pinton P, Rimessi A. Mitochondrial oxidative stress and "mito-inflammation": Actors in the diseases. Biomedicines. 2021;9(1):1–25.

67. Vanier GS. Microwave-assisted solid-phase peptide synthesis based on the Fmoc protecting group strategy (CEM). Methods Mol Biol. 2013;1047:235–49.

68. Overstreet DJ, Lee EJ, Pal A, Vernon BL. In situ crosslinking temperature-responsive hydrogels with improved delivery, swelling, and elasticity for endovascular embolization. J Biomed Mater Res B Appl Biomater. 2022 Aug;110(8):1911–21.

69. Xie Y, Liu C, Huang H, Huang J, Deng A, Zou P, et al. Bone-targeted delivery of simvastatin-loaded PEG-PLGA micelles conjugated with tetracycline for osteoporosis treatment. Drug Deliv Transl Res. 2018 Oct;8(5):1090–102.

70. Mehrotra A, Pandit JK. Preparation and characterization and biodistribution studies of lomustine loaded PLGA nanoparticles by interfacial deposition method. J Nanomedine Biotherapeutic Discov. 2015;5:138.

71. Dandamudi M, McLoughlin P, Behl G, Rani S, Coffey L, Chauhan A, et al. Chitosan-coated PLGA nanoparticles encapsulating triamcinolone acetonide as a potential candidate for sustained ocular drug delivery. Pharmaceutics. 2021 Sep 30;13(10):1590.

72. Liu R, Yu X, Su C, Shi Y, Zhao L. Nanoparticle delivery of artesunate enhances the anti-tumor efficiency by activating mitochondria-mediated cell apoptosis. Nanoscale Res Lett. 2017;12:403.

8. APPENDIX

Appendix 1. ^{1}H NMR analysis of the non-targeted and mitochondria-targeted drug-loaded NPs (project 3)

The chemical structure of both non-targeted QCT-PLGA NPs and targeted 10%TT80-QCT-PLGA NPs was analysed by ^{1}H NMR spectroscopy in deuterium oxide (D_2O). In the spectrum of QCT-PLGA NPs (Figure 8.1A), the aromatic protons of the drug molecule, QCT, were observed around 8.25-8.75 ppm. Also, the -CH_2 and OH protons of PEG polymer were detected around 3.50-4.00 ppm and 2.00-2.50 ppm, respectively. Also, the D_2O protons were seen around 4.50-5.00 ppm. After the conjugation of targeting agent onto the NPs, the previously mentioned peaks coming from the aromatic protons of QCT and -CH_2 and OH protons of PEG were observed at similar ppm values. However, in addition to these, the aromatic protons of TPP molecule were seen around 6.50-7.50 ppm in the spectrum of 10%TT80-QCT-PLGA NPs (Figure 8.1B). This additional peak coming from TPP molecule confirmed the successful addition of the targeting agent to the NPs.

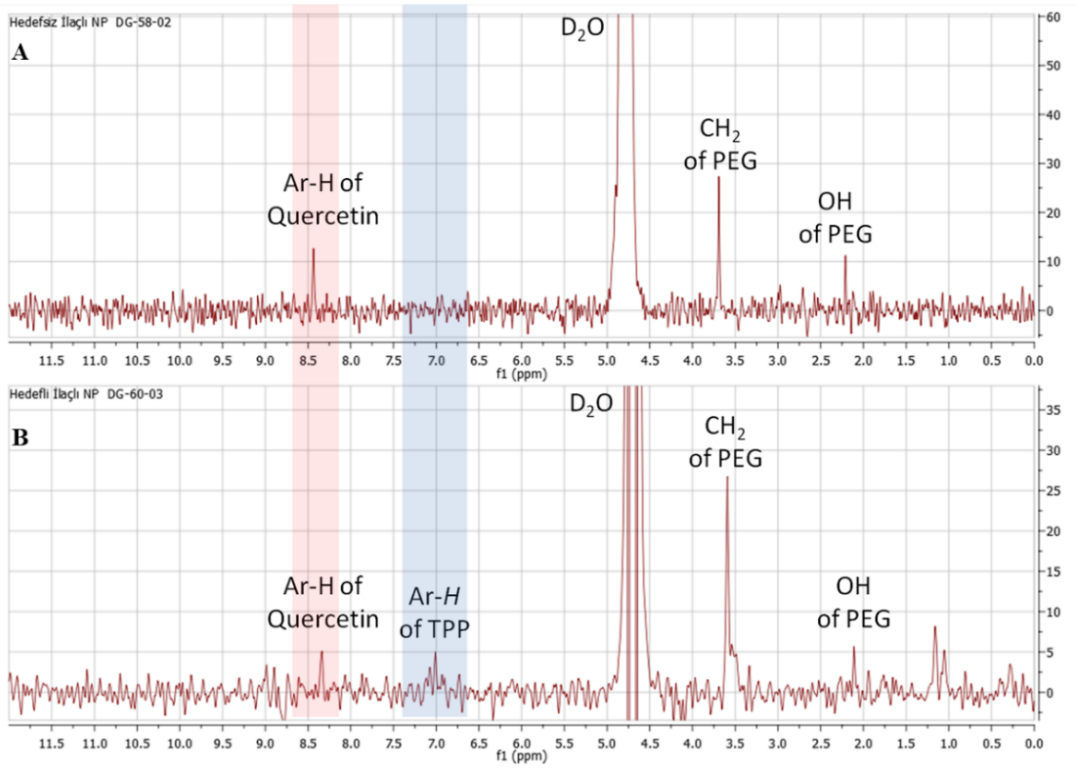

Figure 8. 1. ^{1}H NMR spectrum of the (A) QCT-PLGA NPs (B) 10%TT80-QCT-PLGA NPs.

9. CURRICULUM VITAE